CALIFORNIA INSTITUTE OF TECHNOLOGY

ELECTRON TUBE AND MICROWAVE LABORATORY

EXPERIMENTS ON THE INTERACTION OF A MODULATED ELECTRON BEAM WITH A PLASMA

by

Gary D. Boyd

TECHNICAL REPORT NO. 11-15

May 1959-60

A REPORT ON RESEARCH CONDUCTED UNDER

CONTRACT WITH THE OFFICE OF NAVAL RESEARCH

EXPERIMENTS ON THE INTERACTION OF A MODULATED ELECTRON BEAM WITH A PLASMA

by

Gary D. Boyd

Technical Report 11

CALIFORNIA INSTITUTE OF TECHNOLOGY

Pasadena, California

A Technical Report to the Office of Naval Research

Contract Nonr 220(13)

May 1959

ABSTRACT

New experiments are performed concerning the high frequency interactions of electron beams and plasmas. A modulated (500 Mc and 3000 Mc) electron beam is passed through a uniform plasma region of a mercury arc discharge, after which it is demodulated. Exponentially growing wave amplification along the electron beam is observed for the first time at a modulation frequency equal to the plasma frequency. No constant magnetic fields are used in these experiments. Calculations based on the one dimensional analysis of Bohm and Gross of an electron beam passing through a plasma are made to predict the effects of the random energy of the plasma electrons and collisions. By studying the interaction of a finite diameter beam and a plasma with no thermals or collisions, it is shown that the effect of the finite geometry is to reduce the growth constant.

Recent work by Trivelpiece and Gould has pointed out that a plasma column in free space may propagate forward and backward waves at a velocity small compared to the velocity of light. The experimental techniques of passing a modulated electron beam through the plasma, as described above, are applied to observe traveling wave type of interaction with the slow wave mode of propagation in the absence of any magnetic fields. Theory predicting experimental rates of growth is presented. Experimental results in good agreement with theory are presented.

In the course of verifying plasma density measurements, the excitation of the dipole resonance of a plasma column is considered. Multiple resonances are observed and discussed.

ACKNOWLEDGMENTS

I sincerely wish to extend my appreciation to Professor Roy W. Gould and Professor Lester M. Field for their continued interest and participation in this research. Their contributions have been most valuable.

A great deal of credit for the success of these experiments is attributable to Mr. A. F. Carpenter whose skill and patience in the fabrication of the glass tubes is gratefully acknowledged. Thanks are also extended to Mr. Eric Gelin and Mr. Bob Stratton who constructed the experimental equipment. Mrs. Ruth Stratton is thanked for her patience in the preparation of the manuscript.

Many fruitful discussions were enjoyed with Dr. A. W. Trivelpiece and Professor D. G. Dow with regard to both experiment and theory. Mr. John F. Asmus is thanked for his assistance with experiments and computations.

The contributions of other members of the California Institute of Technology in the education of the author over the past years are too numerous to mention, but are sincerely appreciated.

The author was privileged and fortunate to enjoy fellowships from the Francis Cole, General Electric, Schlumberger and Westinghouse Foundations. Their financial assistance is most appreciated.

TABLE OF CONTENTS

1. INTRODUCTION 1

1.0 Previous Investigations 1

1.1 Interaction of a Modulated Electron Beam with a Plasma at the Plasma Resonant Frequency 6

1.2 Interaction of an Electron Beam with the Surface Slow Wave Propagating Mode of a Plasma Column 7

2. INTERACTION OF A MODULATED ELECTRON BEAM WITH A PLASMA MEDIUM NEAR THE PLASMA RESONANCE FREQUENCY 11

2.0 Definition of a Plasma and Elementary Properties 11

2.1 One-Dimensional Theory of Interaction by the Distribution Function Method Including the Random Energy of the Plasma Electrons 13

2.2 Three-Dimensional Theory Neglecting the Random Energy of the Plasma Electrons 22

3. INTERACTION OF A MODULATED ELECTRON BEAM WITH THE SLOW WAVE SURFACE MODE OF PROPAGATION ON A PLASMA COLUMN 29

3.0 Slow Wave Mode of Propagation 29

3.1 Interaction Impedance and Estimation of Growth Constant 34

4. EXPERIMENTAL PROPERTIES OF THE PLASMA AND THE ELECTRON BEAM 41

4.0 Characteristics of Mercury Arc Discharges 41

4.1 Characteristics of the Electron Beam 44

5. HELIX MODULATION EXPERIMENT 49

5.0 Method of Operation 49

5.1 Experimental Verification of Theory and Plasma Density 51

5.2 Interaction with Surface Wave Mode of Propagation 61

5.3 Experimental Rates of Growth 68

6. CAVITY MODULATION EXPERIMENT 73

6.0 Method of Operation 73

6.1 Growing Surface Waves 78

6.2 Experimental Rates of Growth and Anomalous Effects 87

7. SUMMARY AND CONCLUSIONS 91

7.0 Summary of Results 91

7.1 Conclusions and Future Possibilities 93

Appendix 1 DIPOLE RESONANCE OF A CYLINDRICAL PLASMA COLUMN IN A TRANSVERSE ELECTRIC FIELD 95

Appendix 2 ONE-DIMENSIONAL DISPERSION RELATION BY THE BOLTZMANN EQUATION METHOD 98

REFERENCES 103

1. INTRODUCTION

This thesis is concerned with the amplification mechanisms associated with the interactions of an electron beam, modulated at microwave frequencies, passing through a plasma. The plasma used in the experimental parts of this research is that of an electric discharge in mercury vapor.

1.0 Previous Investigations

Electric discharges in gases have been investigated by a large number of researchers ever since the classic investigations of Langmuir and Mott-Smith (1) in 1924 on the characteristics of low pressure electric arc gas discharges. High frequency plasma electron oscillations have been the subject of many papers (2-25) and in 1929 Tonks and Langmuir (5) defined the electron plasma oscillation frequency and reported on experiments involving them.

Langmuir and Mott-Smith recognized two primary regions in a discharge; the nearly neutral plasma region consisting of the main body of the discharge, and the boundary region or sheath which separates it from the tube and electrode surfaces. This plasma region consists of electrons and ions of approximately equal charge density swarming about in continuous thermal motion due to their random energies. The plasma electrons typically have random energies of several electron volts and the ions only one volt or so. Because of the greater mass of the ions and their smaller energy it is obvious that the random ion current density will be much less than the random electron current density across any imaginary plane in the discharge. In mercury vapor discharges the ratio of random electron current density to ion current

density is typically 400.

Because of the requirements of conservation of energy and momentum, electrons and ions recombine at the walls of the discharge tube and not within the main body of the plasma. Thus there is a continuous flow of ions and electrons to the tube walls where they recombine. Since the random electron current density in the plasma is much greater than the random ion current density, there must be an electric field set up in the sheath separating the plasma from the discharge tube walls which reflects practically all of the electrons back into the plasma. This sheath consists of an excess of positive ions over a thin region of the order of a Debye (35) length thick. The electric field between this excess positive charge and a surface charge accumulation of electrons on the tube wall form a potential barrier which repels all but the most energetic of the plasma electrons.

As a result of the probe measurements of Langmuir and Mott-Smith (1) it was well established that the plasma electrons have a Maxwellian velocity distribution. The above discussion indicates however, that only a small fraction of the plasma electrons have sufficient energy to overcome the positive ion sheath and escape to the discharge tube walls. Therefore it was expected that there should be a depletion in the high velocity tail of the Maxwellian distribution of random energies for the plasma electrons. Such has never been found to be the case. This has been referred to as Langmuir's Paradox by Gabor, Ash and Dracott (21).

In low pressure discharges where the mean free path of the plasma electrons with un-ionized gas atoms is an order of magnitude or more

greater than the tube radius, the plasma electrons "collide" with the sheath many times more often than with gas atoms. Thus collisions with the latter could not be expected to maintain the Maxwellian distribution of the plasma electrons.

The mechanism which seems to be accepted today as the "thermalizing" force for the plasma electrons is that of plasma sheath oscillations (21). To substantiate this conclusion has required many experiments over a long period of years on the nature of such plasma oscillations. Since there are always dissipative forces present in a plasma, there must be some exciting force to maintain these sheath oscillations. This exciting force usually consists of an electron beam penetrating the sheath.

Many experiments have been performed on trying to excite plasma oscillations by a directed electron beam. Such oscillations are then observed with a small probe inserted into the plasma near the beam. Radio frequency signals are then looked for with this probe, and many can be found [(18) and (23) are good examples]. The frequencies of oscillation observed seem to be related to transit time effects of electrons between sheaths more often than they seem to equal the plasma frequency as defined by Tonks and Langmuir (5).

Wehner (14) describes a plasma oscillator which operates on the bunching principles of klystrons and reflex klystrons. Such is felt to be one source of plasma oscillations in discharge tubes. Experiments relating to this have been performed by Looney and Brown (18), Gabor, Ash and Dracott (21), Merrill and Webb (9), and a long list of others (9-23). Certainly some forms of plasma oscillations can be

explained in terms of klystron oscillations.

Looney and Brown's experiment is quite representative and will be described in more detail. A beam of high-energy electrons (several hundred volts) is injected into the plasma of a dc discharge from an auxiliary electron gun. This is found to excite plasma electron oscillations as detected by a small wire probe placed in the plasma. The probe is movable and shows the existence of standing wave patterns of oscillatory energy. Nodes of the pattern coincide with electrodes which bound the plasma. The thickness of the ion sheaths at these electrodes determine the standing wave pattern. It was verified that the energy transfer mechanism from the electron beam to the oscillation of the plasma electrons was established as a velocity-modulation process by transit time considerations between the ion sheaths. Gordon (22) has more recently investigated the energy exchange mechanism involved and performed similar experiments.

Aside from transit time (klystron, etc.) theories of plasma oscillations there have also been developed traveling wave theories (11,26-30) of the interaction of an electron beam with a plasma. These have primarily been investigated by Bohm and Gross (11). The mechanism is essentially that of the double stream amplifier invented by Haeff (28), and independently by Pierce and Hebenstreit (31).

In 1948 Haeff (26) suggested that plasma oscillations in the solar corona may be responsible for certain types of radio frequency electromagnetic energy received from the sun. He visualized that a group of charged particles traveling through the solar corona would interact with the electrons of the corona in such a manner as to amplify statistical fluctuations present in the corona or on the moving group of

particles. This stimulated much interest and there has been a great deal of work concerned with the existence of growing space charge waves on electron beams interacting with plasmas [see Gould (29)].

Looney and Brown in their experiments tried to detect such growing waves along the electron beam interacting with the plasma as predicted by Bohm and Gross. They reported such attempts as "fruitless". Kojima (23) was no more successful in repeating these experiments.

The principal fact to be discerned from previous experiments in this field is that all researchers were concerned with experimental situations in which the mechanism of self-excited plasma oscillations was being investigated. These were naturally occurring oscillations, i.e., they were not forced by a premodulated electron beam, except by Gordon (22). Even then, Gordon's device was basically an oscillator and many resonances were observed at varying densities. He further reports that "there was no evidence that the plasma was resonant when the plasma frequency equaled the beam modulation frequency. No variation of amplitude was observed along the beam" as predicted by Bohm and Gross.

In contradistinction to all of the previous experimental work on plasma oscillations, the research reported in this thesis is concerned with plasma amplifiers, not oscillators. Also the electron beam interacting with the plasma is at all times modulated by an external signal source. The beam is then allowed to pass through the plasma and is then demodulated by an identical microwave coupler.

The experiments to be described here were successful in obtaining

interaction with a plasma at an electron beam modulation frequency equal to the plasma frequency as well as observing growing waves along the electron beam as predicted by Bohm and Gross. Other interesting effects are also reported.

Previous experiments by other workers were unsuccessful because they did not use a modulated electron beam with which to excite the growing wave. They relied upon electron beam noise at the prescribed frequency to excite the growing wave and this did not produce a sufficiently strong detectable signal. Also, since they were dealing with oscillators that were dependent upon sheath boundaries, the observed effects were often extremely complicated. The experiments reported herein are between a modulated electron beam and the uniform plasma of a mercury arc discharge and were not a result of interactions with ion sheaths. Since the devices in this thesis are amplifiers and not oscillators, their behavior is much easier to understand.

1.1 Interaction of a Modulated Electron Beam with a Plasma at the Plasma Resonant Frequency

The first of these experiments was reported upon in a preliminary form by Boyd, Field and Gould (32) and consists of a device as shown in Figure 1.1 . An electron beam at a specified voltage is modulated over a wide frequency range with a short helix which propagates a slow electromagnetic wave at a phase velocity close to that of the electron beam velocity. The electron beam is then passed along the axis of the arc discharge for a distance of 5 cm at which it then leaves the plasma region. The electron beam is then demodulated by another short helix and the energy coupled into the output waveguide.

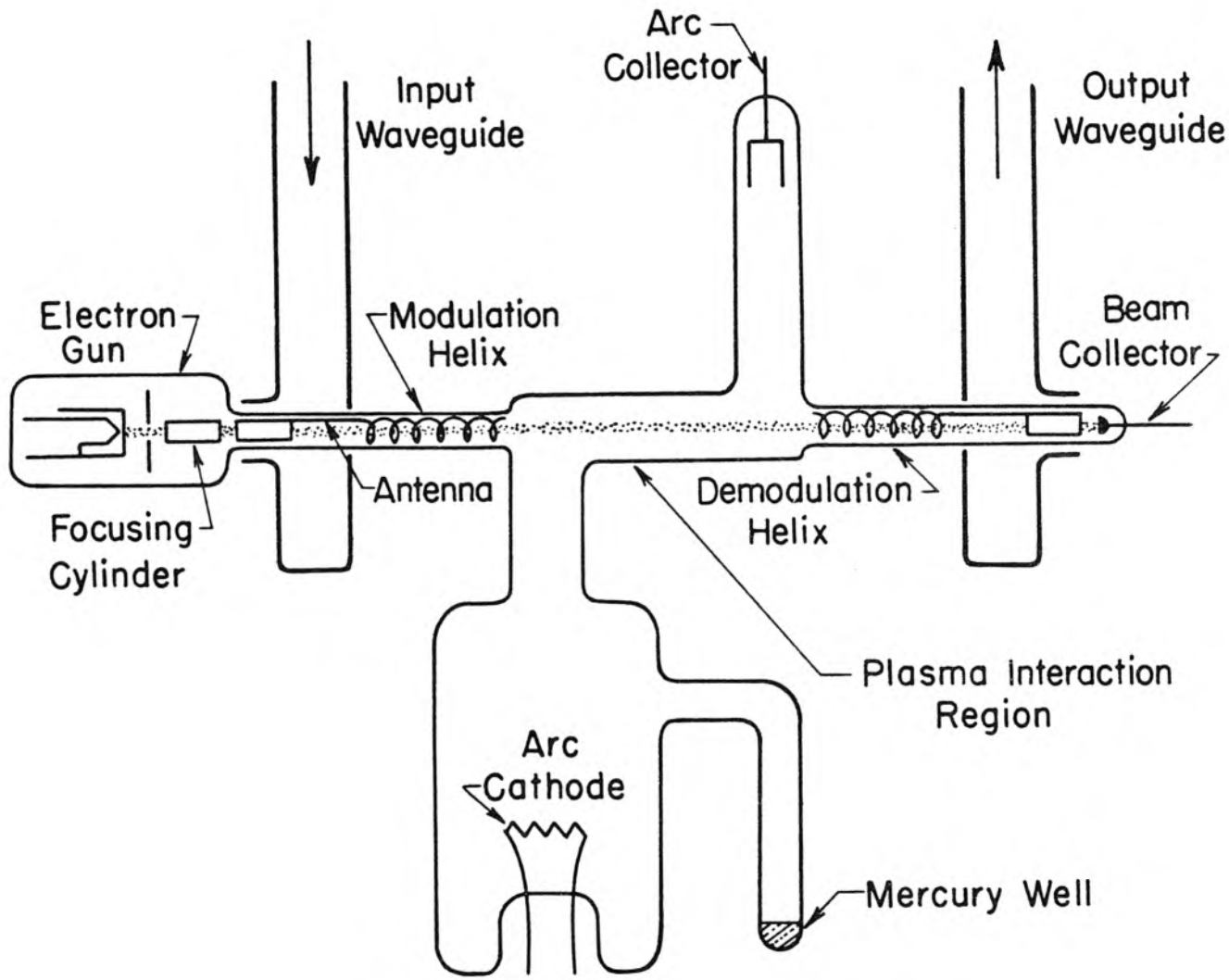

Figure 1.1 Helix Modulation Experiment

With this device experimental verification has been obtained of spatially growing waves in a plasma which is traversed by an electron beam. The growing wave results from the excitation of oscillations in the electron plasma by the electron beam and the interaction of the oscillating electrons back on the beam. In this mode of operation the plasma is a resonating structure as opposed to the form of operation to be described in the following section in which the plasma is a slow wave propagating structure.

The wave amplitude increases exponentially with distance along the beam and the rate of growth reaches a maximum when the excitation frequency, ω , on the electron beam is approximately equal to the plasma frequency ω_p . ω_p^2 is related to the electron plasma particle density n_o by $\omega_p^2 = n_o e^2/m\epsilon_o$, [Tonks and Langmuir (5)]. This thesis will present the theory of this device and the experimental performance.

1.2 Interaction of an Electron Beam with the Surface Slow Wave Propagating Mode of a Plasma Column

During the course of experiments on the above device of Section 1.1 an interaction of the electron beam with the plasma was obtained at a plasma frequency several times that of the excitation frequency on the beam. At the same time in this laboratory, Trivelpiece and Gould (33) were investigating newly found modes of propagation on a cylindrical plasma column. These propagating modes have a phase velocity which is small compared to the velocity of light. The propagating waves are electromechanical in nature and result from the interchange of kinetic energy of the electrons and the stored energy of the electric

field. These slow wave propagating modes have been studied in general by Trivelpiece and Gould with an axial magnetic field. In the special case of no magnetic field there is no charge accumulation within the plasma column, only at the surface of the plasma. The electric fields of this propagating wave are strongest at the surface of the plasma column and are therefore referred to as Surface Waves by Trivelpiece and Gould.

If an electron beam is made to pass along the axis of such a plasma column with its velocity coincident with the phase velocity of the surface wave of propagation, then by familiar traveling wave tube theory [see J. R. Pierce and L. M. Field (34), for a physical description of traveling wave interaction], one should expect spatially growing waves to exist on the system consisting of the electron beam and the slow wave circuit. Such an interaction of an electron beam with the surface wave was observed in the device of Figure 1.1, as well as the interaction at the plasma frequency (that is, when the excitation frequency ω equals ω_p).

To investigate more completely the interaction with the surface wave, however, the tube of Figure 1.1 had severe limitations in that the beam velocity was fixed because of the modulation scheme of using helices and the beam did not pass sufficiently close to the surface of the column to give a strong interaction with the electric fields of the surface wave. Since the phase velocity of the surface wave can be varied by changing the ratio of ω/ω_p (excitation frequency to plasma frequency), it was felt desirable to investigate the surface wave interaction with an electron beam over a range of velocities. The experimental tube of Figure 1.2 was constructed in which the electron

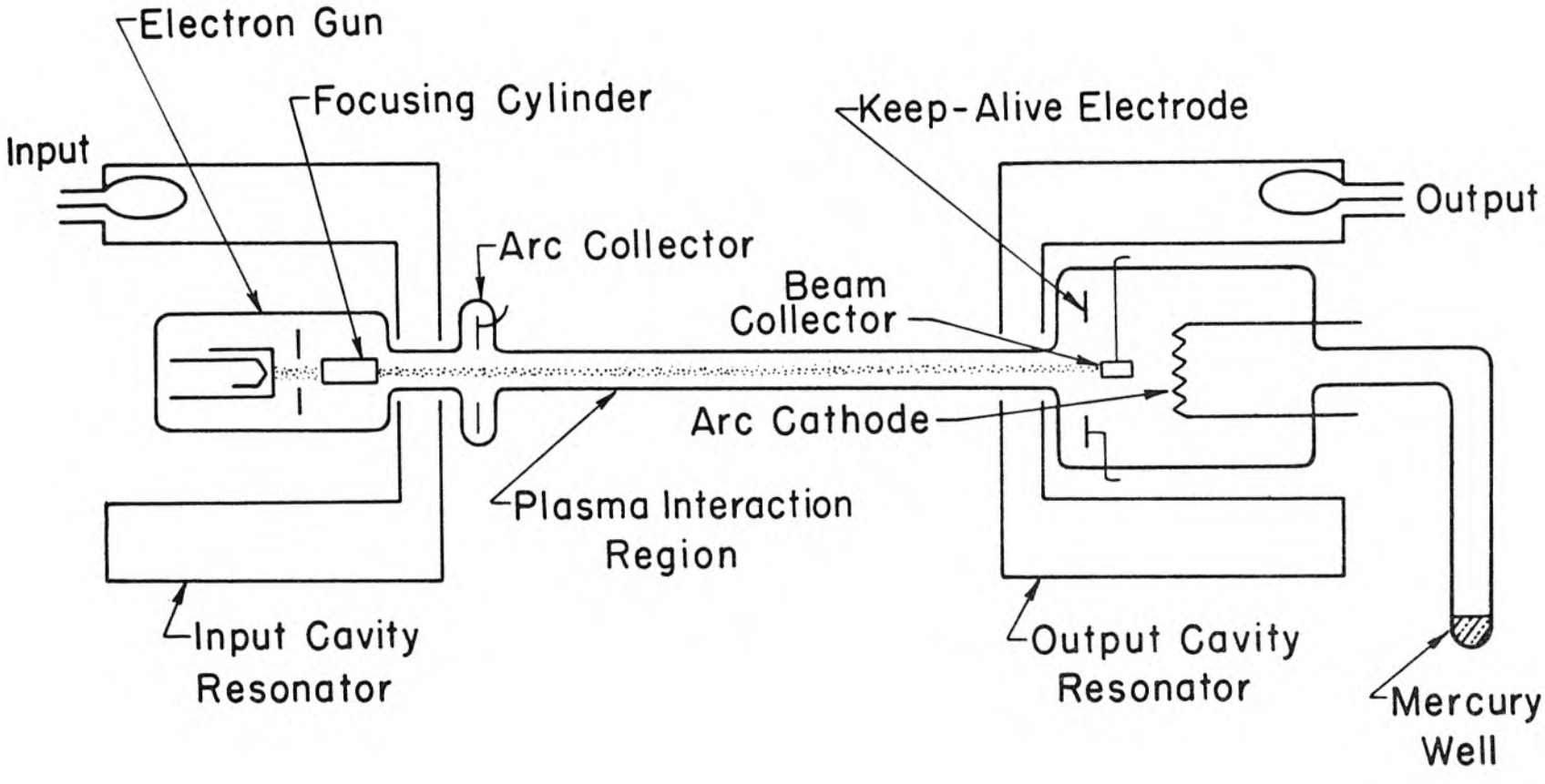

Figure 1.2 Cavity Modulation Experiment

beam is modulated by a resonant cavity. Thus, as opposed to the device of Figure 1.1, the modulation frequency is now fixed but the beam velocity is variable and can be adjusted to synchronism with the phase velocity of the surface wave on the plasma column.

This paper will present experimental data on the operation of this device with a simple description of its theory.

2. INTERACTION OF A MODULATED ELECTRON BEAM WITH A PLASMA MEDIUM NEAR THE PLASMA RESONANCE FREQUENCY

2.0 Definition of a Plasma and Elementary Properties

For the purposes of this paper a plasma will be considered to be a partially ionized gas which is neutral over distances greater than the Debye shielding distance (35). The positive ions of this plasma will be considered to be infinitely massive compared to that of the plasma electrons. This is because only the high frequency properties of the plasma will be under investigation and, under such circumstances, the ions can be considered to be relatively fixed in position, while the electrons oscillate back and forth around such fixed positive charges under the action of external alternating electric fields.

The plasma will have an average electron charge density $\rho_o = -n_o e$ where n_o is the number density of electrons per cubic meter. As the plasma is neutral, the ion charge density will be equal and of opposite sign $-\rho_o$. Since the plasma electrons are in a continuous thermal motion, they have a certain random energy which is often characterized by an equivalent kinetic temperature. The plasma electrons will experience two types of collisions, one being collisions with other particles in the gas (un-ionized gas atoms and ions), and the other being with the walls of the container. In a later section the effects of collisions will be estimated.

In this paper the small-signal sinusoidally time-dependent interaction of an electron beam, modulated at an angular frequency ω, passing through a plasma of plasma frequency ω_p, will be considered. This problem can be approached from either a microscopic or a macroscopic

point of view. In the former case the perturbation in the distribution function for the velocity distribution is obtained, and from this such quantities as the perturbation current density in the plasma are obtained by integrating over all velocity classes. This is the point of view adopted by Bohm and Gross (11). In the latter point of view one obtains the first two moments of the Boltzmann equation which results in the continuity equation and the momentum transport equation. These are then linearized to obtain the small signal perturbation particle density and average velocity. This point of view is used by Spitzer (35) but will not be used here.

Plasma oscillations at the plasma frequency ω_p do not depend on the boundary conditions on the plasma. Such oscillations are independent of the wavelength of the disturbance in a cold plasma and the displacement current and convection current just cancel. Therefore, these plasma oscillations do not give rise to a time varying magnetic field. Thus the electric fields associated with such oscillations may be derived from a scalar potential. It is straightforward to show that the high frequency properties of a cold plasma are mathematically equivalent to a charge-free medium with a relative dielectric constant given by

$$\frac{\epsilon}{\epsilon_o} = 1 - \frac{\omega_p^2}{\omega^2} \quad . \tag{2.0.1}$$

Plasma oscillations also exist at frequencies different from ω_p which depend on boundary conditions. For example, a plasma column in free space, excited by a transverse electric field into dipole oscillations has a normal mode of oscillation

$$\omega_p^2/\omega^2 = 2 \quad . \tag{2.0.2}$$

Such oscillating modes depending on the geometry of the plasma, have been termed "Plasma resonance" by Herlofson (36). In Section 5.1 this resonance condition is used to measure the plasma density of a cylindrical plasma column. In Appendix 1, equation 2.0.2 is derived for the more general case of a cylindrical plasma column surrounded by a layer of glass.

2.1 One-Dimensional Theory of Interaction by the Distribution Function Method Including the Random Energy of the Plasma Electrons

Bohm and Gross (11) have derived a dispersion relation for a one-dimensional electron beam passing through a one-dimensional stationary plasma including the effect of the random distribution of velocities of the plasma electrons. The effect of short range collisions of the plasma electrons is approximately accounted for by the inclusion of the collision frequency ν. Collisions of the beam electrons are ignored. This is reasonable if one visualizes a beam electron collision as removing it from the beam and therefore merely reducing the beam current by some appropriate amount. Plasma electron collisions, on the other hand, tend to damp out plasma oscillations and must be included in some approximate way. In the following expressions all waves are assumed to have a spatial and time dependence of $e^{i(\omega t-\gamma z)}$. γ is the complex propagation constant and will often be written as $\gamma = \beta - i\alpha$ where β and α are real. If the wave grows with distance, α is negative. If the wave propagates with constant amplitude, then $\alpha = 0$ and $\gamma = \beta$. The electron beam has a particle density n_b and thus one may define a beam plasma frequency

$\omega_b^2 = n_b e^2 / m\epsilon_o$. The random distribution of velocities of the electron beam about their mean velocity v_b is neglected. This is valid since the beam electrons come from a hot cathode (1000^oC) and thus have approximately .1 ev of random energy which is small compared to the random energy of the plasma electrons, i.e., of the order of 4 ev. The electron beam voltage in the first experiment is 400 volts which is large compared to both random energies. The plasma electron particle density of n_o is an order of magnitude greater than n_b in the experiments to be performed. The plasma frequency of the "plasma medium" is, of course, $\omega_p^2 = n_o e^2 / m\epsilon_o$.

With this definition of terms the one-dimensional dispersion relation is written (see Appendix 2)

$$1 = \omega_p^2 \frac{(\omega - i\nu)}{\omega} \int_{\underline{u}} \frac{f_o(\underline{u})\, d\underline{u}}{(\omega - \gamma u_z - i\nu)^2} + \frac{\omega_b^2}{(\omega - \gamma v_b)^2} \qquad (2.1.1)$$

where $f_o(\underline{u})$ is the unperturbed distribution function of velocities of the plasma electrons and by $d\underline{u}$ is meant $du_x du_y du_z$. Since an ionized gas has a Maxwellian velocity distribution (1) for the plasma electrons, one may write

$$f_o(\underline{u}) = \left(\frac{m}{2\pi\, kT}\right)^{3/2} e^{-\frac{m}{2kT}(u_x^2 + u_y^2 + u_z^2)} \qquad (2.1.2)$$

where T is the equivalent "temperature" of the plasma electrons; $\underline{u}$ is their random velocity vector. The distribution function in velocity space is normalized as

$$\int_{\underline{u}} f_o(\underline{u})\, d\underline{u} = 1 \quad . \qquad (2.1.3)$$

Substituting equation 2.1.2 into equation 2.1.1, one may evaluate, as does Sumi (24), for the case of $\nu = 0$ (indenting properly around the pole as determined by $\nu \neq 0$) and obtain a function of the error integral of imaginary argument. To be useful for computational purposes, however, this must then be expanded in an asymptotic series and the first few terms taken. The resulting series expression is found to be identical with that obtained by simply expanding the denominator of the integral in equation 2.1.1 in a power series in u_z and integrating term by term. For the purposes of this paper the simpler method will be used. Define the following

$$R = \frac{\frac{1}{2} m v_b^2}{\frac{3}{2} kT} \qquad \Gamma = \frac{\gamma v_b}{\omega} \tag{2.1.4}$$

R is the ratio of the beam electron energy to the average random energy of the plasma electrons. For the experiment of Section 1.1 it will be seen in Section 4.0 that a reasonable value is $R \approx 100$. The complex quantity Γ is the ratio of the propagation constant of the space charge waves to the electronic wave number (ω/v_b) of the electron beam. Thus Γ is a normalized propagation constant and will have a magnitude for reasonable parameters between 1 and 2.

If one integrates over the random velocity components u_x, u_y, u_z after expanding the denominator in equation 2.1.1, one obtains for the dispersion relation

$$1 = \frac{(\omega_p/\omega)^2}{1 - i\frac{\nu}{\omega}} \left\{ 1 + \frac{\Gamma^2}{R(1 - i\frac{\nu}{\omega})^2} + \frac{5}{3} \frac{\Gamma^4}{R^2(1 - i\frac{\nu}{\omega})^4} + \cdots \right\} + \frac{(\omega_b/\omega)^2}{(\Gamma - 1)^2} \quad (2.1.5)$$

In this expression, neglecting collisions, there is a range of parameters over which the normalized propagation constant Γ is complex and a range in which it is real.

Equation 2.1.5 has been solved numerically for a wide range of values applicable to the experiment neglecting collisions. For the special case of $\omega = \omega_p$ some results are given including collisions of the plasma electrons.

One needs only to take the first two terms of the above series for the experimental situation of this paper since $R \approx 100$. Neglecting collisions, equation 2.1.5 becomes

$$1 = \left(\frac{\omega_p}{\omega}\right)^2 \left(1 + \frac{\Gamma^2}{R}\right) + \frac{(\omega_b/\omega)^2}{(\Gamma - 1)^2} \quad (2.1.6)$$

which is a fourth degree polynomial in Γ . This may be placed in a convenient form for computation with the definitions of

$$\sigma = R\left(\frac{\omega_b}{\omega_p}\right)^2 \quad (2.1.7)$$

$$\Lambda = R\left(1 - \frac{\omega^2}{\omega_p^2}\right) \quad (2.1.8)$$

Note that σ is proportional to the ratio of beam electron density to plasma electron density. With the above, one may write equation 2.1.6 as a function of two parameters

$$(\Gamma - 1)^2 (\Gamma^2 + \Lambda) + \sigma = 0 \quad . \quad (2.1.9)$$

If one were to include more terms of the series from equation 2.1.5 in equation 2.1.6 the propagation constant would be a function of three parameters, instead of two.

Equation 2.1.9 has been solved for the complex values of the normalized propagation constant over a range of parameters of σ and $\bigwedge$. These normalized results are presented in the complex γ plane in Figure 2.1. Note that equation 2.1.9 may be solved easily for $\omega = \omega_p$ ($\bigwedge = 0$) resulting in

$$\Gamma = \frac{1}{2} + \frac{1}{2}\sqrt{1 \mp 4i\sqrt{\sigma}} \approx 1 \mp i\sqrt{\sigma} \qquad \sigma \ll 1 \qquad (2.1.10)$$

In Figure 2.2 is shown the maximum value of the imaginary part, α, of γ versus σ. Also the real part, β, of γ corresponding to this maximum value of α is shown.

Inspection of Figure 2.1 reveals that the maximum value of the growth parameter in the range $.003 \leq \sigma \leq 3.0$ corresponds to $-1 \leq \bigwedge \leq +1$ approximately. Practically speaking, a low value of the ratio of electron beam energy to random plasma electron energy would be $R = 30$. The normalized frequency, ω/ω_p, at which the maximum growth parameter occurs corresponding to the above range of σ is in the range $1.016 \geq \frac{\omega}{\omega_p} \geq .983$. For larger values of R the ratio of modulation frequency to plasma frequency is even closer to unity. Therefore, one concludes that the maximum interaction occurs very close to $\omega/\omega_p = 1$.

It is interesting to note in Figure 2.1 that the maximum value of the growth constant α appears to shift from $\omega/\omega_p > 1$ for $\sigma < 1$ to $\omega/\omega_p < 1$ for $\sigma > 1$.

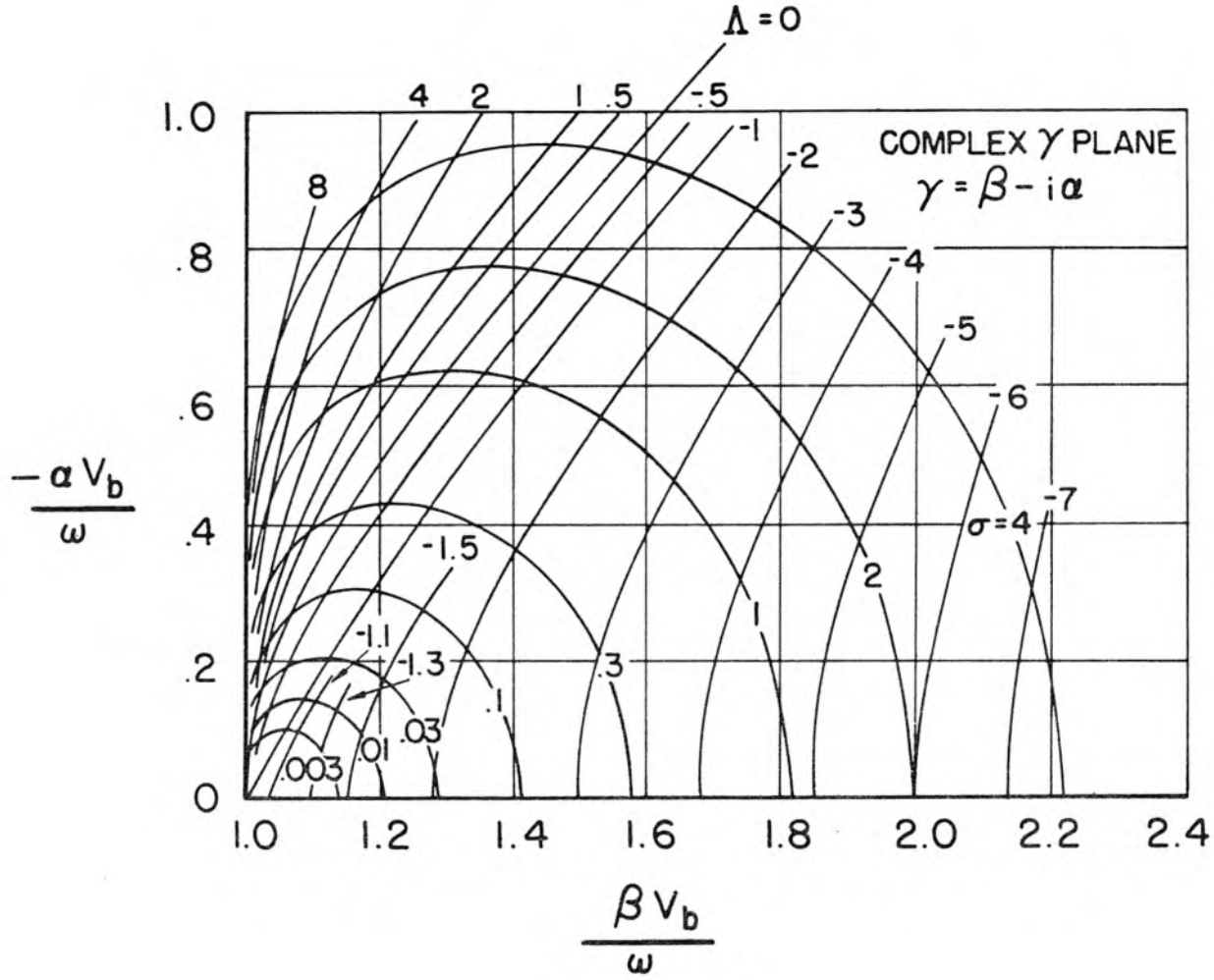

Figure 2.1 Solution of Equation 2.1.9 for the Complex Propagation Constant $\Gamma = \frac{\gamma v_b}{\omega} = \frac{\beta v_b}{\omega} - i\frac{\alpha v_b}{\omega}$ over a range of values of the parameters σ and Λ.

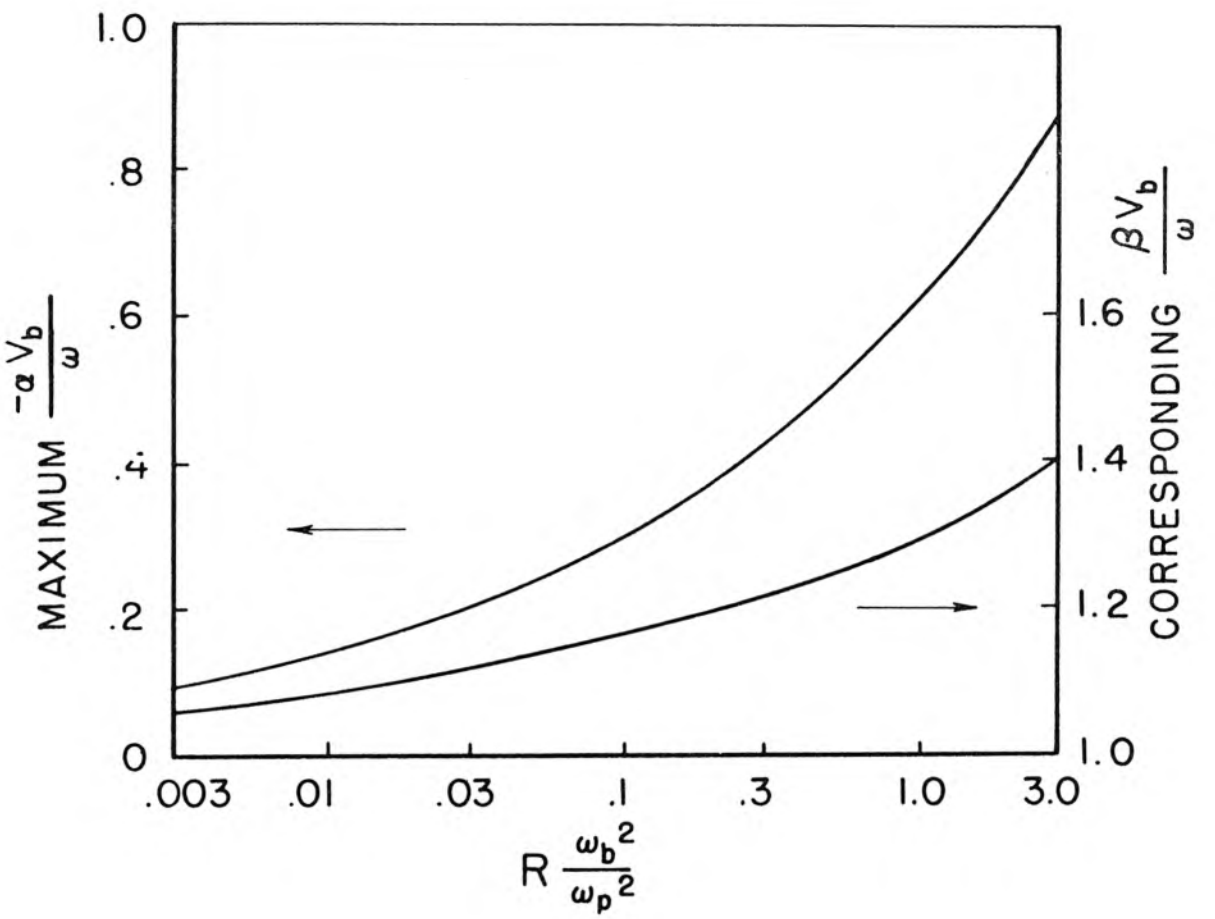

Figure 2.2 Maximum Growth Parameter as Obtained from Figure 2.1 versus a Quantity Proportional to the Ratio of the Beam Electron Density to the Plasma Electron Density.

The presentation of theoretical data that most closely corresponds to the way in which the experimental data is obtained is shown in Figure 2.3 in which the growth constant α is plotted versus ω_p^2/ω^2 for representative values of R and ω_b^2/ω_p^2. Note carefully the suppressed zero of the abscissa.

It is also of interest to estimate the reduction in gain due to collisions. Since the maximum growth constant is closely equal to that at $\omega = \omega_p$ ($\Lambda = 0$) for parameters of interest, it is reasonable to estimate the growth constant with collisions only at $\omega = \omega_p$. Thus from equation 2.1.5 one obtains, taking the first two terms in the series as before,

$$1 = \frac{1}{1 - i\frac{\nu}{\omega}} \left\{ 1 + \frac{\Gamma^2}{R(1 - i\frac{\nu}{\omega})^2} \right\} + \frac{(\omega_b/\omega)^2}{(\Gamma - 1)^2} \quad . \tag{2.1.11}$$

Under the approximation $\nu/\omega \ll 1$ and $\Gamma^2/R \ll 1$, one may neglect ν/ω in the second term of the bracket, as well as when it multiplies $(\omega_b/\omega)^2$. Therefore,

$$\Gamma \approx 1 \pm i \frac{\sqrt{R}\ (\omega_b/\omega)}{\sqrt{\Gamma^2 + iR\frac{\nu}{\omega}}} \quad . \tag{2.1.12}$$

Since this was derived with $\omega = \omega_p$, one may rewrite it as

$$\Gamma \approx 1 \pm i \frac{\sqrt{\sigma}}{\sqrt{\Gamma^2 + iR\frac{\nu}{\omega}}} \quad . \tag{2.1.13}$$

This may be solved by iteration, assuming as a zeroth approximation $\Gamma^2 = 1$ inside the square root.

For the experiments under discussion reasonable values are R = 100

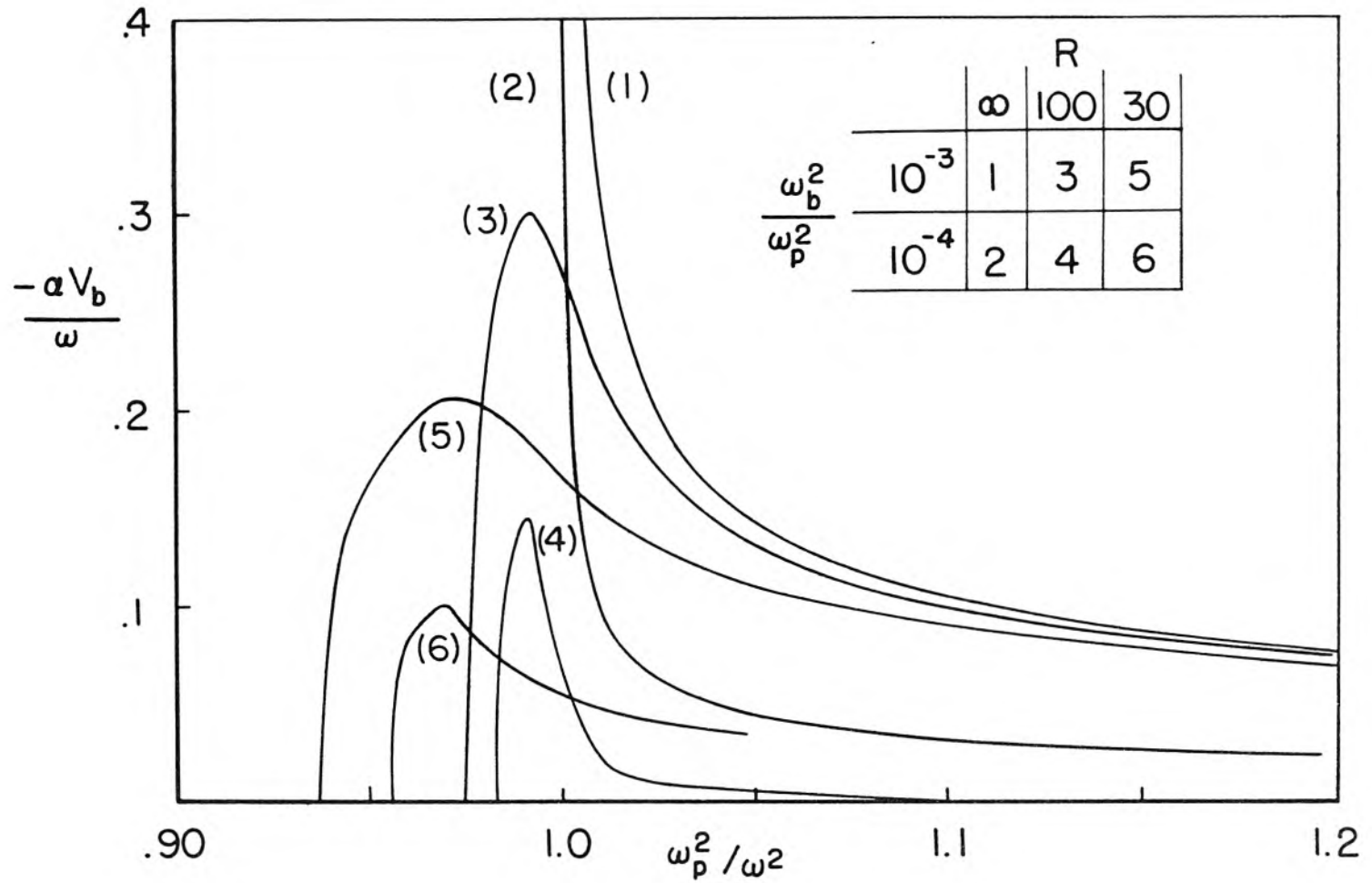

Figure 2.3 Growth Parameter α versus the Normalized Plasma Frequency Squared for Representative Values of R and ω_b^2/ω_p^2. R is the Ratio of the Electron Beam Energy to the Average Random Energy of the Plasma Electrons. ω_b^2/ω_p^2 is the Ratio of the Beam Electron Density to the Plasma Electron Density.

and $\omega_b^2/\omega_p^2 = 10^{-3}$. As will be seen later, in Section 4.0, two interesting values of the collision frequency are $\nu = 3\times10^7$ collisions per second and $\nu = 3\times10^8$ collisions per second. If one assumes $\omega = 2\pi$ (3000 Mc) then

$$\Gamma = 1.08 \pm i\ .265 \qquad \nu = 3\times10^7/\text{sec}$$

$$\Gamma = 1.103 \pm i\ .184 \qquad \nu = 3\times10^8/\text{sec}$$

compared with

$$\Gamma = 1.071 \pm i\ .277 \qquad \nu = 0$$

at $\omega = \omega_p$ from Figure 2.1 . The maximum growth constant for $\omega_b^2/\omega_p^2 = 10^{-3}$, R = 100 at $\omega/\omega_p = 1.0038$ (see Figure 2.3) is

$$\Gamma = 1.15 \pm i\ .30 \qquad \nu = 0 \quad .$$

In the polynomial equation for the propagation constant, equation 2.1.9, the coefficients are all real, implying that complex solutions of this equation come in complex conjugate pairs. By a previous definition the growth constant in nepers per unit length is $\alpha = \omega/v_b \mathrm{Im}(\Gamma)$. For the growing wave α is negative since waves have a spatial dependence of $e^{-\alpha z} e^{-i\beta z}$. The growth constant along the electron beam can then be written as $G = 8.68\alpha$ db per cm, if α is in nepers per cm.

2.2 Three-Dimensional Theory Neglecting the Random Energy of the Plasma Electrons

Plasma oscillations have been previously described as an oscillation of energy between that stored in an electric field and that stored

in the form of kinetic energy of the oscillating electrons. If in a plasma the wavelength of the disturbance is small compared to the free space wavelength corresponding to the frequency of this disturbance, then one may assume that the disturbance propagates at an infinite velocity instead of the velocity of light. This is called the quasi-static approximation and allows one to neglect the magnetic field associated with such disturbances. One may then derive the time varying potential of the electric field of such plasma oscillations as the negative gradient of a scalar. Poisson's equation relates the time varying potential and charge density

$$\nabla^2 \phi_1 = - \rho_1 / \epsilon_o \quad . \tag{2.2.1}$$

It should be pointed out that in the one-dimensional case analyzed in Section 2.1 no such quasi-static approximation is necessary. This is a result of there only being variation in the z direction ($e^{-i\gamma z}$) allowed, and hence only an electric field in the z direction. Then, since the direction of the propagation is parallel to the electric field, the curl of the electric field $\nabla \times \underline{E}_1 = -\gamma \underline{e}_z \times \underline{E}_1 = 0$. Thus there is no time varying magnetic field.

The three-dimensional problem that will be considered here is that of an electron beam of finite radius b passing through an infinite plasma medium. To solve this it will be necessary to compute the sum of the perturbation charge density from the electron beam and the electron plasma. Substituting this into equation 2.2.1 gives a determining differential equation. The random energy of the plasma electrons will be neglected.

To derive the perturbation charge density for a non-drifting plasma

one needs the linearized small signal continuity and force equations.

$$i\omega \rho_{1p} = -\nabla \cdot (\rho_o \underline{v}_{1p}) \tag{2.2.2}$$

$$i\omega \underline{v}_{1p} = -\frac{e}{m} \underline{E}_1 = +\frac{e}{m} \nabla \phi_1 \quad . \tag{2.2.3}$$

Solving for the small signal perturbation plasma charge density ρ_{1p}, one obtains

$$\frac{\rho_{1p}}{\epsilon_o} = +\frac{\rho_o e}{m\epsilon_o \omega^2} \nabla^2 \phi_1 = -\frac{\omega_p^2}{\omega^2} \nabla^2 \phi_1 \quad . \tag{2.2.4}$$

As an aside, notice that if there is only a plasma present, a combination of equations 2.2.4 and 2.2.1 results in the equivalent relative dielectric constant of a plasma as stated in equation 2.0.1 .

When a beam of radius b is present in the plasma, the perturbation charge density of the beam is obtained as above, remembering that the beam velocity vector v_b is in the z direction

$$i\omega \rho_{1b} = -\nabla \cdot (\rho_b \underline{v}_{1b} + \underline{v}_b \rho_{1b}) \tag{2.2.5}$$

$$\frac{d\underline{v}_{1b}}{dt} = \frac{\partial \underline{v}_{1b}}{\partial t} + (\underline{v}_b \cdot \nabla) \underline{v}_{1b} = i\underline{v}_{1b}(\omega - \gamma v_b) = +\frac{e}{m} \nabla \phi_1 . \tag{2.2.6}$$

Note that for convenience the gradient in the z direction is sometimes taken as $-i\gamma$ times the quantity since it was previously assumed that only solutions with z dependence $e^{-i\gamma z}$ were to be allowed. Combining equations 2.2.5 and 2.2.6 one obtains

$$\frac{\rho_{1b}}{\epsilon_o} = +\frac{\rho_b e}{m\epsilon_o (\omega - \gamma v_b)^2} \nabla^2 \phi_1 = \frac{-\omega_b^2}{(\omega - \gamma v_b)^2} \nabla^2 \phi_1 \quad . \tag{2.2.7}$$

Then by superposition $\rho_1 = \rho_{1p} + \rho_{1b}$ which, if substituted into equation 2.2.1 and rewritten slightly, becomes

$$\nabla \cdot \left\{ 1 - \frac{\omega_p^2}{\omega^2} - \frac{\omega_b^2}{(\omega - \gamma v_b)^2} \right\} \nabla \phi_1 = 0 \qquad (2.2.8)$$

as the appropriate differential equation inside the beam and plasma region. In the region where there is just plasma alone, one sets $\omega_b = 0$.

Note that equation 2.2.8 is written in the form $\nabla \cdot \underline{D}_1 = 0$ where $\underline{D}_1$ is the mathematical quantity in the bracket. In this form the applicable boundary condition at the interface between the region containing plasma alone and plasma plus beam, is obvious. That is, the normal component of the quantity $\underline{D}_1$ is continuous between regions. The other necessary boundary condition is that the potential be continuous.

The solutions to equation 2.2.8 are either

$$\left\{ 1 - \frac{\omega_p^2}{\omega^2} - \frac{\omega_b^2}{(\omega - \gamma v_b)^2} \right\} = 0 \qquad r \leq b \qquad (2.2.9)$$

or

$$\nabla^2 \phi_1 = 0 \qquad 0 \leq r \leq \infty \quad . \qquad (2.2.10)$$

The former case, equation 2.2.9, is identical to that of equation 2.1.6, neglecting the random energy. This represents the one-dimensional solution and is independent of beam radius. Note that in the one-dimensional case $\nabla^2 \phi_1 \rightarrow -\gamma^2 \phi_1$. Clearly for waves to exist $\phi_1 \neq 0$ and hence equation 2.2.9 must apply. Equation 2.2.9 corresponds to that derived by Pierce (27) except that he was considering the interaction of beam electrons with ions. The solution of equation 2.2.9 is

$$\Gamma = 1 \pm i \frac{\omega_b}{\omega_p} \frac{1}{\sqrt{1 - \frac{\omega^2}{\omega_p^2}}} \qquad (2.2.11)$$

where Γ is the normalized propagation constant defined by equation 2.1.4 . Equation 2.2.11 is plotted in Figure 2.3 under the designation of $R = \infty$.

In the three-dimensional case of an electron beam of radius b passing through an infinite plasma medium, the appropriate solutions are obtained from equation 2.2.10 . Note that equation 2.2.10 implies that $\rho_{1b} = \rho_{1p} = 0$. This means that the electron beam has no density modulation, only a "rippled boundary" form of modulation at $r = b$ which is the interface between the two regions. Another way to see this is to realize that for the modulation schemes used in the experiments of this thesis--that is, a gridless cavity or a helix--the modulation fields are derived from Laplace's equation. Thus $\nabla \cdot \underline{E}_1 = 0$ and from the force equation 2.2.6 on an electron beam the velocity is divergenceless $(\nabla \cdot \underline{v}_{1b}) = 0$. This and the continuity equation 2.2.5 clearly states that $\rho_{1b} = 0$.

It is apparent that in the experiments presented here the modulated electron beam is "ripple boundary" modulated and not density modulated. An electron beam can be density modulated only by a gridded cavity in which Poisson's equation is applicable rather than Laplace's. The difference between these two types of modulation will have no qualitative effect on the experimental results and only a minor quantitative one.

The solutions to equation 2.2.10 for no angular dependence of the fields are

$$\phi_1 = \frac{I_o(\gamma r)}{I_o(\gamma b)} e^{-i\gamma z} \qquad 0 \leq r \leq b$$

$$\phi_1 = \frac{K_o(\gamma r)}{K_o(\gamma b)} e^{-i\gamma z} \qquad b \leq r \leq \infty \tag{2.2.12}$$

where we require the potential to be finite at the origin and zero at infinity, as well as continuous at $r = b$. Matching the boundary condition on the normal component of $\underline{D}_1$ as given above, one obtains the determinantal equation for a finite size electron beam in an infinite plasma.

$$1 = \frac{\omega_p^2}{\omega^2} + \frac{(\omega_b')^2}{(\omega - \gamma v_b)^2} \tag{2.2.13}$$

where

$$\left(\frac{\omega_b'}{\omega_b}\right)^2 = \frac{1}{1 + \dfrac{I_o(\gamma b)K_1(\gamma b)}{I_1(\gamma b)K_o(\gamma b)}} \quad . \tag{2.2.14}$$

Clearly the only quantitative effect in equation 2.2.13 compared to equation 2.1.6 neglecting the random energy of the plasma electrons, is to replace the electron beam plasma frequency ω_b by a "reduced" beam plasma frequency ω_b' . Note, though, that γ in equations 2.2.13 and 2.2.14 is complex over a certain range of values of (ω/ω_p) but as a reasonable approximation over part of this range [excluding the region where $\mathrm{Im}(\gamma) \gtrsim \mathrm{Re}(\gamma)$] γ in equation 2.2.11 is replaced by the electronic wave number ω/v_b . For $\omega b/v_b \approx 2.5$ as is typical for the experiments in this paper, $(\omega_b'/\omega_b)^2 = .39$. The significant point is, however, that in the one-dimensional limit of $b \to \infty$,

$(\omega_b'/\omega_b)^2 \rightarrow .5$, not 1, which would be expected from the previous one-dimensional treatment. This result is due to the difference between "rippled boundary" modulation and density modulation.

The finite geometry problem including the effects of the random energy of the plasma electrons is quite difficult due to the complexity of the boundary conditions. Also, one cannot easily solve the Boltzmann equation in three dimensions and one is thus forced to use the first two moments of the Boltzmann equation to include the effects of the random energy of the plasma electrons. As an approximation it is assumed that one may take the one-dimensional dispersion relation of 2.1.5 and replace the beam plasma frequency by the reduced beam plasma frequency of 2.2.14. This results in an approximate dispersion relation, including the random energy and collisions of the plasma electrons, for a finite diameter beam in an infinite plasma.

Bohm and Gross' analysis considers one-dimensional disturbances in which there is a density modulation on an electron beam. For the experiments performed in this thesis there is no density modulation in the interior of the beam, but instead there is a rippling of the beam boundary associated with the disturbance. However, the above analysis demonstrates that the dispersion relation for a finite diameter beam can be cast in the same form as obtained by Bohm and Gross when a suitable reduced beam plasma frequency is defined. It is of interest to note that if the electron beam were immersed in an infinite axial magnetic field there would actually be a density modulation. For a finite axial magnetic field both rippled boundary and density modulations would be set up. For the experiments of this thesis no axial magnetic fields are used.

3. INTERACTION OF A MODULATED ELECTRON BEAM WITH THE SLOW WAVE SURFACE MODE OF PROPAGATION ON A PLASMA COLUMN

3.0 Slow Wave Mode of Propagation

Consider a cylinder of non-drifting plasma of radius a filling a glass tube of outer radius c. This glass tube will be considered both in free space and when covered by a conducting layer at its surface of radius c. The random energy of the plasma electrons will be neglected as will collisions. Also, there is no constant magnetic field present.

Trivelpiece and Gould (33) have shown that such a plasma column will propagate a slow electromechanical wave with a phase velocity small compared to the velocity of light. The energy on such a wave oscillates back and forth between the stored energy of the electric field and the kinetic energy of the plasma electrons.

The physical existence of such waves can easily be understood by analogy with the equivalent circuit of a transmission line. A distributed transmission line can be represented by inductance in the longitudinal direction and capacitance in the transverse direction. As was seen in equation 2.0.1, a plasma may be replaced by a charge free medium of relative dielectric constant $(1 - \omega_p^2/\omega^2)$. Therefore, if the frequency ω is less than the plasma frequency ω_p, the displacement current $\partial \underline{D}_1/\partial t = i\omega\epsilon_o(1 - \omega_p^2/\omega^2)\underline{E}_1$ lags the electric field vector $\underline{E}_1$ and the medium appears inductive. Free space is obviously capacitive, however, since the displacement current leads the electric field. If one visualizes a plasma column in free space and $\omega < \omega_p$, then it is inductive in the longitudinal and transverse directions.

But since the column is assumed to be of finite size, one must add in series to this transverse inductance, the capacitance of free space from the edge of the column to infinity. This capacitance can be sufficient to cause the net impedance in the transverse direction to be capacitive and therefore the plasma column in free space appears as a transmission line capable of propagation.

It has been shown (33) that the propagation characteristics of these electromechanical modes are derivable from the quasi-static approximation. In this approximation the perturbation magnetic field is neglected compared to the perturbation electric fields, as long as the phase velocity of such modes is small compared to the velocity of light.

In the quasi-static approximation, the potential satisfies Laplace's equation. As a simple example, consider the two-region case in which the glass tube has a conducting surface at $r = c$. Waves are assumed to vary as $e^{i(\omega t - n\theta - \beta z)}$. Since the propagation characteristics of a plasma column are to be analyzed in the absence of an electron beam, it is clear that the propagation constant will be real, neglecting loss in the plasma and therefore β is used instead of γ.

The time varying potential in each region is given by

$$\phi_1 = \frac{I_n(\beta r)}{I_n(\beta b)} e^{-i(n\theta+\beta z)} \qquad r \leq a$$

$$\phi_1 = \frac{I_n(\beta r)\, K_n(\beta c) - I_n(\beta c)\, K_n(\beta r)}{I_n(\beta a)\, K_n(\beta c) - I_n(\beta c)\, K_n(\beta a)} e^{-i(n\theta+z)} \qquad a \leq r \leq c \,, \quad (3.0.1)$$

where the $e^{i\omega t}$ dependence is assumed.

In the above expressions the potential is finite at the origin, continuous at the plasma-glass interface $r = a$, and zero at the glass-conducting surface interface $r = c$. The remaining boundary condition

to be applied is the continuity of the normal displacement vector at $r = a$ using 2.0.1 for the plasma dielectric and κ for the relative dielectric constant of the glass. One then obtains

$$\left(1 - \frac{\omega_p^2}{\omega^2}\right) \frac{1}{\kappa} = \frac{I_n(\beta a)}{I_n'(\beta a)} \left\{ \frac{I_n'(\beta a)\, K_n(\beta c) - I_n(\beta c)\, K_n'(\beta a)}{I_n(\beta a)\, K_n(\beta c) - I_n(\beta c)\, K_n(\beta a)} \right\} \qquad (3.0.2)$$

where the primes represent the total derivatives of the Bessel functions with respect to the argument. A curve of ω/ω_p versus βa gives the frequency versus propagation constant of these slow surface wave modes of propagation. The phase velocity of such waves is given by ω/β and the group velocity by $\partial\omega/\partial\beta$. The large βa asymptotic frequency of propagation is easily obtainable from equation 3.0.2 as

$$\frac{\omega}{\omega_p} = \frac{1}{\sqrt{1+\kappa}} \quad . \qquad (3.0.3)$$

The dashed curves of Figure 3.1 represent such a plot corresponding to the glass tube used in the cavity modulation experiment of Figure 1.2. In Figure 3.1 it should be noticed that the curves for the angularly independent $(n = 0)$ and the first dependent mode $(n = 1)$ are given. The nearly horizontal dashed curve represents the $n = 1$ mode. For the tube of Figure 1.2 the ratio of the outer radius to the inner radius of the glass is $c/a \approx 1.5$. The glass dielectric constant is $\kappa = 4.60$.

The interaction of interest in this paper is of the electron beam with the angularly independent $(n = 0)$ mode. The curve of the first angular dependent mode is included for pedagogical reasons as well as to illustrate, as shall be seen in Section 6.2, that certain anomalous

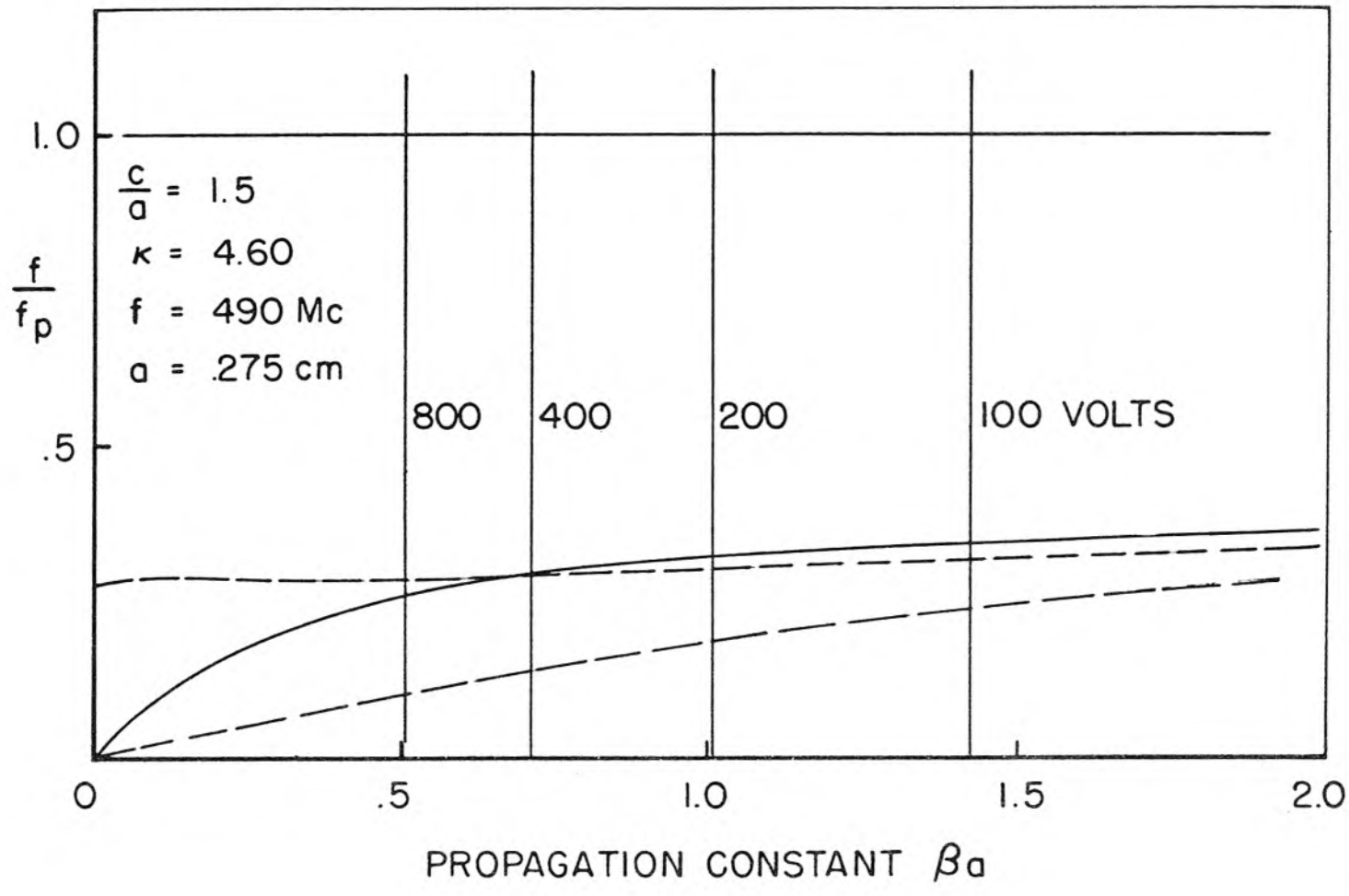

Figure 3.1 Normalized Frequency versus Propagation Constant for the Surface Wave Mode of Propagation on a Plasma-Glass Column in Free Space (Solid Curve) and when Covered with a Conducting Surface (Dashed Curves). For the Latter Case the Upper Dashed Line Represents the n=1 Mode and the Lower Dashed Line the n=0 Mode. The Dimensions Correspond to the Cavity Modulation Tube of Figure 1.2 .

results cannot be explained in terms of interaction with this angularly dependent mode.

The solid curve of Figure 3.1 is for the plasma-glass column in free space. Only the angularly independent $(n = 0)$ mode of propagation is plotted for this case. The vertical lines labeled 800, 400, 200, and 100 volts correspond to constant phase velocity lines at a fixed frequency f. The intersection of these curves with any of the propagation constant curves specifies the operating point at which the electron beam velocity is in synchronism with the phase velocity of the surface wave. According to traveling wave tube theory (30) this is the point of maximum interaction and therefore maximum output signal level. The ω-β curves of Figure 3.1 are dimensionless and apply to any plasma filled glass tube of the given ratio of outer to inner radii and glass dielectric constant. The phase velocity voltage lines apply only for the fixed frequency $f = 490$ Mc and plasma radius $a = .275$ cm, as is appropriate for the experiment performed in this thesis.

If one does not coat the glass tube with a conducting surface at $r = c$, but lets it remain in free space, then the problem is a three-region one of plasma $(r \leq a)$, glass $(a \leq r \leq c)$ and free space $(c \leq r < \infty)$. The propagation characteristics of such a system is obtainable by an analysis as above with an increase in algebraic complications. The determinantal equation for the propagation constants of the angularly independent mode $(n = 0)$ is

$$\left(1 - \frac{\omega_p^2}{\omega^2}\right) \frac{I_1(\beta a)}{I_o(\beta a)} = \frac{-\kappa}{\text{becoth}(\beta c, \beta a)} \cdot \frac{\kappa + \dfrac{K_1(\beta c)}{K_o(\beta c)} \quad \dfrac{1}{\text{betanh}(\beta c, \beta a)}}{\kappa + \dfrac{K_1(\beta c)}{K_o(\beta c)} \quad \text{Betanh}(\beta c, \beta a)} \qquad (3.0.4)$$

where the functions

$$\text{becoth}(\beta c,\beta a) = \frac{I_1(\beta c)\, K_o(\beta a) + I_o(\beta a)\, K_1(\beta c)}{I_1(\beta c)\, K_1(\beta a) - I_1(\beta a)\, K_1(\beta c)}$$

$$\text{betanh}(\beta c,\beta a) = \frac{I_1(\beta c)\, K_1(\beta a) - I_1(\beta a)\, K_1(\beta c)}{I_o(\beta c)\, K_1(\beta a) + I_1(\beta a)\, K_o(\beta c)} \qquad (3.0.5)$$

$$\text{Betanh}(\beta c,\beta a) = \frac{I_o(\beta c)\, K_o(\beta a) - I_o(\beta a)\, K_o(\beta c)}{I_1(\beta c)\, K_o(\beta a) + I_o(\beta a)\, K_1(\beta c)}$$

are defined and tabulated by Birdsall (37).

For the above described glass tube in free space, the propagation frequency curve (ω-β diagram) is plotted as the solid line in Figure 3.1. This curve will be of the greatest interest since normally the tube of Figure 1.2 was operated in free space, though a comparison of experimental data obtained in free space against that obtained with a conducting coating on the tube will be made.

One will notice in Figure 3.1 that a horizontal line is drawn at $\omega/\omega_p = 1$. This corresponds to plasma oscillations discussed previously (neglecting the random energy). The fact that the frequency versus propagation constant diagram is a horizontal straight line coincides with the understanding of plasma oscillations at $\omega = \omega_p$ being independent of the wavelength of the disturbance.

3.1 Interaction Impedance and Estimation of Growth Constant

An electron beam traveling in synchronism with the previously described slow surface wave will interact with the axial electric field of said wave. Under these conditions, a spatially growing wave will result (that is, the propagation constant is complex) in an increasing

amount of radio-frequency energy on the electron beam. This energy results from the conversion of the beam kinetic energy into time dependent fields. Thus the electron beam will slow down slightly as the perturbation wave grows.

The plasma column alone is bilateral, meaning that the surface wave may travel in either direction. In the presence of an electron beam the wave traveling against the electron motion is little affected. The surface wave traveling in the direction of the electron beam plus the fast and slow space charge waves on the electron beam interact and can be described in terms of three waves. For a lossless plasma column, one of these forward waves is attenuated, one is unattenuated, and the third increases in amplitude as it travels; that is, it has negative attenuation. On the average, the electrons travel slightly faster than the phase velocity of the growing wave.

Pierce and Field (34) have compared the situation to one of a breeze blowing past ripples in a stream. The ripples grow larger as the breeze blows them along.

Pierce (30) has shown that an approximate value of the growth constant can be calculated in terms of an interaction impedance defined by

$$Z_o = \frac{E_{1z}^2(0)}{2\gamma^2 \overline{P}_z} \quad . \tag{3.1.1}$$

$E_{1z}(0)$ is the z directed perturbation electric field on the axis and $\overline{P}_z$ is the average z directed power flow of the surface wave in question. In the simplified thin beam analysis the electron beam is assumed to be concentrated on the axis and the space charge effects of

the beam will be neglected. The traveling wave tube interaction parameter C is defined by

$$C^3 = \frac{Z_o I_b}{4V_b} \tag{3.1.2}$$

where I_b and V_b are the electron beam current and voltage. The maximum value of the growth constant can be shown to occur at synchronism between the electron beam velocity and phase velocity of the surface wave. At synchronism the growth constant is given by

$$G = \frac{47.3C}{\lambda_e} \text{ db per cm} \tag{3.1.3}$$

where λ_e is the electronic wavelength in centimeters on the electron beam and is given by

$$\lambda_e = \lambda \frac{v_b}{c} = \frac{2\pi}{\beta} \quad . \tag{3.1.4}$$

In equation 3.1.4 the quantity λ is the free space wavelength corresponding to the frequency of modulation on the electron beam and v_b/c is the ratio of the electron beam velocity to the velocity of light.

To compute the growth constant corresponding to the interaction of an electron beam on the axis of a plasma column of radius a in a glass tube of radius c surrounded by free space, the propagation diagram of such a situation is shown by the solid curve of Figure 3.1, it is necessary to obtain the interaction impedance of equation 3.1.1 which in turn requires the power flow in the z direction. To compute the power flow in this three-region propagating system is somewhat

complex. As a simplification, the power flow will be computed for the two-region problem of a plasma column surrounded by dielectric medium extending to infinity. For small values of the normalized propagation constant βa, the electronic wavelength λ_e in equation 3.1.4 is long compared to the thickness of the glass walls $(c - a)$ of the tube and hence the fields see predominately free space outside of the plasma. For large values of βa the wavelength of the fields on the plasma column are much less than the glass thickness and hence as a fair approximation the surrounding medium to the plasma column appears as a glass dielectric. In the experiment of this paper, the beam velocity can be varied such that $.5 \leq \beta a \leq 1.5$. Since $c/a = 1.5$, clearly $1/8\pi \leq (c - a)/\lambda_e \leq 3/8\pi$. Therefore, the plasma column appears to be in free space.

In the two-dimensional problem the surface wave fields may be written

$$\begin{aligned} E_{1z} &= E_{1z}(0)\, I_o(\beta r) \qquad 0 \leq r \leq a \\ E_{1z} &= E_{1z}(0)\, \frac{I_o(\beta a)}{K_o(\beta a)}\, K_o(\beta r) \qquad a \leq r < \infty \end{aligned} \tag{3.1.5}$$

where $E_{1z}(0)$ is a constant representing the axial electric field strength. The power flow in the z direction for the angularly independent surface wave mode $(n = 0)$ is

$$\bar{P}_z = \frac{1}{2}\mathrm{Re}\int_{\text{Surface}} (\underline{E}_1 \times \underline{H}_1^*)\cdot \underline{dS} = \pi \int_0^\infty E_{1r}\, H_{1\theta}^*\, r\,dr \quad . \tag{3.1.6}$$

The radial electric field is obtained from the axial electric field as $E_{1r} = \frac{i}{\beta}\frac{\partial E_{1z}}{\partial r}$. It should be remembered that the potential from which

these fields were originally derived was obtained from the quasi-static approximation in which the perturbation magnetic field $\underline{H}_1$ is neglected and thus $\nabla \times \underline{E}_1 = 0$. Therefore one may ask if an approximate value of the magnetic field may be obtained now. Such may be obtained from $\nabla \times \underline{H}_1 = i\omega\epsilon \underline{E}_1$ resulting in

$$H_{1\theta} = \frac{\omega}{\beta}\left(1 - \frac{\omega_p^2}{\omega^2}\right)\epsilon_o E_{1r} \qquad 0 \leq r \leq a \tag{3.1.7}$$

$$H_{1\theta} = \frac{\omega}{\beta}\kappa\epsilon_o E_{1r} \qquad a \leq r \leq \infty$$

where κ is the relative dielectric constant of the surrounding medium. If one compares the magnetic field obtained from quasi-static approximation with that obtained from a field analysis, it will be found that they are equal to within the approximation that $\omega_p^2/\beta^2c^2 \ll 1$ where c is the velocity of light.

One may then compute the z directed power flow by equation 3.1.6 and from it the interaction impedance from equation 3.1.1 in ohms as

$$\frac{1}{Z_o} = 2\pi^2\sqrt{\frac{\epsilon_o}{\mu_o}}\left(\frac{a}{\lambda}\right)\kappa(\beta a)I_o^2\left\{\frac{I_o K_1}{I_1 K_o}\left[\frac{I_2}{I_o} - \frac{I_1^2}{I_o^2}\right] + \left[\frac{K_2}{K_o} - \frac{K_1^2}{K_o^2}\right]\right\}. \tag{3.1.8}$$

The Bessel functions are all of argument (βa), κ is the glass dielectric constant and the quantity $[1 - (\omega_p^2/\omega^2)]$ in equation 3.1.7 has been replaced by the determinantal equation of propagation for this two-region geometry

$$1 - \frac{\omega_p^2}{\omega^2} = -\kappa\frac{I_o K_1}{I_1 K_o} \tag{3.1.9}$$

which may be obtained from equation 3.0.2 for the axially symmetric

mode $(n = 0)$ by letting the radius of the glass $c \to \infty$.

The interaction impedance of equation 3.1.8 is plotted in Figure 3.2 corresponding to the experimental tube of Figure 1.2 . In this experiment the modulation cavities are resonant at $f = 490$ Mc ($\lambda = 61.2$ cm) and the plasma radius is $a = .275$ cm. The glass is Nonex 7720, with $\kappa = 4.60$. The interaction impedance is plotted for this value of dielectric constant and $\kappa = 1$.

The true interaction impedance for the three-region problem of plasma-glass-free space will lie between these two curves. Previously though, it was stated that for experimental reasons the beam voltage was only varied such that $.5 \leq \beta a \leq 1.5$ and that for this range of βa the space charge wavelength of the disturbance is long compared to the glass thickness so that actually the medium surrounding the plasma appeared as free space. Therefore the true curve of the interaction impedance will lie closest to the $\kappa = 1$ curve for the region of interest. From equations 3.1.2 and 3.1.3 the growth constant is proportional to the cube root of Z_o , so for the range of interest of βa the variation is unimportant. A representative value of interaction impedance is $Z_o = 800$ ohms.

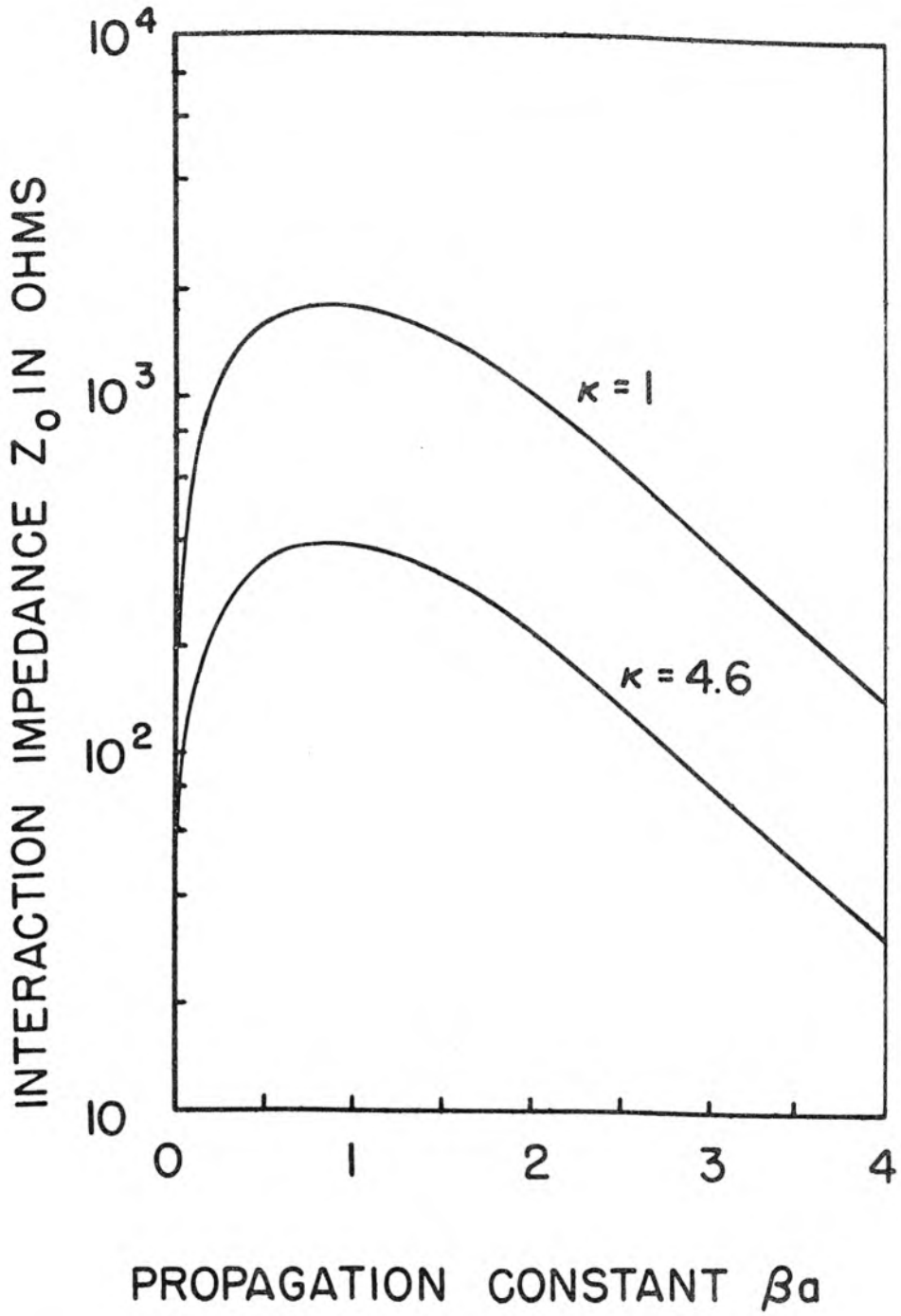

Figure 3.2 Interaction Impedance between an Electron Beam and the Angularly Independent Surface Wave Mode of Propagation. The Plasma Column is Assumed to be Surrounded by a Medium of Dielectric Constant κ which Extends to Infinity. $\kappa = 1$ Corresponds to Free Space and $\kappa = 4.6$ Corresponds to the Glass Used in this Experiment.

4. EXPERIMENTAL PROPERTIES OF THE PLASMA AND THE ELECTRON BEAM

4.0 Characteristics of Mercury Arc Discharges

The plasma used in these experiments consists of the positive column of an arc discharge in mercury vapor. The mercury gas pressure is controlled by the temperature of a pool of mercury in a separate appendage called the mercury "well". In all the experiments of this paper the temperature of the well is maintained at $300 \pm .1^{\circ}$ Kelvin (26.82° C) by a regulated water bath. At this temperature the vapor pressure of mercury is 2.1×10^{-3} mm Hg (2.1 microns). The gas density of mercury atoms is 6.8×10^{13} per cm^3. For a plasma electron frequency of 3000 Mc and 490 Mc the plasma electron density, n_o, is respectively 1.12×10^{11} and $.298 \times 10^{10}$ electrons per cm^3. These plasma densities correspond to an ionization of .165% and .0044% respectively.

In an ionized gas such as a mercury arc discharge, the electrons and ions are in a continuous milling motion and have a quantity of random energy that is often characterized by an equivalent plasma electron temperature T_e. The equivalent ion temperature is typically a third of this (1). The plasma electron temperature may be measured with a Langmuir probe (1). Such measurements have been made, Figure 4.1, on a mercury arc discharge tube of internal diameter 1.04 cm corresponding to the plasma interaction region of the helix modulation tube of Figure 1.1 . These measurements are not as reproducible as one would like, but they do give an average value of $T_e = 36{,}000^{\circ}$ K , corresponding to a random energy for the plasma electrons of approximately 4.7 electron volts. The ionization potential of mercury is 10.4 ev with excitation energy levels as low as 4.66 ev.

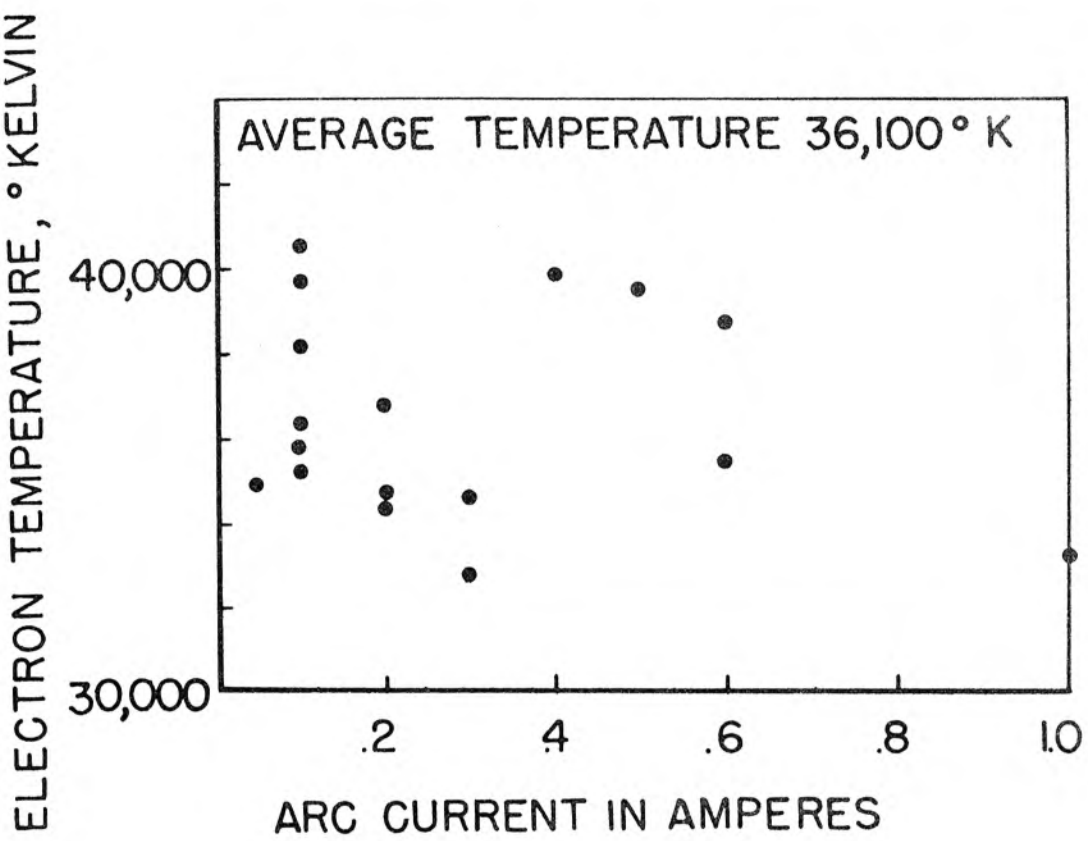

Figure 4.1 Langmuir Probe Measurements of Temperature versus Arc Current as Obtained from an Arc Column of the Size Used in the Helix Modulation Experiments of Fig. 1.1 .

Klarfeld (39) has compiled extensive probe measurements and theoretical calculations of mercury arc plasma column properties versus pressure. For low pressure mercury discharges such as used here, plasma electron density is linearly proportional to arc current. Klarfeld's calculations of plasma density assume that there is no variation with radius. He states, though, that the axial plasma density may be 1.5 to 2 times the plasma density at the edge of the electron sheath. This electron sheath at the tube wall is the order of the Debye length thick, and for a plasma of the above temperature and a density corresponding to a plasma frequency of 3000 Mc this distance is .04 millimeters. The sheath potential drop in a mercury discharge is of the order of 20 volts (assuming the electron and ion temperatures are equal). Klarfeld's curves give an electron plasma temperature of 35,000° K which agrees well with the measurements of Figure 4.1 . He states that the axial voltage gradient for a plasma column as used in Figure 1.1 is approximately .7 volts per cm and .9 volts per cm for the tube of Figure 1.2 . The axial drift velocity of the electrons is equivalent to approximately .2 ev of energy which is small compared to the 4.7 ev of random energy, thus the plasma is essentially stationary.

At the density of mercury atoms as used in these experiments, the mean free path of the un-ionized mercury atoms is approximately 2.62 cm (40). This is greater than the plasma column diameters and therefore collisions with the wall are more numerous than with each other. This also applies to collisions of the plasma electrons with the electron sheath at the tube wall, since the mean free path for collisions

between plasma electrons, at an average energy of 4.7 ev and un-ionized mercury atoms is given by von Engel (40) as 3.5 cm. The collision frequency is therefore approximately 37×10^6 per second which is small compared to the modulation frequencies used of 490 Mc and greater. Or on the basis of collisions with the wall electron sheath for the tube of Figure 1.1, the collision frequency is approximately 129×10^6 per second as obtained by dividing the r.m.s. velocity by the tube diameter of 1.04 cm.

In the present experiments the electron beam voltage ranges from 100 to 1000 volts. The maximum cross section for ionization of a mercury atom by a beam electron in this voltage range, according to von Engel (40), occurs at 100 volts and gives a mean free path for the present density of 26 cm. At 1000 volts the mean free path is 65 cm. For these two cases the fraction of beam electrons traveling a distance of 10 cm without being removed from the electron beam is respectively 68% and 86%.

Mercury vapor was chosen as the gas primarily because of the ease of controlling its pressure, but also because the plasma column voltage gradient is less than that of, say, hydrogen at similar densities.

4.1 Characteristics of the Electron Beam

The electron beam gun used in the experimental tubes of Figures 1.1 and 1.2 are of conventional design as used in traveling wave tubes. In the helix modulation tube of Figure 1.1, the cathode button is .045 inches in diameter. The cavity modulation tube of Figure 1.2 has a cathode button of .090 inches.

As these electron guns are operated in the presence of mercury vapor there is always a supply of ions in the gun region. It is fortunate that these ions do not appear to affect the gun operation adversely, other than to reduce the total current. There is no consistent arcing between gun electrodes to as high as 2000 volts (limit of voltage supply). This is because the product of mercury pressure as used in these experiments (2.1×10^{-3} mm Hg) and electrode separation distance (approximately .5 cm) is two to three orders of magnitude less than that corresponding to Paschen's minimum of the sparking potential. In the first few tubes constructed, oxide-coated cathodes were used, but subsequently L cathodes of type A were found to be more satisfactory. Tubes with oxide-coated cathodes were found to have very limited life, due to destruction of their emitting surfaces by positive ion bombardment. In one case an arc occurred destroying the emitting surface entirely. L cathodes have the advantage of replenishing themselves and being more rugged.

The electron gun appears to be temperature limited at all times as observed by varying the heater power. Also, as one increases the beam voltage from 100 volts to 1000 volts, the beam current will decrease, often by a factor of three or more. This is presumably due to positive ion bombardment of the emitting surface. At higher voltages this destructive action is more pronounced. The voltage dependence of the current is important in the operation of the cavity modulation tube of Figure 1.2 in which the beam velocity is variable. The gun in the helix modulation tube of Figure 1.1 is by necessity operated at a fixed 400 volts as dictated by the helix phase velocity. At a given voltage, however, a more annoying effect from an experimental

point of view, is that the cathode emission current is continuously varying by as much as two to one over an hour or so. It will quite typically vary by 20% within a minute. This effect is presumably due to positive ion bombardment of the emitting surface as well as "poisoning". For instance, due to electrical charging of the glass walls or varying the relative electrode voltages, one may change the positive ion trapping and thus the cathode bombardment.

The electron beam is focused entirely by an electron lens (focusing cylinder, Figures 1.1 and 1.2) just past the gun anode and by space charge forces. No axial magnetic fields are used in this experiment. In the plasma interaction region the space charge repulsion forces of the beam are neutralized by positive ions. To improve the beam focusing many electrode voltages may be adjusted. In the helix modulation tube the first helix is considered fixed relative to the gun cathode at 400 volts corresponding to the helix phase velocity. The focusing cylinder and the electron gun anode voltages may then be adjusted somewhat above or below the first helix voltage. Upon leaving the plasma interaction region the beam is focused by the second helix and beam collector voltages. In practice, one adjusts each of these voltages $\pm 10\%$ or so above and below the first helix voltage so as to maximize the output signal level of the device for a given input signal level. With only the electron beam present, the arc plasma being off, one can visually see the path of the electron beam due to the de-excitation of ions and atoms which have suffered a collision. It is fascinating to see the electron beam cross and uncross as one varies the focusing cylinder voltage relative to the gun anode voltage.

If one defocuses the electron beam with the arc off so that it leaves the first (modulation) helix in a diverging cone, one may observe it reflected from the electron sheath at the glass walls of the cylinder. This electron sheath has, of course, been produced by the beam collisions, since in the above case it was assumed that the arc plasma was off. After reflecting from the electron sheath the beam may even enter the second (demodulation) helix and be collected.

This effect is especially pronounced in a smaller diameter glass column such as used in the cavity modulation tube of Figure 1.2 which has an internal diameter of .55 cm compared to 1.04 cm. In this smaller tube the electron beam has been observed to cross as many as five times in the interaction region of 11 cm length.

Returning the discussion now to the helix tube of Figure 1.1, it is apparent that the same phenomenon of reflection of the electron beam from the electron sheath will occur with the arc plasma on, only the electron beam will no longer be observable. As previously stated, the sheath potential for a mercury arc is approximately 20 volts and thus beam electrons are reflected from the sheath for a divergent beam of half-angle up to 12°, assuming a 400 volt beam. This reflection phenomenon of the beam from the electron sheath will be seen shortly to be necessary in order to explain the interaction with the surface wave of propagation on the plasma column in this helix tube.

The electron beam diameter while passing through the plasma interaction region is seldom of constant diameter, since perfect focusing was found to be very difficult. Also, with the arc on, since the electron beam is not then visible, the only estimate of the quality of the beam focus is the strength of the output signal. Based on visible

observations with the arc off, one concludes that the mean diameter of the electron beam is approximately that of the internal diameter of the focusing cylinder. Such diameters are 3 and 4.8 millimeters respectively for the helix modulation tube, Figure 1.1, and the cavity modulation tube, Figure 1.2 .

The electron beam plasma frequency in terms of beam current, voltage and diameter in MKS units, is $\omega_b^2 = 1.06 \times 10^{16} \; I_b/b^2\sqrt{V_b}$ where the beam radius is b . For the helix modulation tube of Figure 1.1 at 400 volts and a plasma frequency of 3000 Mc, the beam current corresponding to ω_b^2/ω_p^2 equaling 10^{-3} and 10^{-4}, is 1.5 and .15 milliamps respectively. These are reasonable values of beam current for the helix modulation tubes. In the case of the cavity modulation tube the voltage of the beam is an adjustable parameter. A value of 200 volts corresponds approximately to $\beta a = 1$, where the adjustable range is $.5 \leq \beta a \leq 1.5$. From Figure 3.1 for $\beta a = 1$, it is seen for the plasma-glass column in free space that $\omega/\omega_p = .32$. With a modulation frequency of 490 Mc the beam current corresponding to ω_b^2/ω_p^2 equaling 10^{-2} and 10^{-3} is 7.08 and .708 milliamperes, respectively. From these representative numbers it is simple to scale the values to other cases.

The electronic wavelength as defined by equation 3.1.4 is of importance since in traveling wave tube theory one often refers to the interaction length as so many electronic wavelengths. The helix modulation tube operating at 3000 Mc with a 400 volt beam has an electronic wavelength of .396 cm. The cavity modulation tube at 490 Mc with a 200 volt beam, has an electronic wavelength of 1.72 cm.

5. HELIX MODULATION EXPERIMENT

5.0 Method of Operation

A schematic of the helix modulation tube is pictured in Figure 1.1 . The actual device has evolved through four principal stages as shown in Figure 5.1 A,B,C,D . The glass tube through which the plasma and beam interact remained the same in all of the tubes of Figure 5.1 . The inside glass diameter, 2a , is 1.04 cm and the ratio of outside diameter to inner is $c/a \approx 1.2$. The dielectric constant is $\kappa \approx 4.71$. The interaction region between helices is 5 cm in all but tube A .

In Figure 1.1 the energy is coupled from the S band waveguide, (TE_{10} mode) onto the helix by means of a wire antenna on the end of the helix which is parallel to the electric field. The waveguide height has been reduced to 1 cm to minimize over-all beam length. The input and output helices are each 3 cm long. At a distance of approximately one-fourth of a guide wavelength from the helix antenna in the waveguide is an adjustable short which is adjusted for maximum output signal strength during operation. Only limited data has been taken concerning the input match from waveguide to beam but a representative number for the input voltage standing wave ratio is 3:1 .

The method of operation of the tubes of Figure 5.1 is to modulate the electron beam at some frequency between 2.2 kMc (kilomegacycles) and 4.0 kMc, and to observe the output signal from the demodulation helix as one sweeps the arc current. It is known (39), that the plasma density, and thus plasma frequency squared, is linearly proportional to arc current for low pressure arc discharges. By the elementary theory of Section 2, the output signal level should be a maximum when the arc

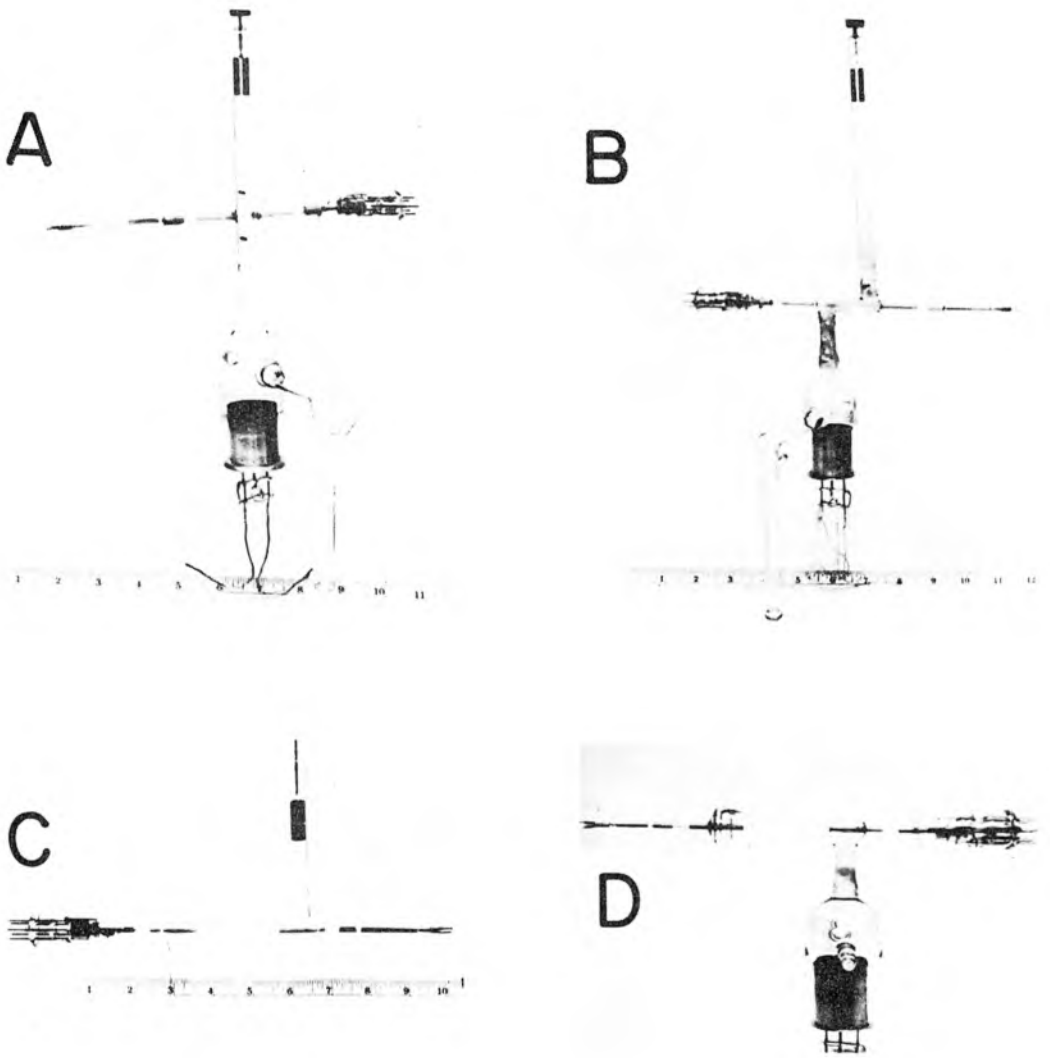

Figure 5.1 Helix Modulation Tubes at Various Stages of Development. Tube A Contains Langmuir Probes with which Plasma Temperature Measurements were Made. The Plasma Interaction Region of Tubes C and D are More Uniform than that of Tube B, Since the Beam Need Not Pass Through the Bend in the Plasma Column. The Arc is Significantly Easier to Strike in Tube D than in Tubes B and C .

current is such that the modulation frequency ω equals the plasma frequency ω_p. This value of arc current for interaction will change as one changes the input frequency. For convenience, the arc current is swept at 60 cps by an a.c. voltage in series with the d.c. arc voltage. The detected output signal is filtered by a low pass filter with a 10^{-4} second time constant.

Typical operation is shown in Figure 5.2 for various values of the modulation frequency. The abscissa is proportional to the plasma arc current and ordinate to the detected output power which is proportional to linear gain. The numbered vertical line at the far left is the zero of arc current. A plot of frequency squared versus arc current from photographs such as Figure 5.2 is shown in Figure 5.3 for several experimental runs by the curves labeled G. Experimental runs G_2 and G_3 were on tube C and were taken a month apart. The points of G_1 were obtained on tube B and were previously reported (32).

5.1 Experimental Verification of Theory and Plasma Density

The experimental observation that points G_1, G_2, and G_3 lie on straight lines with a remarkably small spread, passing nearly through the origin, is in itself strong evidence that the interaction observed is that predicted by Bohm and Gross (11) and discussed in Chapter 2. That the modulation frequency equals the plasma frequency on the axis of the discharge where the electron beam passes may only be ascertained from an independent measurement of plasma density. The fact that such straight lines extrapolated to zero frequency do not pass exactly through the origin but to the left of the origin may be

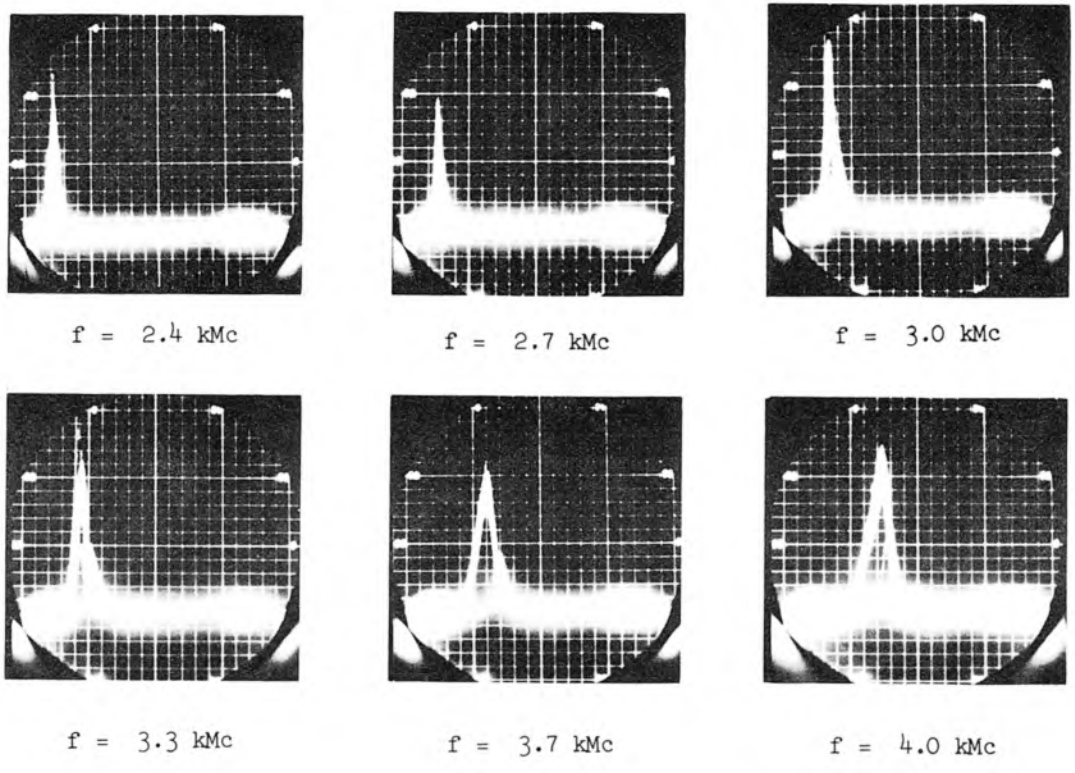

Figure 5.2 Detected Output Signal versus Arc Current as Obtained from Helix Tube C for Various Modulation Frequencies. The Electron Beam Cathode Current is Respectively, 1.8, 2.0, 1.2, 1.2, 1.5, 1.5 milliamperes.

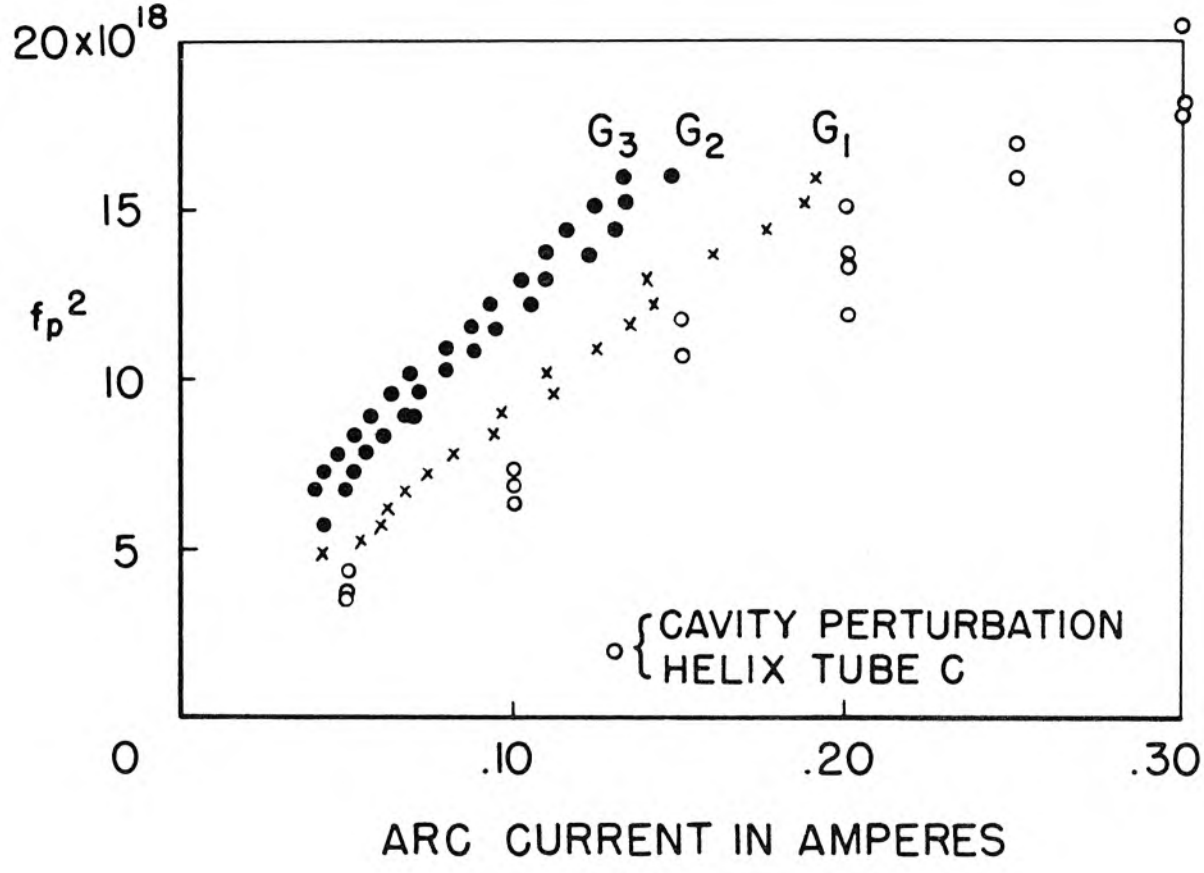

Figure 5.3 Measured Values of Plasma Frequency Squared versus Arc Current. G_1 Obtained from Helix Tube B . G_2 and G_3 Obtained from Helix Tube C . The Circles Represent Measurements of the Average Plasma Frequency over the Cross Section of the Plasma Interaction Region of Helix Tube C as Obtained by Perturbing the Resonant Frequency of a Microwave Cavity.

explained in terms of the plasma produced by beam collisions. It may also be possible that the curves depart from a straight line to pass through the origin as the arc current is reduced. This was not verified as the S band waveguide used to couple to the helices would not propagate at significantly lower frequencies. The contribution of the electron beam to the production of plasma electrons will be estimated later in this section.

The slow undulation of curves G_2 and G_3 can be explained as due to the slow variation of the water bath temperature since the experimental points in curves G_2 and G_3 were taken in sequential time order. The points of G_1 were not taken in order. The mercury well water bath was regulated to $\pm .1^{\circ}$C which theoretically allows a 2% variation in mercury vapor pressure neglecting any thermal time constants in the system.

The difference between curves G_2 and G_3 is most probably due to differences in the quality of beam focusing between the two experimental runs if the explanation of beam electron collisions causing the zero frequency intercept is correct. It may also very likely be caused by inaccuracies in the zero point of the arc current in the photographs of Figure 5.2 since curves G_2 and G_3 are shifted horizontally with respect to one another by approximately .01 amperes corresponding to half of one division in Figure 5.2 . The slopes of curves G_2 and G_3 are quite equal, a condition which would be required by either hypothesis.

It is essential in order to verify the theory of interaction with the plasma resonance at $\omega = \omega_p$ that the electron plasma density be measured by an independent method. The method that has proven to

be the most suitable though, unfortunately, not the first tried, is that of perturbing the resonant frequency of a microwave cavity (41). Since a plasma may be represented by a relative dielectric constant $1 - \omega_p^2/\omega^2$, then inserting it into a resonant cavity will perturb the resonant frequency according to $\Delta f/f = \Delta\bar{W}/\bar{W}$ where $\Delta\bar{W}$ is the change in the average stored energy resulting from the insertion of the dielectric column.

Such measurements have been made with a split S band rectangular cavity operating in the TE_{101} mode. The plasma column interaction region of tube C of Figure 5.1 was placed parallel to the electric field in the above cavity. Measurements of plasma density versus arc current were made and are plotted as circles in Figure 5.3 . Recall that the measurements G_2 and G_3 were made on the same tube C , whereas G_1 is from tube B .

The cavity perturbation technique measures average plasma electron density, whereas the growing wave experiment at $\omega \approx \omega_p$ measures the axial plasma density, since the electron beam diameter is small compared to the plasma column diameter. Thus the difference in slopes between the cavity data and that of growing wave data G_2 or G_3 is probably attributable to the radial variation of plasma electron density in the plasma column.

Howe (42) has discussed the radial variation of electron density but points out that the use of ambipolar diffusion theory is not really applicable when the mean free path of the mercury vapor is of the order of the tube diameter or greater. Normally one can approximate the radial electron density variation by a parabolic variation from the tube axis to some finite value at the tube walls. Of course,

this neglects the rapid variation of the plasma density in the electron sheath to zero, but is satisfactory as long as the sheath thickness is small compared to the tube radius. From Figure 5.3 the ratio of the slopes of curves G_2 or G_3 and the cavity data is approximately 1.42. Based on the assumption that the variation is parabolic, one then estimates that the edge plasma density is .4 of the axial plasma density which seems to be a reasonable number.

In the preliminary report (32) of this work, the independent method of measuring density was by scattering microwaves from a plasma column, see Appendix 1. In such an experiment the plasma arc column is inserted in a rectangular TE_{10} waveguide so that the axis of the column is perpendicular to both the electric field and the direction of propagation. When the reflection coefficient of the column is plotted versus arc current at a fixed frequency, several distinct maxima are found (32). The principal or first resonance (36) occurs at $\omega_p^2/\omega^2 = 2$ (modified by a straightforward correction for the glass walls which, in the case of the tube of Figure 1.1, gives $\omega_p^2/\omega^2 = 2.81$) and corresponds to dipole resonance of the plasma column. It can be shown that with a monotonic density variation radially, reflection should occur at nearly the average density. These multiple resonances have been experimentally observed by others (6),(7),(44),(45),(46), but are unexplained in the literature. Much speculation has occurred that these multiple peaks may be caused by the radial charge density variation (36),(43),(47),(48), but Keitel based on his own work (49), criticizes these results as erroneous (50). Recently, Gould (51) has succeeded in predicting an infinity of peaks by the approximate inclusion of the effects of the random energy of the plasma electrons. Such

random velocities succeed in coupling the plasma resonance at $\omega_p^2/\omega^2 = 2$ to the plasma oscillations near $\omega = \omega_p$.

For the purposes of this paper only the principal resonance is of use in measuring the plasma density. The minor peaks will not be considered further. As mentioned in the preliminary report (32), there was an appreciable discrepancy between the estimated average plasma density obtained by the scattering experiments and the axial density as measured by the electron beam. This discrepancy was caused by the erroneous assumption that the positive column of an arc discharge is independent of bends in the column. That is, the scattering measurements were performed for convenience on a long straight arc column made from an identical piece of glass as used for the plasma interaction region of the helix tube of Figure 1.1 . The plasma density versus arc current was then mistakenly assumed the same in both tubes at identical conditions of mercury pressure. That such is not the case is apparent in Figure 5.4, where cavity perturbation measurements made on a long straight plasma column are compared with the data presented in Figure 5.3 obtained from the helix tube model C of Figure 5.1 . Both measurements were made with the same rectangular TE_{101} cavity. Also in Figure 5.4 are measurements of average plasma density as obtained from the principal resonance of the scattering experiment (designated by the points S). Likewise, the line labeled K represents an estimate of average plasma density by Klarfeld (39) and is based on a compilation of Langmuir probe measurements. The crosses labeled W are measurements of average plasma density on said straight column as obtained from the slow wave propagation method (33) by Trivelpiece. All the measurements on the straight column agree

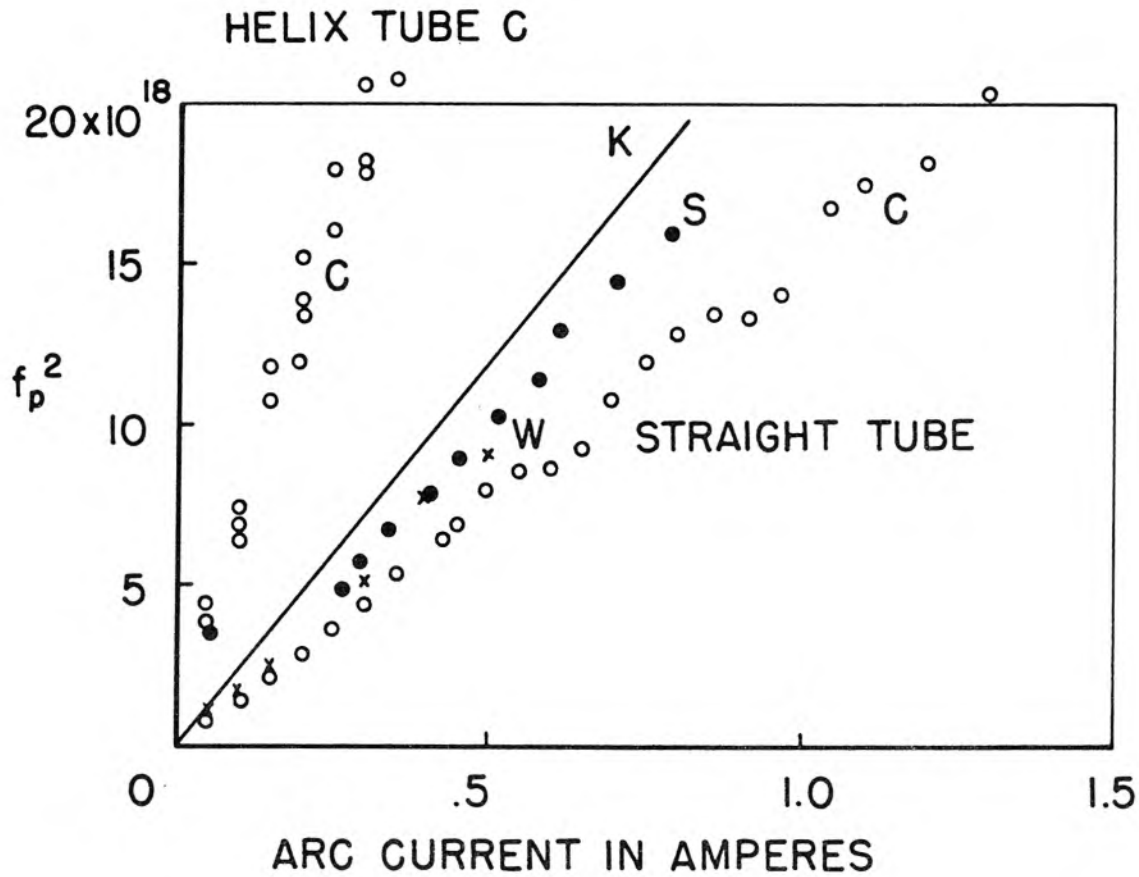

Figure 5.4 Measured Values of Average Plasma Frequency Squared versus Arc Current. The Circles Represent Density Measurements as Obtained by the Cavity Perturbation Technique (C). Such Measurements were made on both Helix Tube C and on a Straight Discharge Tube of the Same Dimensions. On the Straight Discharge Tube, Plasma Density Measurements were also Obtained by the Scattering (S) Method and the Slow Wave Propagation Method (W). Klarfeld's Estimated Value is Also Shown (K).

reasonably well as they all measure average density but differ considerably from the cavity measurements on the plasma interaction region between the helices of tube C shown in Figure 5.1 .

One must conclude, based on the experimental results of Figure 5.4, that the plasma electron density versus arc current of a short plasma column (such as the interaction region of Figure 1.1) depends on the end conditions to a large extent. In figure 5.1B it may be seen that the beam passes through the bends in the arc column whereas in tube C the helices and their surrounding small glass tube project through the bends. Thus the geometry at the ends of the plasma interaction region is different for helix tubes B and C and therefore one might expect the plasma densities, for a given arc current, to be different. This explains the slope discrepancy in Figure 5.3 between G_1 , which was obtained on helix tube B, and G_2 and G_3 , which were obtained on helix tube C .

One may even go so far as to explain why helix tube C has a higher plasma density for a given value of arc current than does tube B as seen in Figure 5.3 . Note that the arc column is more restricted by the bends in tube C than tube B . This is because the small glass tube supporting the helix passes through the bend of tube C but not tube B . It is known that constricting an arc column raises the voltage gradient along it so one might expect that the voltage drop through the bend of tube C should be greater than that of tube B . Therefore, plasma electrons passing around the bend of tube C might be expected to have more energy than tube B and thus have a greater probability of producing an ionizing collision.

The contribution of the electron beam to the production of plasma electrons will now be estimated. For a 400 volt electron beam as used in the helix tubes the mean free path (40) for beam electrons to ionize Hg atoms is 43.7 cm. It is possible to compute a rate of ion production, r_b, in ions per sec per centimeter length of the beam for a typical beam current of, say 1.5 ma, as is typical for Figure 5.2. From Klarfeld (39), knowing the plasma electron temperature, one can compute the rate of ion production due to the plasma electrons, assuming a plasma density corresponding to a plasma frequency of 3000 Mc, in ions per sec per centimeter length of the arc column. The ratio $r_p:r_b$ is approximately 113, which implies a small beam contribution compared to that of the plasma electrons. This is experimentally substantiated by the fact that in the cavity perturbation experiments, which measure the average plasma density throughout the cross section of the tube, there is no detectable shift in the resonant frequency due to the electron beam.

In Figure 5.3 the intercept at zero frequency for curve G_1 or G_2 is approximately -.01 ampere. The arc current for interaction at 3000 Mc is approximately .1 ampere for G_1. Assuming that the beam contribution theory is correct, this implies that the ratio of the rates of ion production due to plasma electrons and due to the beam electron collisions is approximately 10:1. To explain the discrepancy between 113 and 10 one must assume that the plasma electrons produced by the electron beam remain, at least for several cycles of the signal frequency, within the beam radius of .15 cm (Section 4.1). The plasma column radius is .52 cm. Over the beam cross section the ratio of

$r_p : r_b$ becomes 113 $(.15/.52)^2 \approx 9.4$ which is satisfactory.

To substantiate this assumption of the plasma electrons produced by beam electron collisions remaining for several cycles within the beam radius, it is necessary to know the average random energy of the electrons produced by ionizing collisions between beam electrons and mercury atoms. Such an answer is not easily obtained but, for the sake of argument, assume that such random energy is 4.7 ev, corresponding to that of the plasma electrons. A traversal frequency across the beam is obtained by dividing the corresponding one-dimensional random velocity by the beam radius. Such a traversal frequency is approximately 500 Mc which is a reasonably small fraction of 3000 Mc implying that a plasma electron produced by a beam electron collision remains within the beam radius for several cycles of the modulation field. Mott and Massey (52) show a curve of the energy distribution of ejected electrons for hydrogen at various beam voltages although, unfortunately, not for Hg. This and related calculations indicate that the average random energy of the ejected electron may range from the above assumed value to several times that value. This is, however, a satisfactory order of magnitude calculation.

5.2 Interaction with Surface Wave Mode of Propagation

During the course of experimentation on the helix tube it was found that an interaction occurred at a plasma frequency greater than the modulation frequency. Such interactions for various frequencies are shown in Figure 5.5 where the detected output signal is shown versus arc current. The arc current increases from left to right and is zero at the numbered vertical line at the far left. Two interactions occur,

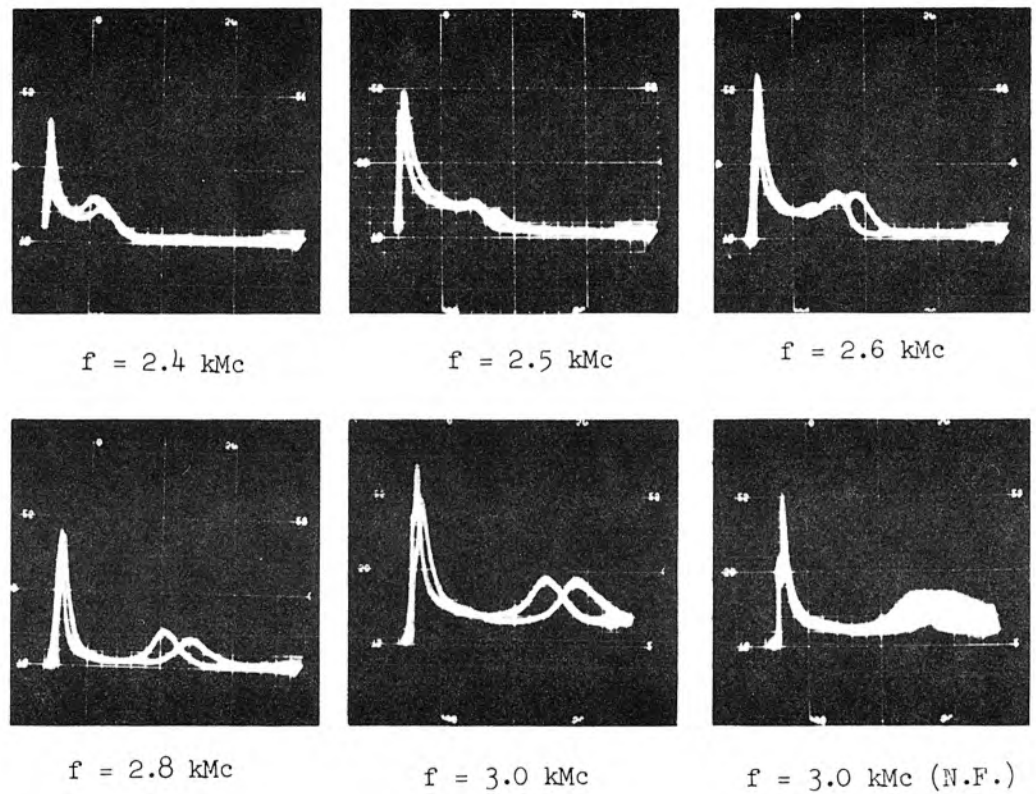

Figure 5.5 Detected Output Signal versus Arc Current as Obtained from Helix Tube C. The Strongest Interaction is at $f = f_p$. The Second Interaction Peak is Presumably with the Surface Wave Mode of Propagation. The Electron Beam Cathode Current is Approximately .6 Milliamperes in All Cases.

the one at lower arc current being at $\omega = \omega_p$, and the other one presumably with the axially symmetric surface wave mode of propagation. Note in Figure 5.5 that there are two photographs at 3.0 kMc. The second one is with the detected output signal of the amplifier not filtered (N.F.). The noise that is apparent will be discussed later.

The surface wave frequency versus propagation constant diagram for the helix tube is shown in Figure 5.6. The vertical lines are both for phase velocities corresponding to a 400 volt electron beam at two different frequencies. Their intersection with the surface wave ω-β diagram represents the ratio f/f_p at which the electron beam is synchronous with the slow wave of propagation on the plasma column. As can be seen in Figure 5.6, the intersections for this helix tube at its fixed beam velocity occur at large values of βa for frequencies in the range 2.5 to 4.0 kMc. The interaction occurs at $f_p^2/f^2 = 6.0$.

In order to obtain the operation as shown in Figure 5.5 instead of that of Figure 5.2, it is necessary to defocus the electron beam such that it is reflected by the electron sheath into the second helix. This is accomplished by first obtaining the pure $\omega = \omega_p$ interaction as in Figure 5.2. This in itself is often very difficult as all the different electrodes through which the beam passes have voltages which must be adjusted a slight amount about the synchronous voltage. The criterion of optimization is to maximize the output signal strength and to obtain a sharp response as in Figure 5.2 . If then, at this condition of optimum performance, the second (demodulation) helix is shifted a few percent in voltage, the output signal strength at the peak of the interaction in Figure 5.2 decreases, necessitating an increase in the

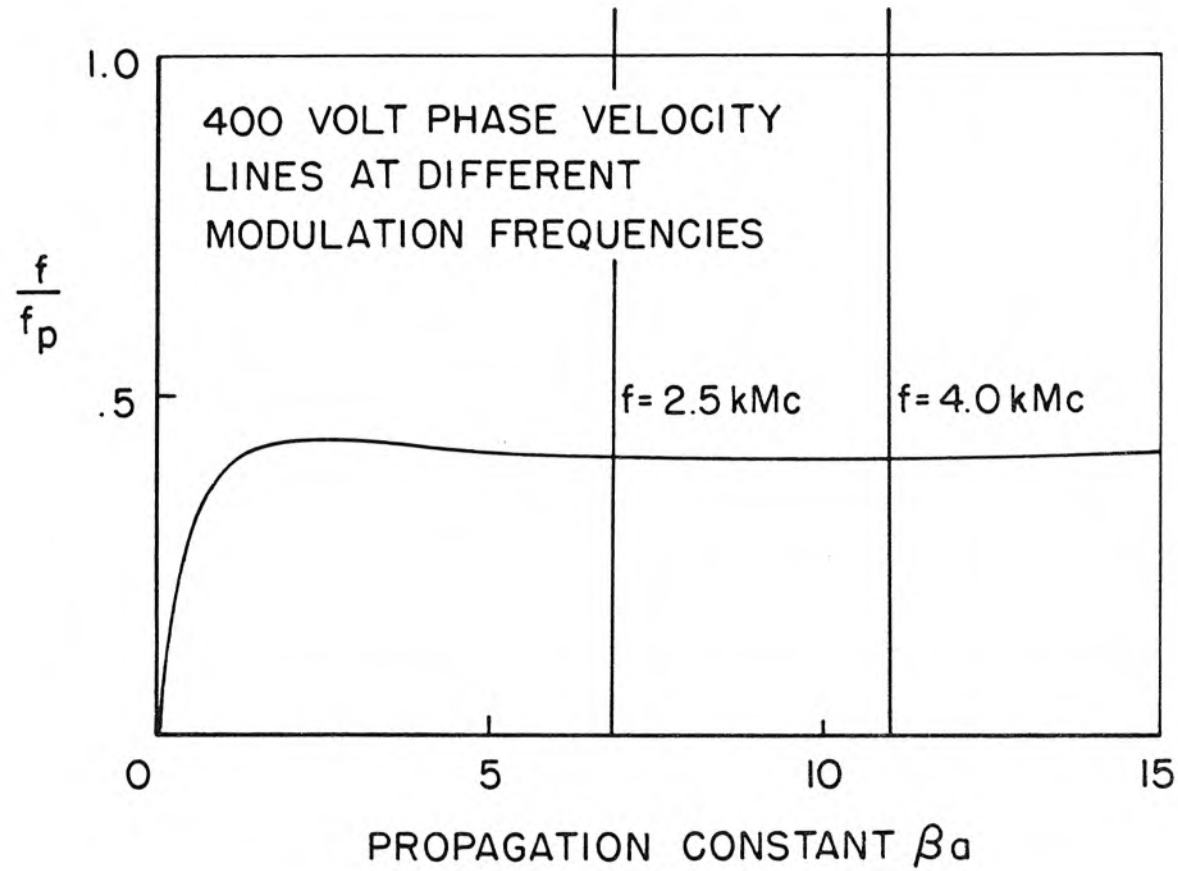

Figure 5.6 Normalized Frequency versus Propagation Constant for the Surface Wave Mode of Propagation on a Plasma-Glass Column in Free Space of Dimensions Corresponding to the Helix Modulation Tube of Figure 1.1 .

oscilloscope sensitivity. When the decrease of the principal interaction reaches approximately 20 db the second interaction is of appreciable magnitude as seen in Figure 5.5.

From photographs such as Figure 5.5 one is able to plot the arc current corresponding to the two interaction peaks versus the modulation frequency squared. Typical results from helix tube C are shown in Figure 5.7. Also included are the cavity perturbation measurements of average plasma frequency versus arc current which were previously presented in Figure 5.3. The points G_4 correspond to the body resonance interaction at $\omega = \omega_p$ and agree well with curves G_2 and G_3 of Figure 5.3. The experimental points of both interactions lie on good straight lines and have zero frequency intercepts to the left of the origin. The fact that the intercept of the purported surface wave interaction lies to the left of the principal interaction is unexplained.

The ratio of the slopes of these two experimental lines is 4.3 compared to the theoretical value of 6.0. The effect of the radial charge density variation is unfortunately in the direction which will increase the theoretical value of the ratio. This is because the surface wave fields interact with the edge plasma density, whereas the body resonance interaction occurs when the modulation frequency equals the axial plasma density. This discrepancy is unexplained.

The mechanism of the reflection of a divergent electron beam from the electron sheath was described previously. It is necessary to postulate that such is occurring in order to explain the interaction of the surface wave mode of propagation with the electron beam of the helix tube. This is because the electric fields of the surface wave

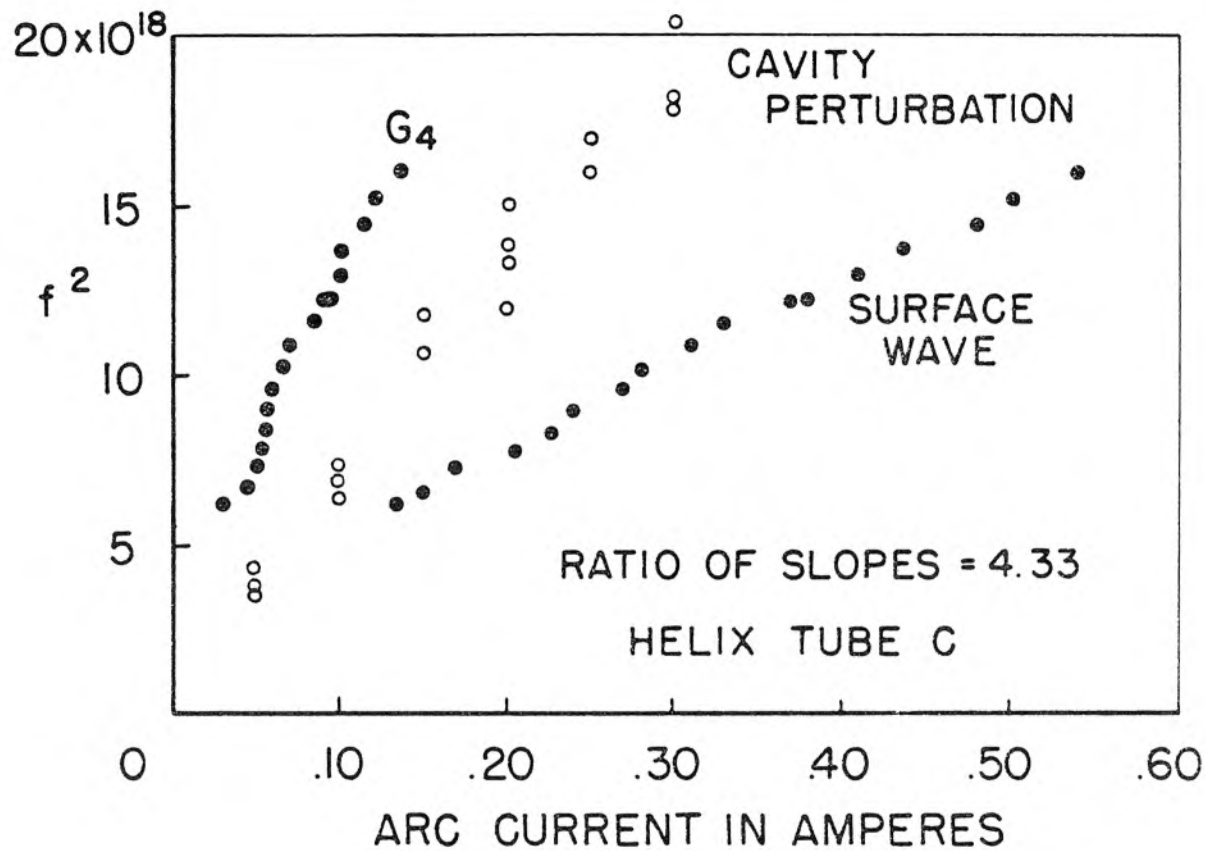

Figure 5.7 Frequency Squared versus Arc Current at Which the Two Interactions of Data Similar to Figure 5.5 Occur. The Circles Represent Experimental Measurements of Average Plasma Frequency Squared versus Arc Current as Obtained by the Cavity Perturbation Method.

at the surface of the electron beam are a factor of 88 weaker [$I_o(\beta a)/I_o(\beta b)$ for f = 2.5 kMc] than at the surface of the plasma column of Figure 1.1, and hence significant interaction will not occur if the electron beam is well focused and remains close to the axis. Strong interaction with the surface wave will occur only if the beam is made to pass close to the surface of the plasma column.

In Figure 5.5 are shown two photographs of the interaction at 3.0 kMc. These were taken in immediate succession. The filtered and nonfiltered detected output signal is shown. Obviously there is an appreciable noise or hash present and because of this the detected output signal is normally filtered for the experiments of this paper. The noise spectrum appears to be rather broad although it probably has a maximum in the 10 kc to 20 kc range. This noise vanishes when the input signal level is removed (except when the tubes are oscillating) and may be associated with density fluctuations from moving striations (53). Since both the interaction with the body resonance at $\omega = \omega_p$ and the surface wave appear to be extremely noisy, it would appear that the devices described in this paper are of limited usefulness unless one can circumvent this difficulty in some manner.

Also in evidence in Figures 5.2 and 5.5 is hysteresis in the trace. This implies that the arc plasma electron density differs for a given arc current depending on whether the 60 cps arc sweep voltage is in the increasing or decreasing part of the cycle. This may possibly be caused by space charge build up and decay on the glass walls, or by non-equilibrium heating effects in the arc column. The exact mechanism is not understood. For consistency, the first occurring peak is normally chosen in this thesis from which curves are plotted.

5.3 Experimental Rates of Growth

The theoretical rates of growth including the beam plasma frequency reduction factor, but neglecting collisions, may be computed from section 2 with the conditions of section 4. Assuming a 400 volt beam, $R = 400/4.7 = 85$. At 3000 Mc assuming an electron beam current of .1 and 1.0 ma, the growth constant G is 12.4 and 26.1 db per cm. As seen in section 2.1, collisions of the plasma electrons can significantly reduce these growth constants.

Experimentally the maximum net gain observed between the input and output waveguides of the device of Figure 1.1 performed on tube D of Figure 5.1 is +25 db. Under this condition the electron cathode current was 2.0 ma and that reaching the beam collector was .48 ma. When the arc was turned off, but the beam left on, the net loss was as little as 10 db if the beam remained well focused. This implies an electronic gain of 35 db or a growth constant of 7 db per cm. The above operation is shown in Figure 5.8.

It should not be implied though, that such high net gains were always observed. On tube C, for example, the highest net gain observed was +8 db with a cathode current of .8 ma. Turning the arc off, the net loss was approximately 30 db with the beam well focused. This again predicts a growth constant of 7 or 8 db per cm.

Many times with the tube operating as in Figure 5.2, the device would show a net loss of 10 db or so. Adjusting the device well enough to show net gain is quite difficult and requires much adjustment.

Under the most favorable circumstances the growth constant was estimated at only 7 or 8 db per cm. This discrepancy of experiment and theory is most likely explained by inhomogeneities in the axial plasma density,

since the inclusion of collision effects, as in Section 2.1, fails to reduce the gain to sufficiently near that required by experiment. By inhomogeneities in the axial plasma density is meant either a gradual or statistical variation in the plasma electron density along the axis of the plasma interaction region of Figure 1.1.

It can be seen in Chapter 2 that the theoretical bandwidth of this amplification device is less than one percent. As an example, consider a beam current of .15 ma; the bandwidth as defined by the half power points is then .2%. The experimental curves of Figure 5.2 indicate a bandwidth up to 40% or so. Based on the narrowness of the theoretically predicted bandwidth, it is easy to understand how a few percent change of electron density along the plasma interaction region of Figure 1.1 could drastically reduce the observed growth constant and make comparison with theory very difficult.

The helix modulation experiment has also been found occasionally to oscillate without external feedback. The output versus arc current under such circumstances is similar to Figure 5.2 and 5.8 and is only discernable in that the output does not disappear when the input is turned off.

The output signal level versus arc current such as Figure 5.8 should be compared to that of Figure 2.3. The vertical axis of the latter figure is, of course, proportional to the logarithm of the output signal level of Figure 5.8. The fact that the output signal falls off less rapidly at arc currents above the maximum interaction current than below is seen in the second through fourth photographs of Figure 5.8 which were obtained from tube B. These latter three cases were used to form Figure 2 of the preliminary report (32). The electronic gain

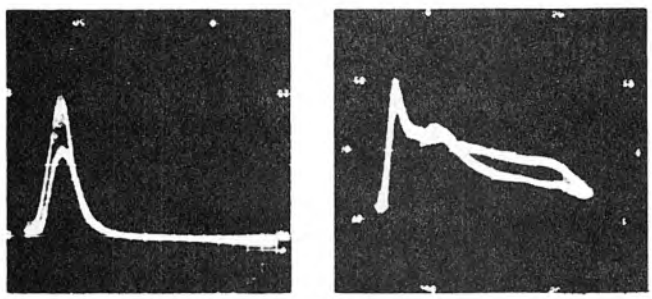

f = 3.0 kMc TUBE D

f = 2.5 kMc TUBE B

f = 3.0 kMc TUBE B

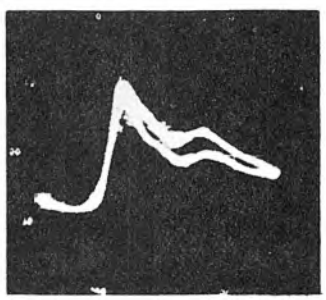

f = 3.5 kMc TUBE B

OUTPUT VERSUS ARC CURRENT

HORIZONTAL CALIBRATION: 20 DIVISIONS = .40 AMPERES

Figure 5.8 Detected Output Signal versus Arc Current. Tube D in This Photograph Showed a Net Gain of +25 db. The Electron Beam Cathode Current is 2 Milliamperes for Tube D and .8, 1.0, .9 Respectively, for the Data of Tube B .

of tube B in the latter three cases was much less than that of the first photograph of Figure 5.8 which was obtained from tube D. The data obtained from tube B substantiates the general shape of the theoretical curves of Figure 2.3. The second bump in the output is presumably due to surface wave interaction.

The primary advantage of tubes C and D over B is that the beam passes through a more uniform region of the arc column. The advantage of tube D over C is that the arc is much easier to strike. Tube A of Figure 5.1 showed interaction but was never very satisfactory and was quickly discarded for the more ideal geometries. It served its purpose in encouraging our initial efforts.

A direct experimental observation at $\omega = \omega_p$ of growing waves along the electron beam obtained by moving an antenna along the outside of the glass column is very difficult to observe. There are two main reasons for this. The first is that the fields fall off as $K_o(\beta r)$ from the edge of the beam to the edge of the plasma column. This factor becomes quite large for the helix modulation tube, since βa ranges between 6 and 11 as seen in Figure 5.5. The second is concerned with the coupling of plasma oscillations at $\omega = \omega_p$ to outside the plasma column. Note from equation 2.0.1 that when the modulation frequency equals the plasma frequency the equivalent dielectric constant is zero inside the plasma medium. Therefore, the displacement vector is zero inside this equivalent plasma dielectric. From the boundary condition on the continuity of the normal displacement vector at a charge free interface it is then apparent that if the displacement vector is zero inside the plasma the normal electric field must be zero outside the plasma surface. From a theorem in electrostatics it is known that if the normal component of the electric field is zero over a surface,

there is no field outside this enclosed region. As applied to the experiments of this thesis these considerations indicate why it is difficult to detect oscillation fields at the plasma frequency outside the plasma body. Of course the above discussion neglects the effects of the random energy of the plasma electrons and plasma density inhomogeneities.

When this experiment was tried on helix tubes C and D, the results were negative, i.e., no growing wave at $\omega = \omega_p$ could be recognized amid the background radiation of the helices, etc. When this was tried on the cavity modulation tube at $\omega = \omega_p$ the experiment was successful and will be discussed further in Sections 6.2 and 6.3 . The experiment was successful there probably because the electron beam passed closer to the surface of the column as well as operating at values of βa between .5 and 1.5 .

This difficulty in detecting plasma oscillations with an r-f probe outside the plasma emphasizes one of the points that has made the experiments in this thesis successful. That is, in these experiments one generally couples to the modulated electron beam emerging from the plasma as opposed to coupling to radio frequency fields. The other main point is that in these experiments the growing wave is excited by a modulated electron beam and therefore usable signal levels may be reached in a shorter distance than if left to grow from the inherent noise on an electron beam. For these reasons one can appreciate why Looney and Brown (18) were unsuccessful in detecting growing waves, in the direction of their unmodulated electron beam, as had been predicted by Bohm and Gross (11).

6. CAVITY MODULATION EXPERIMENT

6.0 Method of Operation

To more fully investigate the interaction of an electron beam with the slow surface wave mode of propagation on a plasma column, the cavity modulation tube of Figure 1.2 was constructed. The resulting tube and its split 490 Mc re-entrant cavities are shown in Figure 6.1 . The cavity gap is .150 inches and each cavity has a tuning plunger capable of shifting the resonant frequency as much as 2.4% . The cavity gap fields must penetrate through the glass to the beam. This results in poor coupling of the cavity to the beam, but this is not of great importance, since for this experiment it is the interaction mechanism that is of importance and not the over-all net gain.

In the helix tube experiments, interaction with the surface wave was observed but only at a fixed phase velocity as specified by the helices. Also, because of the high frequency and large plasma column diameter, interaction was observed only far out on the asymptote of βa as seen in Figure 5.6 . Weak interaction was obtained because the electron beam diameter was small compared to the plasma column.

In Figure 3.2 it was seen that the maximum interaction impedance occurred in the range $.5 \leq \beta a \leq 1.5$, whereas the helix tube had values of βa greater than 6 for frequencies of interest. Of further interest was the fact that for $\beta a < 2$ the value of ω/ω_p changed with βa . For the beam voltage and frequencies as used in the helix tube, the surface wave interaction occurred at a constant value of ω/ω_p . To verify the interaction properties with the surface wave it is of interest to vary the beam velocity in the range $.5 \leq \beta a \leq 1.5$ and see that the arc current at which interaction occurs varies as

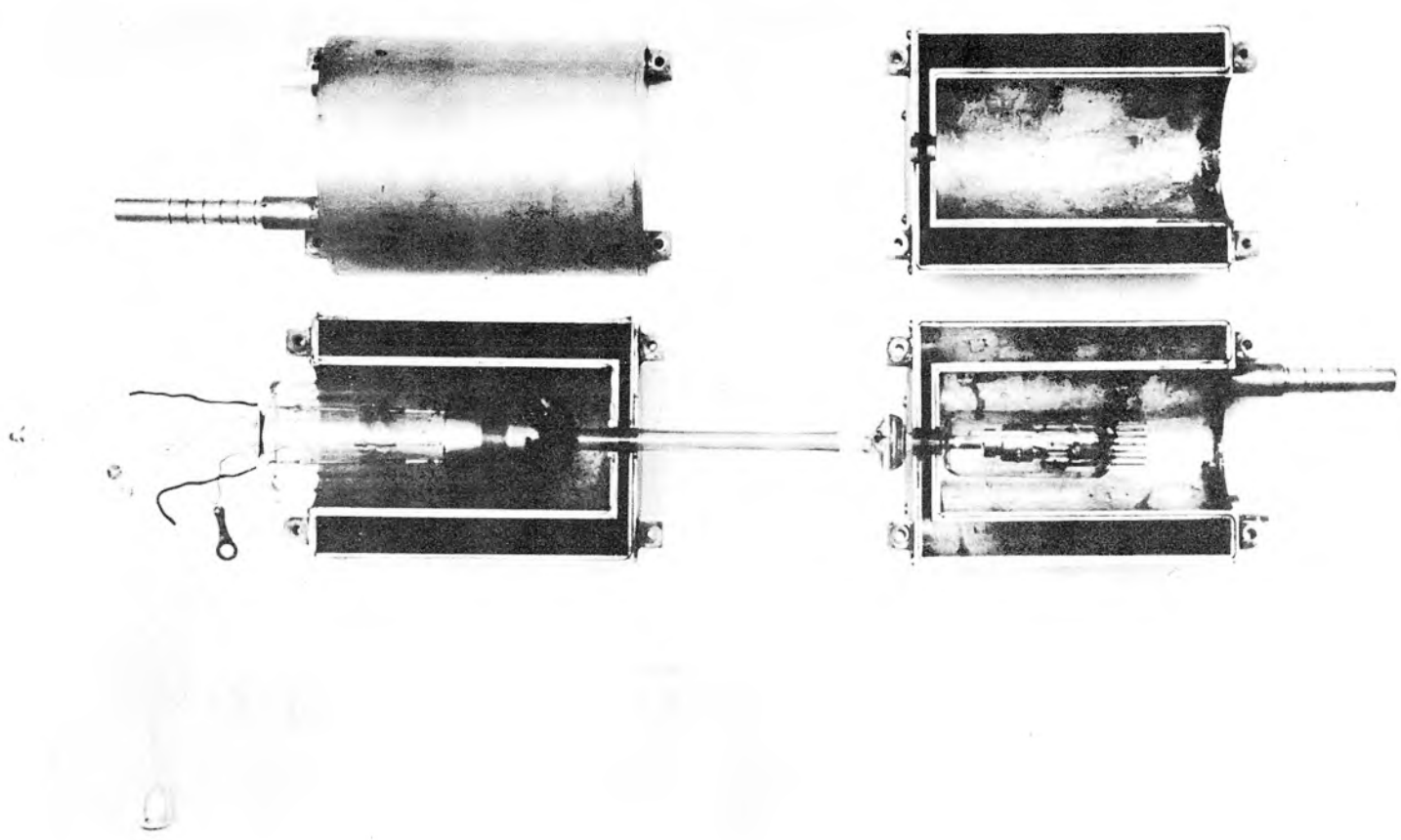

Figure 6.1 Cavity Modulation Tube and Split 490 Mc Re-entrant Cavities. Note Tuning Plungers which May Shift Resonant Frequency up to 2.4% .

prescribed by theory.

Typical experimental results obtained from the device of Figure 6.1 are shown in Figures 6.2 and 6.3 . In Figure 6.2 the detected (and filtered) output signal is presented versus arc current for different electron beam voltages. The zero of arc current is the numbered vertical line at the far left. As the beam velocity increases the phase velocity of the slow surface wave mode of propagation must also increase to remain in synchronism. It is seen in Figure 3.1 that as the velocity increases, βa decreases and f/f_p decreases. The tube of Figure 6.1 is operated at a fixed frequency of 490 Mc. Thus for increasing synchronous velocity the plasma frequency must increase. This is seen to be true in Figure 6.2 where the interaction peak shifts toward higher arc currents as the beam velocity is increased. In Figure 6.3 the arc current is held fixed and the beam velocity is swept (at 60 cps). As before the interaction occurs at increasing beam voltages as the plasma density is increased by way of the arc current.

To obtain the operation shown in Figure 6.2 requires a considerable amount of adjustment of the electrode voltages along the electron beam to focus it well. Of course, with the arc on, the beam cannot be seen so the only measure of the quality of the beam focus is the strength of the output signal level and the current reaching the beam collector shown in Figure 1.2 . Actually, the current reading is only of limited usefulness, since current readings to electrodes surrounded by plasma can be very misleading. This is because the plasma appears to d.c. electrode voltages as a medium of finite conductivity. Thus between any two electrodes there flows a current (ions being collected

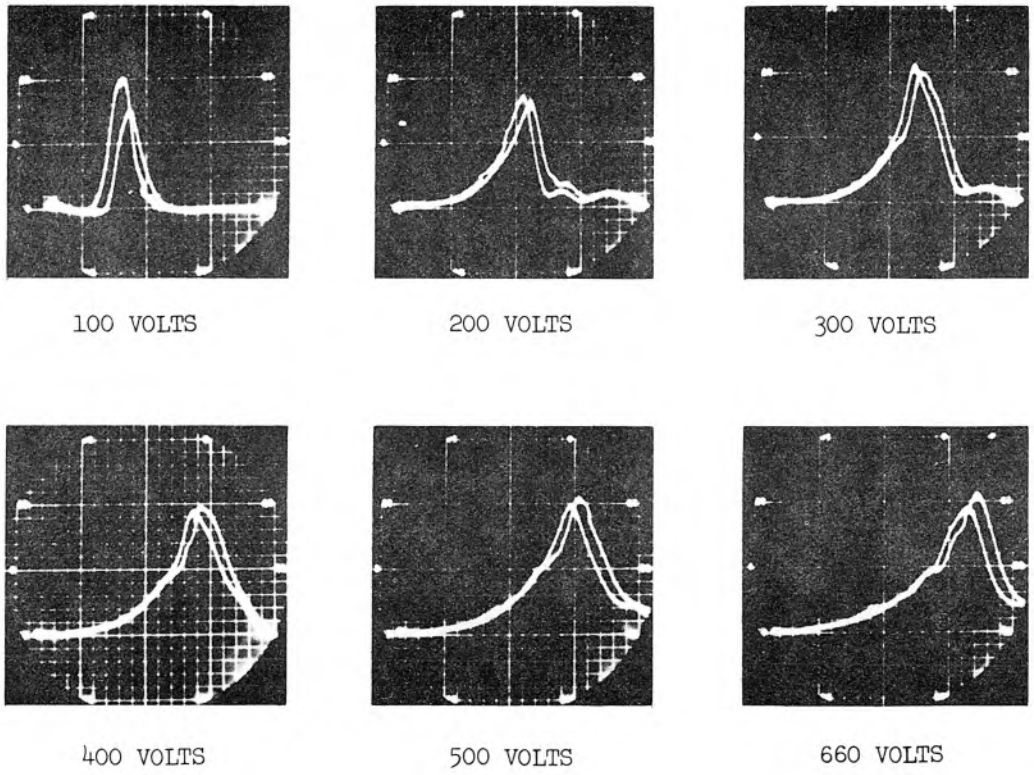

Figure 6.2 Detected Output Signal versus Arc Current at Various Electron Beam Voltages. The Electron Beam is Interacting with the Angularly Independent Surface Wave Mode of Propagation on the Plasma-Glass Column in Free Space. The Electron Beam Cathode Current is 1.8, 1.0, 1.0, .40, .44, .48 milliamperes, Respectively.

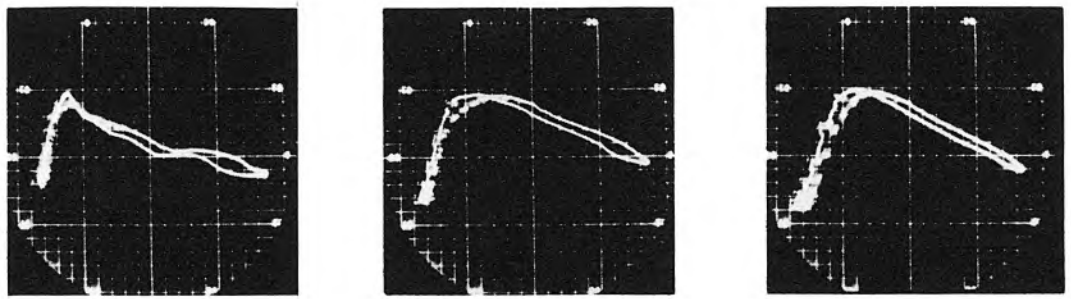

I_{ARC} = .020 AMP.

I_{ARC} = .030 AMP.

I_{ARC} = .040 AMP.

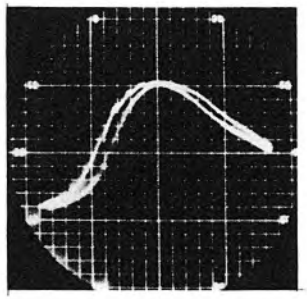

I_{ARC} = .050 AMP.

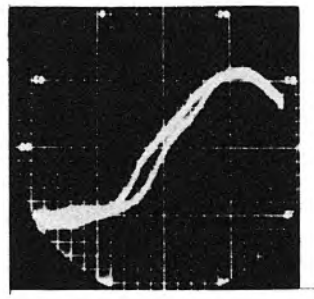

I_{ARC} = .060 AMP.

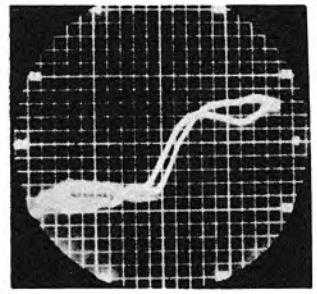

I_{ARC} = .075 AMP.

OUTPUT VERSUS BEAM VOLTAGE

HORIZONTAL CALIBRATION: 20 DIVISIONS = 800 VOLTS

Figure 6.3 Detected Output Signal versus Electron Beam Voltage at Various Arc Currents. The Electron Beam is Interacting with the Angularly Independent Surface Wave Mode of Propagation on the Plasma-Glass Column in Free Space. The Average Electron Beam Cathode Current is .37 Milliamperes.

at one electrode and electrons at the other) resulting from the plasma alone. The current reading at any electrode is the algebraic sum of current resulting from the conducting medium and the electron beam current collected by that electrode. The measure of beam current used in this paper is taken as the electron gun cathode current. It is reasonably isolated from the plasma region. Naturally all the cathode current does not remain in the beam when it reaches the plasma interaction region due to interception by the various electrodes along the way.

6.1 Growing Surface Waves

Since the electric field resulting from the surface wave interaction is strongest at the surface of the plasma column, a probe on the exterior of the column is capable of coupling to the surface waves. If one moves an antenna probe along such a column a growing standing wave pattern will be apparent as seen in Figure 6.4 for several values of the beam voltage. The electron beam travels from left to right. The standing wave pattern is a result of the propagating surface waves being partially reflected from the ends of the plasma column. That is, the plasma column appears as a mismatched transmission line. The growing wave envelope is a result of the interaction between the surface wave and the electron beam. As noted in Figure 6.4, the probe is moved between the input and output cavities a distance of 8.7 cm. Directly above three of the growing wave patterns are photographs obtained of detected output signal strength versus arc current corresponding to that beam voltage. After the photographs were taken, the arc current sweep was turned off and the current adjusted to the value corresponding to the maximum output signal strength. At this fixed value

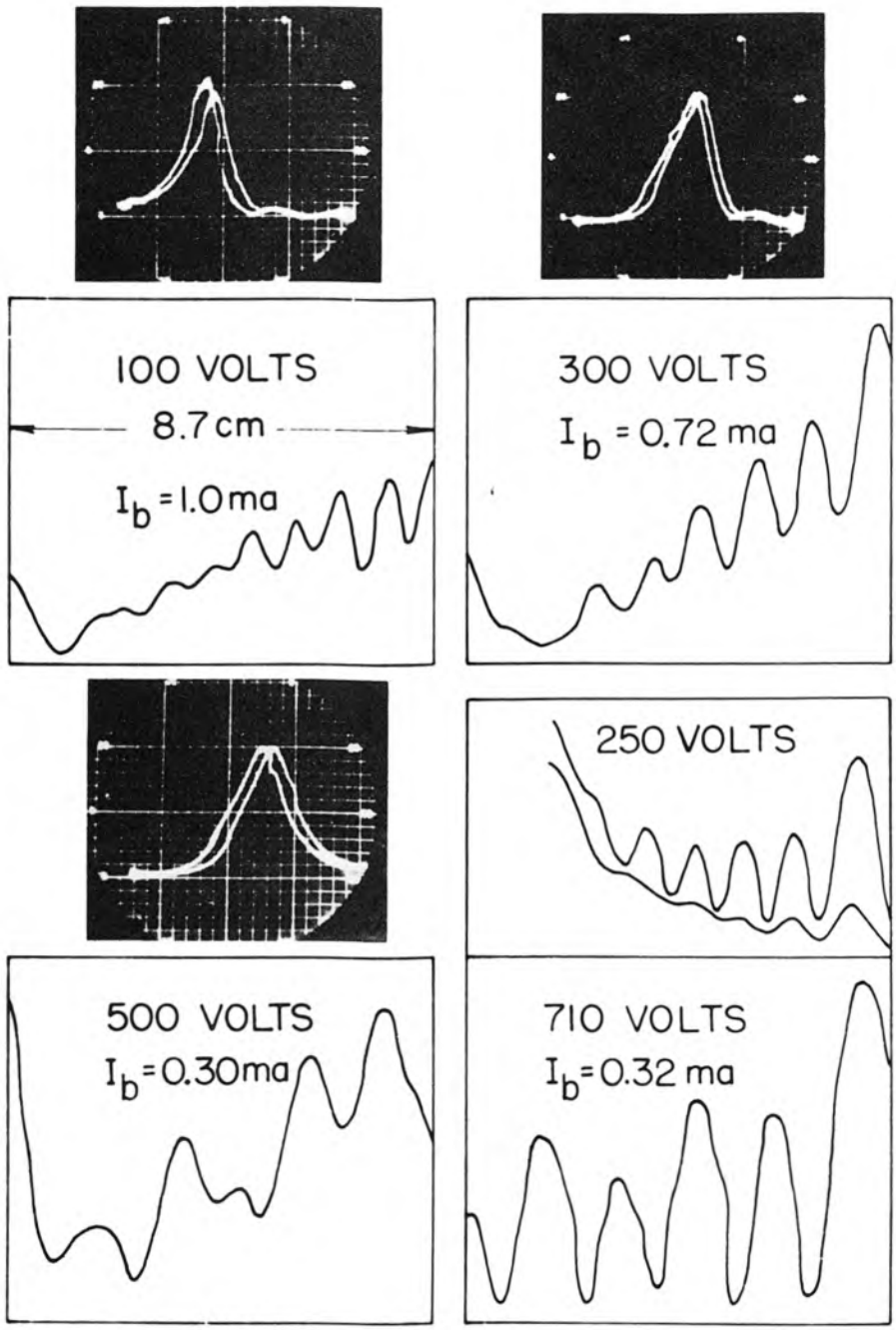

Figure 6.4 Growing Surface Waves Resulting from the Interaction of an Electron Beam Traveling from Left to Right with the Angularly Independent Mode of Propagation. The Horizontal Calibration for the Photographs is 20 Divisions Equals .050 Amperes.

of arc current, the probe is then moved along the plasma column with the resulting standing wave pattern.

In Figure 6.4 the signal strength versus distance along the plasma column is especially of interest for the 250 volt electron beam case. The upper curve is with the electron beam present and shows a growing standing wave. The lower curve is with the electron beam current greatly reduced by lowering the cathode temperature. In this latter case the signal strength decays for most of the distance along the interaction region due to losses in the slow surface wave mode of propagation. The 250 volt beam curves of Figure 6.4 clearly show that an electron beam interacting with the surface wave mode of propagation produces a growing wave.

From the standing wave pattern one may measure the electronic wavelength on the plasma column. This agrees reasonably well with that predicted from the known beam voltage. In fact, this wavelength measurement is a better measure of the velocity of propagation than the beam voltage, since no electrode voltage gives a true measure of the potential existing in the plasma interaction region. As is well known, an electrode in a plasma drawing no current is at a potential less than the plasma potential by a voltage equal to the sheath potential. This and such associated phenomena as the anode (arc) drop, all cause the plasma interaction region potential to be somewhat different from that of any of the beam electrodes.

As a further verification of the properties of the surface wave interaction, it is of interest to plot experimental ω-β diagrams corresponding to Figure 3.1 . To do this, one must have a measure of plasma density versus arc current. This was accomplished by the cavity

perturbation method discussed in Section 5.1 . Plasma density versus arc current is shown in Figure 6.5 and was obtained from the interaction region of the plasma column of the tube of Figure 6.1 . Several runs are shown and indicate a significant variation. The experimental points indicated by dots and circles were obtained with the previously used rectangular TE_{101} cavity. The crosses were obtained with the plasma column placed along the axis of a cylindrical TE_{111} cavity simultaneously with the operation of the surface wave interaction experiment. The experiment was being operated as in Figure 6.3 where the beam voltage was being swept at a 60 cps rate and the arc current was held constant.

It is apparent that the density versus arc current is not very reproducible, in that the function seems to split at approximately .05 amperes. The interaction region of the plasma column of Figure 6.1 is not an infinitely long column and thus the plasma density versus arc current might well be affected by the conditions on the electrodes at the ends of the interaction region. Experimentally, such is found to be the case, i.e., varying the electron beam electrode voltages affects the plasma density somewhat, though not in a reproducible way. For the degree of sophistication and accuracy attained thus far in this experiment, the plasma density versus arc current will be assumed to be given by the straight line of Figure 6.5 .

Knowing the plasma density versus arc current, it is possible to obtain experimental ω-β diagrams from data such as Figures 6.2 and 6.3 . Such a diagram is presented in Figure 6.6 . The dots, circles and deltas represent measurements made with the plasma column in free space and thus should coincide with the solid curve. The dots and deltas correspond to data such as Figure 6.2 where one sweeps the arc current.

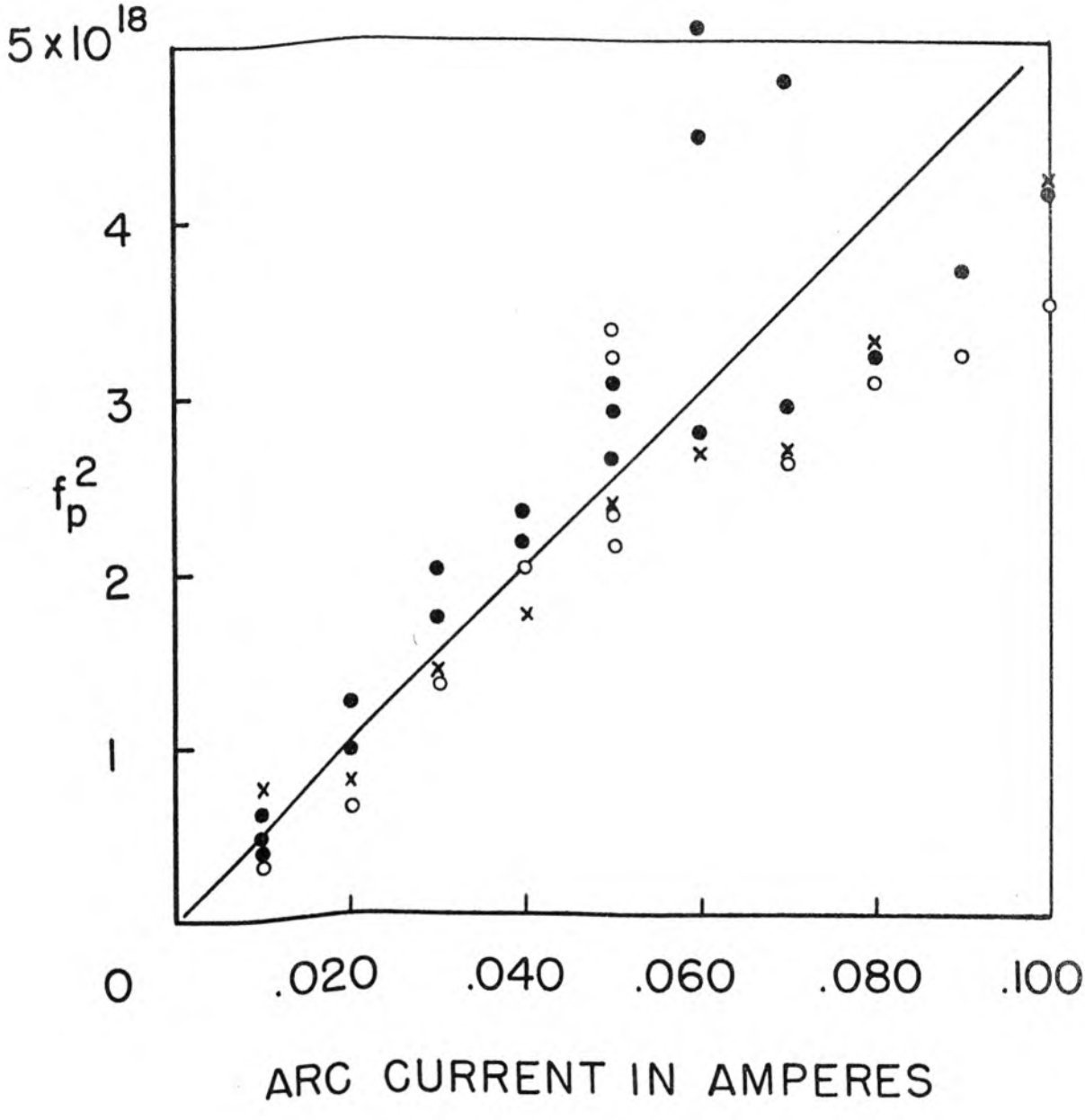

Figure 6.5 Cavity Perturbation Measurements of Plasma Frequency Squared versus Arc Current Obtained on the Cavity Modulation Tube of Figure 6.1

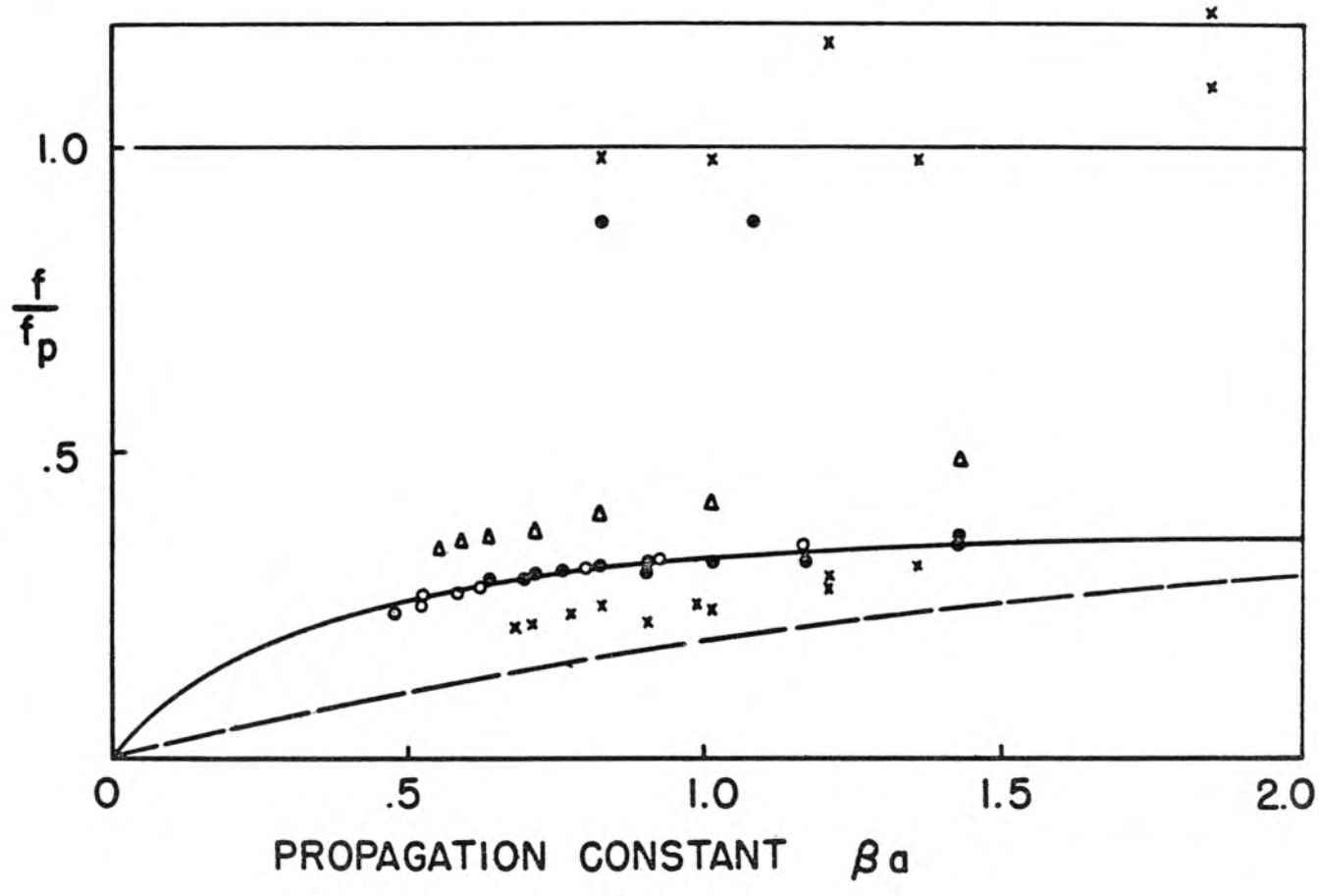

Figure 6.6 Experimental Surface Wave Frequency versus Propagation Constant. The •, ○, and △ Correspond to Measurements on the Plasma-Glass Column in Free Space and Should Lie on the Theoretical Solid Curve. The Data × Correspond to Measurements on the Plasma-Glass Column when Coated with a Conducting Surface and Should Lie on the Theoretical Dashed Curve.

The circles correspond to data such as Figure 6.3 where the beam voltage is swept. The crosses represent data obtained when the plasma column was coated by a metallic conductor (silver paint) at the surface of the glass tube and thus should coincide with the dashed curve. The significant experimental verification is that the experimental curve formed by the crosses lies below the curves formed by the dots, deltas and circles. All of the curves have the general shape as required by theory. The closeness with which they lie to the theoretical curves is, of course, proportional to the calibration of the ordinate in Figure 6.6 as obtained from Figure 6.5 . The effect of the radial variation in charge density would be to raise the experimental points upward in Figure 6.6 and thus would increase the discrepancy. This correction should not be too great, however, as the cavity perturbation technique measures average plasma density and the surface wave interaction measures somewhere between average and edge density. Note that the ordinate of Figure 6.6 is inversely proportional to the square root of arc current and the abscissa is inversely proportional to the square root of the beam voltage.

Besides demonstrating the interaction between an electron beam and the surface wave mode of propagation, the cavity modulation tube also shows interaction with the body resonance of the plasma at $f = f_p$. Three such interactions are shown in the top row of Figure 6.7 where the detected output signal versus arc current is shown. The first occurring peak (at lower arc current) corresponds to interaction with the body resonance as discussed in Chapter 2. The surface wave interaction is at the higher arc currents. From experimental curves similar to Figure 6.7 one obtains points as shown in Figure 6.6 near the

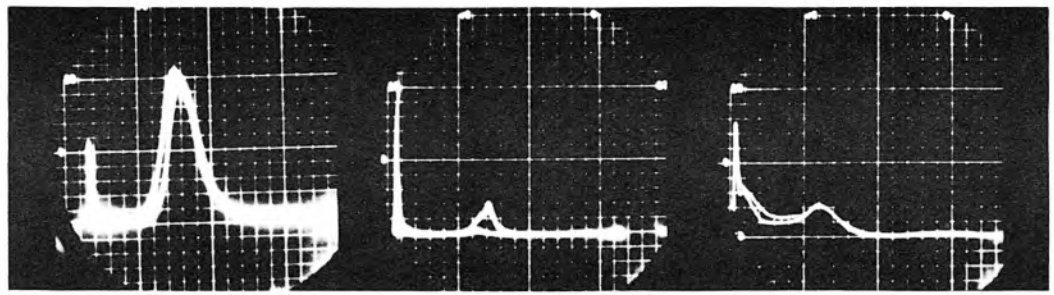

100 VOLTS 100 VOLTS 140 VOLTS

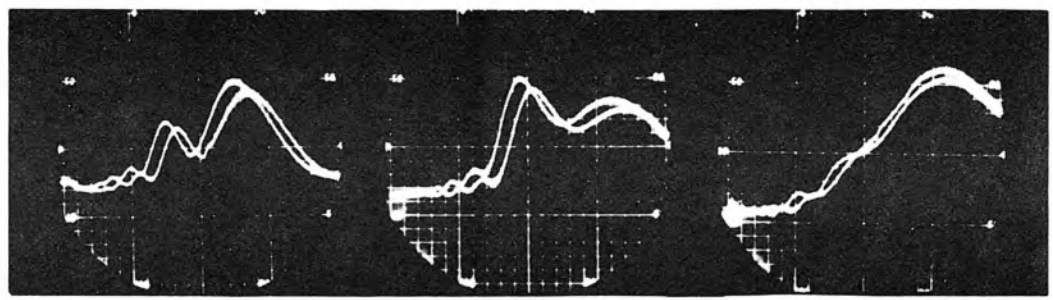

I_{ARC} = .040 AMP. I_{ARC} = .060 AMP. I_{ARC} = .080 AMP.

TOP ROW: OUTPUT VERSUS ARC CURRENT

HORIZONTAL CALIBRATION: 20 DIVISIONS = .10, .10, .20 AMPERES, RESPECTIVELY

BOTTOM ROW: OUTPUT VERSUS BEAM VOLTAGE

HORIZONTAL CALIBRATION: 20 DIVISIONS = 1000 VOLTS

Figure 6.7 Top Row: Interaction with Both the Body Resonance at $f = f_p$ and the Surface Wave Mode of Propagation. The Electron Beam Currents are Respectively, 2.2, 1.5, .57 Milliamperes.
Bottom Row: Anomalous Behavior of Output Signal versus Electron Beam Voltage at Different Arc Currents.

horizontal line $f/f_p = 1$. Since the interaction with the body resonance is at a small value of arc current (7 milliamperes approximately), the accuracy of scaling the photographs is poor. Also this small value of current is quite near the extinguishing value of the arc which causes experimental difficulties. For these reasons the experimental interaction points at $f = f_p$ in Figure 6.6 are no better than 20% .

6.2 Experimental Rates of Growth and Anomalous Effects

The surface wave interaction with an electron beam is experimentally demonstrated in Figures 6.2 and 6.3 . In the latter case the electron beam voltage is swept while holding the arc current constant. It is sometimes observed, however, that curves such as the bottom row of Figure 6.7 are obtained. These indicate several subsidiary peaks in output signal strength at lower voltages than the surface wave interaction.

As can be seen from a study of Figure 3.1, these lower voltage interactions (at a fixed arc current) lie on the lower side of the angularly independent, $n = 0$, surface wave diagram and thus cannot be explained in terms of interaction with the $n = 1$ mode of propagation. A possible explanation is in terms of the Kompfner "dip" phenomena (54,55).

Net gain has been obtained with the cavity modulation tube as was obtained with the helix modulation tubes C and D . The top row left photograph of Figure 6.7 corresponds to a net gain of +5 db. Net gain as high as +8 db has been observed. A more interesting experiment by far is to measure the rate of growth from curves similar to Figure 6.4 obtained by moving a probe along the outside of the glass column. If the growth constant is large enough, the growing wave predominates and the output signal will increase exponentially with distance. By replotting the average of the maxima and minima of the growing standing wave pattern on semilog paper, one can obtain the growth constant in db per cm. Data obtained in this manner is presented in Table 6.1 which follows.

BEAM VOLTAGE	BEAM CATHODE CURRENT IN MILLIAMPERES	GROWTH IN DB PER CM
143	3.0	.70
170	1.65	.61
185	1.6	.66
200	.73	.99
200	1.1	.78
200	1.2	.68
200	1.2	.72
200	1.2	.80
200	1.4	.85
500	.22	.44

Table 6.1 Experimental Growth Constants for Surface Wave Interaction with an Electron Beam as Obtained from the Cavity Modulation Tube

As can be seen, the spread in data is such that at a fixed voltage (200 volts as used here) the measured growth constant is not sufficiently reproducible that the dependence of the growth constant upon beam current could be verified. The main conclusion to be drawn is that such growing waves exist and that for a 200-volt beam and 1 ma beam current, a representative growth constant would be .8 db per cm. Theoretically from equations 3.1.2 and 3.1.3, one may compute a growth constant of 2.75 db per cm for a 1 milliampere, 200 volt beam. The interaction impedance, Z_o , was assumed to be 800 ohms as seen in Section 3.1 . This discrepancy between experiment and theory is probably due to the neglect of loss in the plasma column, a factor which is known to be significant.

In addition to the surface wave interaction, it was found that the body interaction could also be observed (Figure 6.7). A moving antenna

along the plasma column indicated a growing standing wave pattern in the direction of the electron beam similar to those observed in Figure 6.4 for the surface wave interaction. For the reasons discussed in Section 5.3, the signal picked up by the probe is very weak and is difficult to observe. For instance, the body resonance signal decreases 20 db or so relative to the surface wave signal when one changes from the output cavity to the probe at the surface of the plasma-glass column. Experimental growth constants are tabulated in Table 6.2.

BEAM VOLTAGE	BEAM CATHODE CURRENT IN MILLIAMPERES	GROWTH IN DB PER CM
215	1.0	.94
215	1.0	1.07
225	1.3	1.31
225	1.3	1.42

Table 6.2 Experimental Growth Constants for Body Resonance ($f=f_p$) Interaction with an Electron Beam as Obtained from the Cavity Modulation Tube

The reason that growing waves at $f = f_p$ are detectable with a probe outside the plasma column of the cavity tube but not the helix tube, is probably a result of two factors. The first is that βa is typically 1 in the cavity tube and 8 or so in the helix tube. Thus the fields are relatively stronger outside the cavity tube than the helix tube. The second factor is that, in the cavity tube the electron beam passes closer to the tube walls.

The theoretical rate of growth for the cavity modulation tube at $f = f_p$ may be computed from Section 2 including the beam plasma frequency reduction factor but neglecting collisions. Assuming a 200 volt electron beam, $R = 200/4.7 = 42.6$. At 490 Mc assuming an electron beam current of 1 ma the growth constant G is 10.2 db per cm. This discrepancy with

experiment is most likely a result of collisions of the plasma electrons since a representative collision frequency (Section 4.0) of 100 Mc is a far greater fraction of 490 Mc than of 3000 Mc.

Measurements of the growing standing wave pattern at $f = f_p$ indicate that the reflected wave has a phase velocity large compared to the forward beam velocity and thus is probably a reflected electromagnetic wave.

The above experimental measurement of growth constant along an electron beam at $f = f_p$ is a direct confirmation of the theories of Bohm and Gross (11). Previous investigators such as Looney and Brown (18) were unsuccessful in observing such results. Their lack of success is chiefly attributable to not using a modulated electron beam. In these previous experiments the electron beam-plasma interaction region was too short for an appreciable signal strength to build up from the noise level.

7. SUMMARY AND CONCLUSIONS

7.0 Summary of Results

Two new experiments on the interaction of a modulated electron beam with a plasma medium have been performed. One type of interaction is that between an electron beam and the plasma acting as a resonant, non-propagating medium. Such body resonance interaction occurs at $f/f_p \approx 1$. The modulated electron beam excites plasma oscillations which react back on the beam increasing the modulation and thus a growing wave exists in the beam direction. The interaction is independent of the electron beam velocity, in that the wave is carried by the electron beam and not by propagation through the plasma medium.

The other type of interaction studied in this paper is between an electron beam and a plasma column acting as a slow wave propagating structure. Such a plasma column acting as a transmission line is a three-dimensional effect, i.e., its propagation characteristics depend on the finite cross section of the plasma column. In the absence of an axial magnetic field such slow waves propagate on the surface of the plasma column. The interaction of an electron beam with such surface waves as observed in this paper occur in the range $.2 < f/f_p < .5$. The interaction is velocity dependent in that the interaction occurs when the electron beam velocity is synchronous with the phase velocity of the surface wave on such a plasma column. The helix modulation experiment and cavity modulation experiment of Figures 1.1 and 1.2 respectively, were designed to investigate these interactions.

The helix modulation experiment operated at a fixed beam velocity and over a wide frequency range. Because the plasma column radius was large compared to the beam radius, the principal interaction observed was with the body resonance at $f/f_p \approx 1$. The principal features of this amplifying mechanism were found to be in qualitative agreement with the one-dimensional analysis of many previous workers, i.e., the existence of growing waves on the electron beam were found at a frequency equal to the plasma frequency of the medium through which the electron beam passed. The linear dependence of the modulation frequency squared versus interaction arc current as seen in Figure 5.3 is in agreement with theory. This device also shows interaction with the surface wave mode of propagation.

The cavity modulation experiment operated at a fixed frequency and over a wide synchronous velocity range. The electron beam filled an appreciable fraction of the plasma column cross-section and interacted strongly with the surface wave mode of propagation. An experimental frequency versus propagation constant diagram such as Figure 6.6 is found to be in good agreement with the theoretical curves. Interaction was also obtained with the body resonance at $f/f_p = 1$ for small values of arc current.

Net gain has been obtained in both experiments. Exponential growth constants along the beam were measured by means of a traveling probe for both interactions and were considerably less than predicted theoretically including only the random energy of the plasma electrons and the beam plasma reduction factor. Collisions and plasma inhomogeneities probably account for the reduction in gain.

7.1 Conclusions and Future Possibilities

Results have been reported for two new experiments that verify existing theories of the interaction of a modulated electron beam with a plasma medium. The experiments are difficult to perform because of the uncertainty in the focusing of the electron beam. The amplifying mechanisms in both experiments appear to be extremely noisy. This is probably due to the random energy of the plasma electrons which results in collisions with mercury atoms and the electron sheaths at boundaries of the plasma. Unless this can be overcome, these devices may not be of great practical importance.

One of the most fascinating future experiments to be performed with a device such as the cavity modulation tube is to immerse the entire apparatus in a strong axial magnetic field. This would probably eliminate beam focusing problems and consequently result in far more reproducible results. Further, if the magnetic field were sufficiently high that the cyclotron radius of the plasma electrons due to their random energy were small compared to the plasma column radius, then one might expect to lower the collision frequency with the electron sheath. If this were so, one would hope that the high frequency loss of slow waves on such a plasma column might be reduced, and with it the noise on such waves. The noise mechanism is, however, more probably associated with striations and oscillations in the arc column.

Aside from these considerations, the effect of an axial magnetic field would change the propagation characteristics of the plasma column in a most interesting way, as discussed by Trivelpiece and Gould (33). They have shown that with a magnetic field there exists a backward wave propagating mode (phase and group velocities in opposite

directions) with which backward wave interaction and thus oscillation is possible. Structureless oscillators are an intriguing concept from the millimeter wave point of view but this is beyond the results of the present thesis.

Appendix 1

DIPOLE RESONANCE OF A CYLINDRICAL PLASMA COLUMN IN A TRANSVERSE ELECTRIC FIELD

Consider the plasma column of an arc discharge tube placed across a waveguide such that the column axis is perpendicular to the direction of propagation in the guide. The guide is assumed to be propagating in the TE_{10} mode and the electric vector is perpendicular to the column axis. The experiment is shown in Figure A1.

The condition of dipole resonance is easily obtained [Herlofson (36)] if one assumes that the guide wavelength of the propagating wave is large compared to the plasma column radius. Such is the case for the experiments performed in Section 5.1 . Therefore, in determining the normal modes of oscillation of the plasma column one may use the quasi-static approximation and derive the fields from the negative gradient of the potential. The effect of the glass walls will be included and the plasma column is assumed to have a uniform charge density.

In the quasi-static approximation the time varying potential satisfies Laplace's equation, $\nabla^2 \phi_1 = 0$. The radius of the plasma is assumed to be a . The outer radius of the glass tube is c . The appropriate solutions are

$$\begin{aligned} \phi_1 &= A_n \frac{\cos n\theta}{r^n} && r \geq c \\ \phi_1 &= \left\{ B_n r^n + \frac{C_n}{r^n} \right\} \cos n\theta && c \geq r \geq a \\ \phi_1 &= D_n r^n \cos n\theta && r \leq a \end{aligned} \qquad \text{(A1.1)}$$

The equivalent dielectric constant of the plasma is

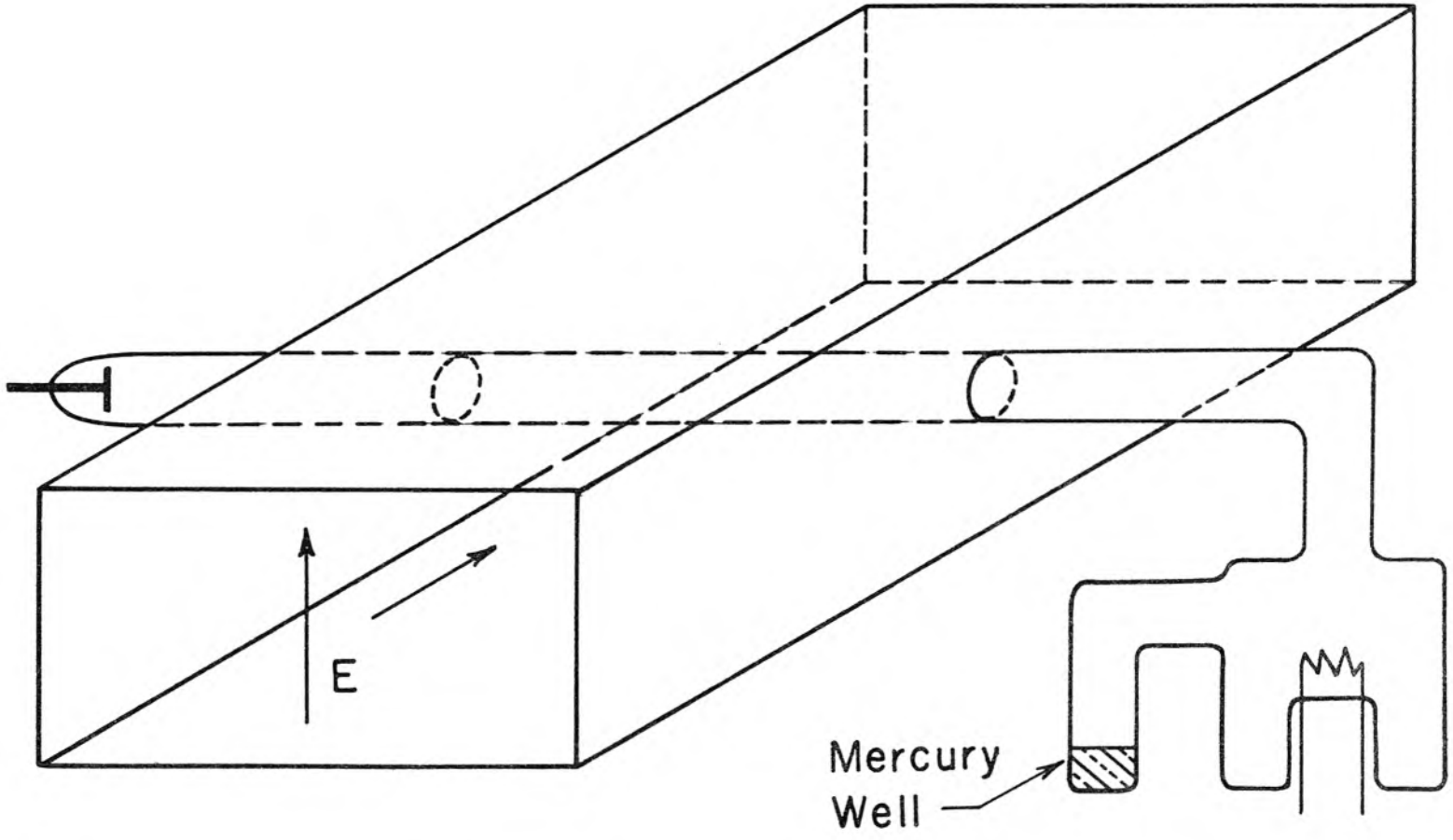

Figure A1. Dipole Scattering and Resonance from a Plasma Column.

$$\frac{\epsilon}{\epsilon_o} = 1 - \frac{\omega_p^2}{\omega^2} \tag{A1.2}$$

Applying the boundary conditions of continuity of the tangential electric field and normal displacement at $r = a$ and $r = c$ one obtains the set of simultaneous equations

$$\begin{aligned} &A_n - B_n (c^{2n}) - C_n = 0 \\ &B_n(a)^{2n} + C_n - D_n (a^{2n}) = 0 \\ &A_n + B_n (\kappa c^{2n}) - C_n \kappa = 0 \\ &D_n(a^{2n}) - C_n - D_n \left(\frac{\epsilon}{\kappa \epsilon_o}\right) = 0 \end{aligned} \tag{A1.3}$$

where κ is the relative dielectric constant of the glass tube enclosing the plasma. For there to be a solution, the determinant of the coefficients must be zero. Making the substitution

$$\Delta = \left(\frac{c}{a}\right)^{2n} - 1 \tag{A1.4}$$

one obtains as the condition for resonance

$$\frac{\omega_p^2}{\omega^2} = 1 + \frac{2 + \Delta(1 + \kappa)}{2 + \Delta[1 + (1/\kappa)]} \tag{A1.5}$$

In the case that there is no glass surrounding the plasma this becomes $\omega_p^2/\omega^2 = 2$ which was given as equation 2.0.2 . Note that this is independent of the mode n of oscillation. In Section 5.1 measurements of dipole resonance were obtained on a plasma column constructed from the same glass as used in the helix modulation tubes of Figure 5.1 . Substituting the appropriate numerical constants one finds dipole resonance at $\omega_p^2/\omega^2 = 2.81$.

Appendix 2

ONE-DIMENSIONAL DISPERSION RELATION BY THE BOLTZMANN EQUATION METHOD

The dispersion relation of an electron beam passing through a plasma, including the random energy of the plasma electrons, has been obtained by Bohm and Gross (11) from the Boltzmann equation.

The Boltzmann equation may be written as

$$\frac{\partial f}{\partial t} + (\underline{u} \cdot \nabla_r) f + \frac{\underline{F}}{m} \cdot \nabla_u f = \left(\frac{\partial f}{\partial t}\right)_{\text{collisions}} \qquad \text{(A2.1)}$$

where $f(\underline{r},\underline{u},t)$ is the fraction of the number of electrons per unit volume in six-dimensional phase space in the vicinity of the point $(\underline{r},\underline{u})$ at time, t. This is not the customary definition which is the number (as opposed to the fraction) of electrons per unit volume. The fraction of electrons within the volume $dx\,dy\,dz$ at a position $\underline{r}$ in the velocity range du_x, du_y, du_z centered about $\underline{u}$ is given by $f(\underline{r},\underline{u},t)\,du_x\,du_y\,du_z$. The Boltzmann equation states that df/dt, the rate of charge of f along the trajectory of the particles, is entirely the result of encounters among the particles. The external force $\underline{F}$ is assumed conservative. The long-range interaction force of the plasma electrons is included in the force term as

$$\underline{F} = -e(\underline{E} + \underline{u} \times \underline{B}) \quad . \qquad \text{(A2.2)}$$

The plasma is assumed stationary and steady magnetic fields are assumed to be absent.

If the time varying disturbances in the plasma are small, one can linearize equation A2.1 . Let the equilibrium distribution function be

denoted by f_o and the small signal perturbation distribution function by f_1. The equilibrium distribution is assumed to be independent of position. One then obtains

$$\frac{\partial f_1}{\partial t} + (\underline{u} \cdot \nabla_r) f_1 - \frac{e}{m} (\underline{E}_1 + \underline{u} \times \underline{B}_1) \cdot \nabla_u f_o = \left(\frac{\partial f}{\partial t}\right)_{\text{collisions}} . \quad \text{(A2.3)}$$

Since the velocities of the plasma electrons are small compared to the velocity of light, the magnetic force can be neglected compared to the electric force. The effect of short-range collisions of the plasma electrons is approximated by letting

$$\left(\frac{\partial f_1}{\partial t}\right)_{\text{collisions}} = -\nu f_1 \quad . \quad \text{(A2.4)}$$

For the case of longitudinal oscillations of the plasma electrons as considered in this thesis, the direction of propagation and the electric field are assumed parallel and in the z direction. Equation A2.3 can then be solved in the one-dimensional case, where time and spatial dependence are assumed to be given by $e^{i(\omega t - \gamma z)}$, resulting in

$$f_1(\underline{u}) = \frac{e}{m} \frac{E_1 \frac{\partial f_o(\underline{u})}{\partial u_z}}{i(\omega - \gamma u_z) + \nu} \quad \text{(A2.5)}$$

f_1 being defined as the perturbation in the fraction of electrons per unit volume in phase space. By definition

$$\int_{\underline{u}} f_o(\underline{u}) \, d\underline{u} = 1 \quad . \quad \text{(A2.6)}$$

The small signal time varying current density is given by

$$\underline{J}_1 = -e\, n_o \int_{\underline{u}} \underline{u}\, f_1(\underline{u})\, d\underline{u} \qquad \text{(A2.7)}$$

where n_o is the total number of electrons per unit volume of the equilibrium distribution and is assumed to be uniform throughout space. After substituting equation A2.5 and integrating by parts one obtains

$$\underline{J}_1 = i\omega\epsilon_o\, \chi_\ell\, \underline{E}_1 \qquad \text{(A2.8)}$$

where χ_ℓ is defined as the longitudinal susceptibility of the plasma. If the equilibrium distribution function $f_o(\underline{u})$ is symmetrical in velocity space then the longitudinal susceptibility is given by

$$\chi_\ell = -\omega_p^2 \frac{(\omega - i\nu)}{\omega} \int_{\underline{u}} \frac{f_o(\underline{u})\, d\underline{u}}{(\omega - \gamma u_z - i\nu)^2} \qquad \text{(A2.9)}$$

where $\omega_p^2 = n_o e^2/m\epsilon_o$ is the plasma frequency.

Equation A2.9 is the longitudinal susceptibility of the plasma. It is also necessary to obtain the susceptibility of the modulated electron beam which passes through the electron plasma. The random distribution of velocities of the beam electrons about their mean velocity v_b is neglected. Starting with the linearized equation of motion and continuity in one dimension and assuming a time and space dependence $e^{i(\omega t - \gamma z)}$ as before, one obtains (see Section 2.2)

$$i\, \underline{v}_{1b}\, (\omega - \gamma v_b) = -\frac{e}{m}\, \underline{E}_1 \qquad \text{(A2.10)}$$

$$\omega\, \rho_{1b} = \gamma J_1 \quad . \qquad \text{(A2.11)}$$

It is convenient to define a beam plasma frequency in terms of the beam electron density by $\omega_b^2 = -\rho_b e/m_o$. The small signal time varying current density is given by

$$\underline{J}_1 \approx \rho_b \underline{v}_{1b} + \underline{v}_b \rho_{1b} \quad . \tag{A2.12}$$

From equations A2.10, A2.11 and A2.12 one can eliminate ρ_{1b} and v_{1b} and obtain

$$\underline{J}_1 = i\omega\epsilon_o \chi_\ell \underline{E}_1 \tag{A2.13}$$

where the electron beam susceptibility χ_ℓ is given by

$$\chi_\ell = - \frac{\omega_b^2}{(\omega - \gamma v_b)^2} \quad . \tag{A2.14}$$

Adding equations A2.9 and A2.14 gives the total susceptibility to longitudinal oscillations of an electron beam passing through an electron plasma.

It is now necessary to find what requirement must hold on the total susceptibility of the beam plus plasma system. The two systems may be superimposed since all equations are linear. For the situation under discussion of longitudinal oscillations in one dimension in which the electric field is parallel to the direction of propagation, (as opposed to transverse wave propagation), it is apparent that

$$\nabla \times \underline{E}_1 = 0 \tag{A2.15}$$

since the total spatial dependence is $e^{-i\gamma z}$. Therefore, the electric field can be derived from

$$\underline{E}_1 = - \nabla \phi_1 \quad . \tag{A2.16}$$

Poisson's equation then follows from $\nabla \cdot \epsilon_o \underline{E}_1 = \rho_1$

$$\nabla^2 \phi_1 = - \rho_1 / \epsilon_o \quad . \tag{A2.17}$$

The continuity equation

$$i\omega \rho_1 = - \nabla \cdot \underline{J}_1 \tag{A2.18}$$

and the convection current

$$\underline{J}_1 = i \omega \epsilon_o \chi_\ell \underline{E}_1 \tag{A2.19}$$

defined in terms of a susceptibility, can then be combined with equation A2.17 to give

$$(1 + \chi_\ell) \nabla^2 \phi_1 = 0 \quad . \tag{A2.20}$$

χ_ℓ now represents the <u>total</u> susceptibility of the plasma <u>plus</u> the beam. The solution $\nabla^2 \phi_1 = 0$ is not of interest in one dimension and thus the dispersion relation for longitudinal oscillations becomes

$$\chi_\ell = -1 \quad . \tag{A2.21}$$

The total susceptibility from equations A2.9 and A2.14 of the plasma and beam system when combined with equation A2.21 results in

$$1 = \omega_p^2 \frac{(\omega - i\nu)}{\omega} \int_{\underline{u}} \frac{f_o(\underline{u})\, d\underline{u}}{(\omega - \gamma u_z - i\nu)^2} + \frac{\omega_b^2}{(\omega - \gamma v_b)^2} \tag{A2.22}$$

which is the one-dimensional dispersion relation given by equation 2.1.1 .

REFERENCES

(1) I. Langmuir, H. Mott-Smith, Gen. Elec. Rev. 27, 449, 538, 616, 762, 810, (1924).

(2) I. Langmuir, Phys. Rev. 26, 585 (1925).

(3) A. F. Dittmer, Phys. Rev. 28, 507 (1926).

(4) F. M. Penning, Physica 6 , 241 (1926) ;
Nature 118, 301 (1926) .

(5) L. Tonks, I. Langmuir, Phys. Rev. 33, 195, 990 (1929).

(6) L. Tonks, Phys. Rev. 37, 1458 (1931).

(7) L. Tonks, Phys. Rev. 38, 1219 (1931).

(8) M. J. Druyvesteyn, N. Warmoltz, Physica 4, 51 (1937).

(9) H. J. Merrill, H. W. Webb, Phys. Rev. 55, 1191 (1939).

(10) E. B. Armstrong, Nature 160, 713 (1947).

(11) D. Bohm, E. P. Gross, Phys. Rev. 75, 1851 (1949)
75, 1864 (1949)
79, 992 (1950) .

(12) T. R. Neill, Nature 163, 59 (1949).

(13) E. B. Armstrong, K. G. Emeleus, Inst. of Elec. Engrs. Proc. 93, Part 3, 390 (1949).

(14) G. Wehner, J. Appl. Phys. 21, 62 (1950).

(15) T. R. Neill, K. G. Emeleus, Roy. Irish Acad. Proc. 53A, 197 (1951).

(16) E. B. Armstrong, K. G. Emeleus, T. R. Neill, Roy. Irish Acad. Proc. 54A, 291 (1951).

(17) D. Gabor, Brit. JAP 2, 209 (1951).

(18) D. H. Looney, S. C. Brown, Phys. Rev. 93, 965 (1954).

(19) K. G. Emeleus, R. A. Bailey, Brit. JAP 6, 127 (1955).

(20) R. A. Bailey, K. G. Emeleus, Roy. Irish Acad. Proc. 57A, 53 (1955).

(21) D. Gabor, E. A. Ash, D. Dracott, Nature 176, 916 (1955).

(22) E. I. Gordon, Thesis, Mass. Inst. of Technology (1957).

(23) S. Kojima, K. Kato, S. Hagiwara, Jour. Phy. Soc. Japan 12, 1276 (1957).

(24) M. Sumi, Jour. Phys. Soc. Japan 13, 1476 (1958).

(25) M. Sumi, Phys. Rev. Letters 2, 37 (1959).

(26) A. V. Haeff, Phys. Rev. 74, 1532 (1948);
Phys. Rev. 75, 1546 (1949).

(27) J. R. Pierce, JAP 19, 231, (1948).

(28) A. V. Haeff, Proc. IRE 37, 4 (1949).

(29) R. W. Gould, PhD Thesis, California Inst. of Technology (1956).

(30) J. R. Pierce, Traveling Wave Tubes, D. Van Nostrand Co., (1950).

(31) J. R. Pierce, W. B. Hebenstreit, B.S.T.J. 28, 33 (1949).

(32) G. D. Boyd, L. M. Field, R. W. Gould, (L) Phys. Rev. 109, 1393 (1958); Proc. Symp. Electronic Waveguides, Polytechnic Press of the Polytechnic Inst. of Brooklyn, p.367 (1958).

(33) A. W. Trivelpiece, PhD Thesis, C.I.T. (1958); R. W. Gould, A. W. Trivelpiece, Proc. Inst. of Elec. Eng. 105B, 516 (1958).

(34) J. R. Pierce, L. M. Field, Proc. IRE 35, 108 (1947).

(35) L. Spitzer, Physics of Fully Ionized Gases, Interscience Pub., Inc. (1956).

(36) N. Herlofson, Arkiv for Fysik 3, 247 (1951).

(37) C. K. Birdsall, Memorandum for File ETL-12, July 1, 1953, Hughes Aircraft Company.

(38) H. Mott-Smith, I. Langmuir, Phys. Rev. 28, 727 (1926).

(39) B. Klarfeld, Jour. Of Phys., Acad. of Sc. USSR 5, 155 (1941).

(40) A. von Engel, Ionized Gases, Oxford University Press (1955).

(41) M. A. Biondi, S. C. Brown, Phys. Rev. 75, 1700 (1949);
K. B. Persson, Phys. Rev. 106, 191 (1957);
S. J. Buchsbaum, S. C. Brown, Phys. Rev. 106, 196 (1957).

(42) R. M. Howe, JAP 24, 881 (1953).

(43) T. R. Kaiser, R. L. Closs, Phil. Mag. 43, 1 (1952).

(44) D. Romell, Nature 167, 243 (1951).

(45) A. Dattner, Ericson Technics 2, 309 (1957).

(46) F. I. Boley, Nature 182, 790 (1958).

(47) V. R. Eshleman, Tech. Report 49, Electronics Res. Lab., Stanford University (1952).

(48) R. E. B. Makinson, D. M. Slade, Austr.Jour. Phys. 7, 268 (1954).

(49) G. H. Keitel, Proc. IRE 43, 1481 (1955).

(50) G. H. Keitel, Austr. Jour. Phys. 9, 144 (1956).

(51) R. W. Gould, Private communication.

(52) N. F. Mott, H. S. W. Massey, The Theory of Atomic Collisions, Second edition, Oxford (1949).

(53) K. W. H. Foulds, Jour. Electronics 2, 270 (1956).

(54) R. Kompfner, Brit. Jour. Inst. Radio Engrs. 10, 283 (1950).

(55) H. R. Johnson, Proc. IRE 43, 874 (1949).

Nonr 220(13)

DISTRIBUTION LIST

Chief of Naval Research 2
Navy Department - CODE 427
Washington 25, D. C.

Director, Naval Research Lab.
Washington 25, D. C.
Attn: CODE 5240 1
CODE 7130 1
CODE 2000 6
CODE 5430 1

Commanding Officer 1
ONR Branch Office
1000 Geary Street
San Francisco, California

Scientific Liaison Officer 25
ONR, London
c/o Navy 100, Box 39, FPO
New York, New York

Commanding Officer 1
ONR Branch Office
1030 E. Green Street
Pasadena, California

Commanding Officer 1
ONR Branch Office
The John Crerar Library Bldg.
86 E. Randolph Street
Chicago, 1, Illinois

Commanding Officer 1
ONR Branch Office
346 Broadway
New york 13, New York

Officer-in-Charge 3
Office of Naval Research
Navy No. 100
Fleet Post Office
New York, New York

Chief, Bureau Aeronautics EL4 1
Navy Department EL43 1
Washington 25, D.C. EL45 1

Chief, Bureau of Ordnance
Navy Department Re 4 1
Washington 25, D. C. Re 9 1

Chief of Naval Operations Op 20X 1
Navy Department Op 421 1
Washington 25, D.C. Op 55 1

Director, Naval Ordnance Lab. 1
White Oak, Maryland

Director, Naval Electronics Lab 1
San Diego 52, California

Dept. of Electronics Physics 1
U.S.Naval Post Grad. School
Monterey, California

Commander Code 366 1
Naval Air Missile Test Center
Point Mugu, California

U.S. Naval Proving Ground 1
Attn: W. H. Benson
Dahlgren, Virginia

Commander 1
U.S.Naval Air Development Center
Johnsville, Pennsylvania

Committee on Electronics 1
Research and Development Board
Department of Defense
Washington 25, D. C.

Director, Natl. Bureau of Stds. 1
Washington 25, D. C.
Attn: Div.14.0 CRPL, Librarian

Commanding Officer 1
Engineering Res.and Dev. Lab.
Fort Belvoir, Virginia

Ballistics Research Labs. 2
Aberdeen Proving Ground
Maryland
Attn: D.W.H. Delaasso

Chief, Ordnance Develop. Div. 2
Natl. Bureau of Standards
Connecticut Av, VanNess St, NW
Washington 25, D. C.

Commanding Officer 1
Frankford Arsenal
Bridesburg, Philadelphia, Pa.

Thermionics Branch 5
Signal Corps Eng. Labs.
Evans Signal Lab, Bldg. 42
Belmar, New Jersey

Commanding General 1
Air Research and Dev. Command
ATTN: RDSBTL(Hq.Tech.Library)
Andrews Air Force Base
Washington 25, D. C.

Commanding General WCLC 1
Wright Air Devel.Center WCLRC 1
Wright-Patterson AF Base, Ohio

Commanding General CRRE 1
AF Cambridge Research Center
230 Albany Street
Cambridge 39, Massachusetts

Commanding General RCRW 1
Rome Air Development Center
Griffiss Air Force Base
Rome, New York

Commander 5
Armed Services Tech. Info.
ATTN; TIPDR
Arlington Hall Station
Arlington 12, Virginia

Director CR4582 1
Air University Library
Maxwell AF Base, Alabama

Chief, Western Division 1
Air Research and Devel.Command
Office of Scientific Research
P.O.Box 2035, Pasadena, Calif.

Microwave Laboratory 1
Stanford University
Stanford, California
Attn: F.V.L. Pindar

University of Michigan 1
Electron Tube Laboratory
Ann Arbor, Michigan
Attn: J. Rowe

Mr. John S. McCullough 1
Eitel-McCullough, Inc.
San Bruno, California

Johns Hopkins University 1
Radiation Laboratory
1315 St. Paul Street
Baltimore 2, Maryland
Attn: M. Poole, Librarian

Raytheon Corporation 1
Waltham, Massachusetts
Attn: Librarian

Cascade Research 1
53 Victory Lane
Los Gatos, California

Engineering Library 1
Stanford University
Stanford, California

Research Lab.of Electronics 1
Massachusetts Inst. of Tech.
Cambridge 39, Massachusetts

Sloane Physics Laboratory 1
Yale University
New Haven, Connecticut
Attn: R. Beringer

Mr. H. J. Reich 1
Department of Elec. Eng.
Yale University
New Haven, Connecticut

Electron Tube Section 1
Electrical Engineering Dept.
University of Illinois
Champaign, Illinois

Chairman, Div. of Elec. Eng. 1
University of California
Berkeley 4, California

Technical Report Collection 1
303A, Pierce Hall
Harvard University
Cambridge 38, Massachusetts

Laboratory for Insulation Res. 1
Massachusetts Inst. of Tech.
Cambridge 39, Massachusetts
Attn: A. von Hippel

Chief, West Coast Office 1
Signal Corps Eng. Labs.
75 So. Grand Avenue
Pasadena, 2, California

Periodicals Librarian 1
General Library
California Inst. of Technology

Lincoln Laboratory 1
Massachusetts Inst. of Tech.
Cambridge 39, Massachusetts

Signal Corps Resident Engineer 1
Electronic Defense Lab.
P.O. Box 205
Mountain View, California

Cornell Aeronautical Laboratory 1
Cornell Research Foundation
Buffalo 21, New York

Director, Electronics Defense 1
Engineering Research Inst.
University of Michigan
Ann Arbor, Michigan

Georgia Inst. of Technology 1
Atlanta, Georgia
Attn: Librarian

Fred D. Wilimek 1
Varian Associates
611 Hansen Way
Palo Alto, California

John Dyer 1
Airborne Instrument Laboratory
Mineola, L.I., New York

Bell Telephone Laboratories
Murray Hill, New Jersey
Attn: Librarian 1
J. R. Pierce 1

Hughes Aircraft Company 1
Culver City, California
Attn: Mr.Milek, Tech.Librarian

RCA Laboratories 1
Princeton, New Jersey
Attn: Mr.Herold and H.Johnson

Federal Tele. Laboratories
500 Washington Avenue
Nutley, New Jersey
Attn: W. Derrick 1
K. Wing 1

Technical Library 1
G.E. Microwave Laboratory
601 California Avenue
Palo Alto, California

Columbia Radiation Laboratory 1
538 W. 120th Street
New York 27, New York

Countermeasures Laboratory 1
Gilfillan Brothers, Inc
1815 Venice Boulevard
Los Angeles, California

The Rand Corporation 1
1700 Main Street
Santa Monica, California
Attn: Librarian

Technical Library 1
Research and Development Board
Pentagon Building
Washington 25, D. C.

Motorola Riverside Res. Lab. 1
8330 Indiana Avenue
Riverside, California
Attn: Mr. John Byrne

Chief, Bureau of Ships 816 1
Department of the Navy 820 1
Washington, D. C. 840 1

Advisory Group on Electron Tubes 1
346 Broadway (8th Floor)
New York 13, New York

Supervisor of Research Lab. 1
Electrical Engineering Bldg.
Purdue University
Lafayette, Indiana

W. E. Lear 1
University of Florida
Department of Electrical Eng.
Gainesville, Florida

Director, Microwave Res. Inst. 1
Polytechnic Inst. of Brooklyn
55 Johnson Street
Brooklyn 1, New York

Material Lab. Library, 912B 1
New York Naval Shipyard
Brooklyn 1, New York

University of Washington
Dept. of Electrical Engineering
Seattle, Washington
Attn: E. A. Harrison 1
A. V. Eastman 1

University of Colorado 1
Department of Elec. Engineering
Boulder, Colorado

Ramo-Wooldridge Corporation 1
Control Systems Division
P.O. Box 900B
Hawthorne, California
Attn: Librarian

Electrical Engineering Dept. 1
Princeton University
Princeton, New Jersey

National Union Radio Company 1
350 Scotland Road
Orange, New Jersey
Attn: Dr. A. M. Skellet

Dr. J. E. Shepherd 1
Sperry Gyroscope Company
Great Neck, L.I., New York

W. L. Maxson Corporation 1
460 West 34th Street
New York 1, New York
Attn: M. Simpson

Bertram G. Ryland, Manager 1
Spencer Laboratory
Raytheon Manufacturing Co.
Burlington, Mass.

Dr. E. D. McArthur 1
Electron Tube Laboratory
General Electric Company
Schenectady, New York

General Electric Company 1
Electronic Components Division
Power Tube Department
Microwave Lab. at Stanford
Palo Alto, California

Office of Technical Services 1
Department of Commerce
Washington 25, D. C.

Professor W. P. Dyke 1
Linfield College
McMinnville, Oregon

Stanford Electronics Labs. 1
Stanford University
Stanford, California
Attn: Electronics Lab.Library

Mr. E. C. Okress, Tech.Director 1
P.O. Box 284
Electronic Tube Division
Westinghouse Electric Corp.
Elmira, New York

Mr. Gilbert Kelton 1
Security Officer
Philips Laboratories
Irvington-on-Hudson, New York

University of Colorado 1
Engineering Experiment Sta.
Boulder, Colorado
Attn: W. G. Worcester

Dr. Z. Kaprielian 1
Electrical Engineering Dept.
University of Southern Calif.
Los Angeles 7, California

Dr. G. E. Barlow 1
Australian Joint Service Staff
Box 4837
Washington 8, D. C.

R. E. McGuire, Librarian 1
Office of the Director of Res.
Boeing Airplane Company
P.O. Box 3707
Seattle 24, Washington

Dr. Donald W. Kerst 1
General Atomic
P. O. Box 608,
San Diego, California

Image Instruments, Inc. 1
51 Waldorf Road
Newton Upper Falls 64, Mass.

Radiation Laboratory 1
Tech. Information Division
University of California
Berkeley 4, California

Sylvania Electric Products Inc. 1
Waltham, Massachusetts
Attn: Charles A. Thornhill

Dr. J. M. Lafferty, Manager 1
Physical Studies
General Electric Company
P.O. Box 1088
Schenectady, New York